This is to certify that the
dissertation entitled

ADSORPTION OF BIO-RENEWABLE SUBSTRATES ON
SUPPORTED METAL CATALYST IN WATER

presented by

LARS PEEREBOOM

has been accepted towards fulfillment
of the requirements for the

Ph.D. degree in Chemical Engineering

Dennis J Miller
Major Professor's Signature

9/17/07
Date

ADSORPTION OF BIO-RENEWABLE SUBSTRATES ON SUPPORTED METAL CATALYST IN WATER

By

Lars Peereboom

A DISSERTATION

Submitted to
Michigan State University
in partial fulfillment of the requirements
for the degree

DOCTOR OF PHILOSOPHY

Department of Chemical Engineering

2007

ABSTRACT

ADSORPTION OF BIO-RENEWABLE SUBSTRATES ON SUPPORTED METAL CATALYST IN WATER

By

Lars Peereboom

Biomass-based organic substrates are attractive feedstocks for chemicals production because they are available in quantity and can undergo a variety of reactions to form useful products. In our efforts to understand the mechanisms of aqueous transformations of these substrates over supported noble metal catalysts, we seek to probe interactions between the substrate and catalyst metal and between the substrate and catalyst support. This dissertation recounts our work to measure the extent of substrate adsorption on the catalyst surface and on the support based on difference—i.e. by measuring (via HPLC analysis) the initial and final concentrations of substrate in solution. We have developed a novel flow microreactor system (recirculating batch reactor or RBR) with in-line substrate detection and a high catalyst metal to solution ratio. Polyol and organic acid interactions with both the unsupported Ru metal catalyst and the carbon support have been examined, the former in the RBR and the latter in batch systems.

Volumetric gas phase chemisorption of H_2 and CO onto unsupported Ru catalyst gives 4.5 umol H_2/g Ru and 8.7 μmol CO/g Ru, respectively. These quantities are consistent with dissociative H_2 chemisorption (H:M = 1). Quantities of biorenewable substrates adsorbed on a "H_2-free" (evacuated) Ru surface from water under argon at 25 °C are ~0.6 μmol sorbitol/g Ru, ~0.8 μmol/g Ru for C3 alcohols

and polyols, and ~4.0 μmol/g Ru for C3 organic acids. Degradation products are seen during adsorption of polyols, especially sorbitol. When the metal surface is pre-saturated with H_2 and is under H_2, no significant adsorbtion of polyols is seen. In contrast, the adsorption of acids is unaffected by the presence of hydrogen. Sequential adsorption of glycerol (GO) followed by propylene glycol (PG) shows that GO inhibits the adsorption of PG, while reversing the order of adsorption shows no inhibition of GO adsorption by PG.

Single and multiple component physical adsorption on activated carbon catalyst supports was examined over a broad range of concentrations (0.005 M to 1.5 M) and temperature (298 – 433 K). To obtain adsorption data relevant to glycerol hydrogenolysis, adsorption of a combination of GO and PG (0.5 M total) was examined over the same temperature range. An extended Langmuir isotherm model, using single components' adsorption parameters, accurately predicted the two-component adsorption behavior.

Adsorption of combined lactic acid (LA) and propionic acid (PA) on activated carbon was not predictable with an extended Langmuir model. We therefore proposed a new model with two modes of adsorption: the filling of micro-pores, and adsorption on macro-pore surfaces. When this new model was expanded to multiple components, it accurately predicted the multicomponent LA + PA adsorption using single component adsorption parameters.

Adsorption of biorenewable substrates on catalyst metal and on the catalyst support has been characterized. Adsorption in both cases can significantly influence the rate of reaction of these biomass substrates to value-added products.

In memory of Ilse Morgan

ACKNOWLEDGMENT

I would like to thank Dr. Dennis Miller for his guidance and support as my research advisor through my Ph.D. studies (especially the editing). I also thank Dr. James E Jackson, Carl T. Lira, Lawrence T. Drzal, and Greg M Swain for serving on my graduate committee. Special thanks to Lisa Benton (my wife) for emotional and financial support. She put up with me for many years of graduate school.

TABLE OF CONTENTS

LIST OF FIGURES

LIST OF TABLES

1 INTRODUCTION

The Miller group at Michigan State University focuses on the evolving technology of renewable resource refining. We seek to produce commodity chemicals from readily available bio-based feedstocks. Recent group members studied itaconic acid production,[1] lactic acid hydrogenation to propylene glycol[2], stereoretentive amino alcohol synthesis[3], the processing of sugar alcohols to value-added polyols[4, 5], and the hydrogenation of glycerol to propylene glycol.[6]

Our current focus is to understand the mechanism of aqueous hydrogenolysis/hydrogenation of bio-based intermediates (polyols, organic acids, amino acids, alkyl amines, amides, ...) over noble metals. For example, in glycerol hydrogenolysis the first step in the proposed mechanism (**Scheme 1-1**) is the dehydrogenation and adsorption of the substrate as an aldehyde-like intermediate. Although the exact mechanism of adsorption is not known, we seek to probe interactions between substrate molecules and the metal catalyst surface to better understand binding energy, adsorbed structure, and competition for surface sites.

Scheme 1-1: Proposed sequence of steps for GO hydrogenolysis to EG, PG and LA

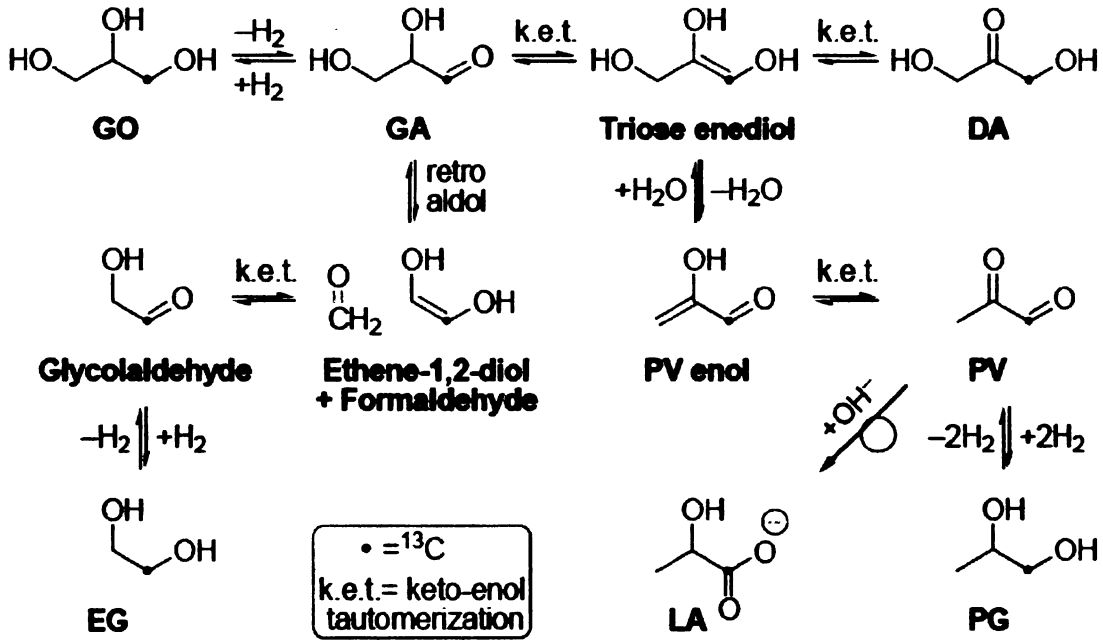

1.1 Significance

Global energy demands keep increasing, fueling development of alternative renewable energy supplies and bio-based chemical intermediates. Aqueous phase processing and/or conversion of these bio-based materials is becoming important because of low environmental impact. Unfortunately, little is known about aqueous phase processing/conversion of bio-based materials like glycerol. Many of these processes use metal catalysts which follow the general mechanism in **Scheme 1-2**. The first step is adsorption of reactant (A) onto the catalyst metal site (M). Even if this is not the rate determining step it is still involved in the reaction kinetics. Understanding the mechanism of this adsorption

in aqueous media is important. The other steps are conversion of reactant to product (B) on the metal and then product desorption from metal

Scheme 1-2

$$A + M \longrightarrow A^{*}\text{-}M \ (+C) \longrightarrow B^{*}\text{-}M \longrightarrow B + M$$

For example, the side product of biodiesel formation is glycerol, which has low fuel value and limited industrial uses. On the other hand, the conversion of glycerol to propylene glycol is a good value adding process because propylene glycol has much greater industrial potential as a solvent, heat-transfer fluid, and as a chemical feed stock. Optimizing the conversion of glycerol to propylene glycol is thus an important goal, one which would greatly benefit from a detailed understanding of the reaction mechanism.

1.2 Objectives

Understanding the adsorptive properties on active metals and supports of glycerol, glycols, organic acids, and related substrates derivable from renewable resources will give insight into the reactivities of our catalysts. To develop such an understanding, the following objectives need to be accomplished.

1. Develop a system to measure the adsorption of bio-based substrates on metal surfaces under elevated pressures and temperatures.
2. Study the adsorption of glycerol, propylene glycol, ethylene glycol and others individually and in mixtures on ruthenium sponge metal.
3. Study the adsorption of these same species on the carbon support and develop a model for this adsorption.

4. Compare the reactivity and selectivity between supported and unsupported ruthenium catalysts for conversion of selected biorenewable feed stock species, with emphasis on correlating reactivity with the adsorption results.

2 LITERATURE REVIEW

2.1 Hydrogenolysis of glycerol

The hydrogenolysis and degradation of polyols has been studied extensively. The dissertation of Mike Shafer from our group has a large collection of references and patents.[5] Selected patents dealing with hydrogenolysis of glycerol include Crabtree's 2005 patent[7] that mainly focuses on hydrogenolysis of sugar alcohols, but also includes glycerol. Their system uses an organic phosphine and ruthenium or osmium. The use of organic phosphine alone makes this impractical. Suppes' 2005 patent[8] has a more practical approach and will be discussed below.

Glycerol hydrogenolysis over ruthenium on carbon (Ru/C) has been studied by several groups. Kovacs et al. in our group did detailed qualitative mechanistic studies using deuterium labeling.[6] Lahr and Shanks focused on kinetics under neutral to basic conditions[9, 10] while Tomishige et al. looked at addition of Amberlyst 15, a strong cationic resin.[11] Suppes et al.[12] and Rosier et al.[13] looked at a range of metal catalysts while Perosa and Tundo used Raney nickel.[14]

2.1.1 Kovacs's et al.

Kovacs et al.[6] propose a mechanistic pathway for catalytic hydrogenolysis of glycerol to propylene glycol, ethylene glycol, and lactic acid over ruthenium on carbon (**Scheme 1-1**). The first step is dehydrogenation of glycerol to a

glyceraldehyde analog, followed by one of two paths: (1) cleavage to the enediol of hydroxyacetaldehyde, which, with or without tautomerization, is reduced to ethylene glycol, or (2) keto-enol tautomerization to the enediol, which then dehydrates and tautomerizes to pyruvaldehyde. Subsequent hydrogenation or water addition and rearrangement leads to propylene glycol or lactic acid, respectively. The presence of base promotes enolization and dehydration of the glyceraldehyde, favoring propylene glycol and lactate formation. Kovacs et al. substantiated this reaction mechanism by conversion, isotopic labeling, reaction of proposed intermediates, and computational molecular modeling studies.

2.1.2 Lahr and Shanks

Lahr and Shanks studied the hydrogenolysis of glycerol (GO) over 5% ruthenium on carbon with emphasis on understanding the reaction mechanism. As a control, they looked at the degradation of propylene glycol (PG) and ethylene glycol (EG).[10] The degradation of both EG and PG were independent of solution concentration (i.e. zero order), while initial rate data for GO conversion gave a reaction order of 0.45 to 1. They also reported that the presence of EG inhibited the conversion of GO, while PG had no effect. Studies of mixtures of EG and PG suggested that EG forms a stronger bond than PG with the Ru surface, thus explaining why EG inhibits GO conversion. Based on these results, they developed a reaction model based on Langmuir-Hinshelwood kinetics where the polyol adsorbs on Ru, undergoes dehydrogenation to form an aldehyde intermediate, desorbs into the solution, and then undergoes degradation with the

base. They proposed that the rate limiting step is the dehydrogenation of the adsorbed polyol.

In 2005, Lahr and Shanks expanded on this system by studying the effects of sulfur and temperature.[9] The degradation rates of PG and EG are similar when they are reacted individually. The apparent activation energy and the relative reaction rates were unaffected by the addition of sulfur. The degradation rate becomes immeasurable at S/Ru ratios >0.5. The addition of sulfur only seems to block the active sites and does not alter the degradation chemistry. The relative degradation rate of EG:PG was 4:1 in an equimolar mixture and was unaffected by temperature. This indicates strong competition between EG and PG on the metal surface.

For the reaction of glycerol over Ru exposed to sulfur, the apparent activation energy increased while the absolute rate decreased greatly. The selectivity to PG increased with increase in sulfur concentration on the catalyst. This effect was also reported by Montassier et. al[15]. Shanks proposes that there are two different pathway to PG; the surface dehydration of glyceraldehyde becomes more favored than the solution phase dehydration reaction upon addition of sulfur.

2.1.3 Tomishige et al.

In 2005, Tomishige and coworkers[11] tested the hydrogenolysis of GO over Ru, Pt, Pd, and Rh on carbon without any acid or base at 180 °C and 80 bar for 10 hours. Under these conditions, the Ru/C gave 6.3% conversion with 18%

selectivity to PG while the other metals gave conversions of 1% or less but with higher selectivity.

They studied Ru/C with a range of solid acids of which Amberlyst 15 gave the best conversion, 40% at 140 °C and 80 bar H_2. Selectivity to PG was low at 43%. Decreasing the temperature to 120 °C did improve the selectivity to PG (60%) but conversion was only 33% after 40 hours. Curiously, the use of sulfuric acid resulted in only 3.2% conversion under the conditions that gave 43% with Amberlyst 15. They suggest that H_2SO_4 interacts with Ru surface sites, perhaps being reduced to sulfide that adsorbs and blocks GO access.

2.1.4 Suppes et al.

Suppes et al.[12] focused on the use of copper-chromite as a hydrogenolysis catalyst because their reactions with Ru, Pd, Pt, Ni, and Cu catalysts showed that copper-chromite gave 55% conversion and 85% selectivity after 24 hours at the following conditions: 80% GO in solution; 5% bulk copper-chromite; 200 °C, and 200 psi H_2. They propose a two step mechanism where glycerol is dehydrated to acetol, and acetol is reduced to PG. They filed a patent[8] on a two step process where glycerol is dehydrated under reduced pressure to form acetol. This acetol is then hydrogenated to PG at the same temperatures with the addition of H_2 (200psi). No mechanistic details were suggested for the dehydration.

All experiments were done in a batch reactor and only conversion of GO and selectivity to PG after 24 hours was reported. Solution pH and the possible presence of lactic, acetic, formic, and other acids was not mentioned. This is

somewhat troubling, because they also report that the catalyst loses activity before the reaction goes to completion. They performed a parametric study to understand the effects of catalyst reduction temperature, catalyst loading, reaction temperature, hydrogen pressure, and initial water content. A reduction temperature of 300 °C gave the best conversion and selectivity. Conversion increased with catalyst loading, but selectivity had a maximum of 85% at 5% loading. They speculate that higher loadings result in increases in the decomposition of the product. The effects of temperature follow the same trend as the catalyst loading with a maximum at 200 °C. For these cases, it would be beneficial to have the selectivity and conversion at different times in the reaction. Increasing hydrogen pressure from 50 to 300 psi resulted in a steady increase in the conversion and selectivity. Conversion was 65% with a selectivity of 90% at 300 psi, the maximum value they examined. Decreasing the initial water content increased the conversion but the selectivity went through a maximum of 85% at 20% water. In all cases, they reported that, except for an H_2 pressure of 300 psi, the selectivity decreased when the conversion was >55%. This might be a clear indication that PG degradation is important, as reported by Shanks et al.[10]

2.1.5 Rosier et al.

Rosier et al.[13] looked at hydrogenolysis of ~20 wt% GO in water over CuO/ZnO, Pd/C, Rh/C catalysts at 180 °C and 80 bar H_2. Their conversions were generally <30% after 168 hours and PG selectivities <70%. Rh/C with H_2WO_4 gave best selectivity to PG. In switching from water to sulfolane as solvent, the 1,3-propanediol (1,3 PDO) was favored over PG by 2:1, but the 1,3-PDO

selectivity was only 12%. The observed rate and selectivity changed if the stainless steel autoclave was lined with Teflon. The lined reactor showed conversions ~twice that of the unlined reactor, and the 1,3-PDO/PG ratio increased from 0.1 to 0.5. Metal leaching was confirmed by testing the reaction mixtures. The addition of iron salts decreased the conversion and increased the 1,3-PDO/PG ratio. The addition of copper salts drastically reduced the conversion while still increasing the 1,3-PDO/PG ratio. They proposed a reaction scheme that includes several different pathways to PG and 1,3-PDO. The complexation of the 1,2- or the 1,3-OH groups to the metal and subsequent hydrogenolysis of the "free" hydroxide is proposed.

2.1.6 Perosa and Tundo

Perosa and Tundo[14] used wet Raney Ni as catalyst and neat glycerol at high loading (2g Ni to 8g GO) at 190 °C and 10 atm H_2, and obtained 63% GO conversion and selectivity to PG of 77%. The only byproducts that they reported are CO_2 and ethanol, identified by GC-MS and NMR respectively. CO_2 was identified by GC-MS, but quantities were based on mass loss. Addition of 2 g tetrabutylphosphonium bromide or $(C_6H_{13})_3C_{14}H_{29}PCl$ decreased the conversion and selectivity. It should be noted that these ionic liquids created a two-phase system at reaction conditions. The lack of 1,3-propanediol was used as evidence that it was not formed in the reaction scheme, but the absence of 1,3-PDO could also result from its rapid degradation as shown by Tomishige[11].

2.2 Aqueous phase adsorption on activated carbon

The literature is filled with adsorption studies, but very few deal with aqueous phase adsorption of small molecules on solid adsorbents. Most deal with adsorption of large bio molecules which are relatively easy to detect and will not be discussed in this paper. An extremely useful source is http://adsorption.org/awm/ by Adam W. Marczewski, Ph.D. This site has a great general overview of adsorption and detailed model descriptions and references. Several good reviews exist[16-18] that cover general solution phase adsorption.

For modeling single species adsorption, several common isotherm models are used including Langmuir, Freundlich, and Sips (Generalized Freundlich). Equations for these isotherms are defined by Marczewski and are shown in Equations 2-1, 2-2, and 2-3.

Langmuir $$q = \frac{q_m k C}{1 + kC} \quad (2\text{-}1)$$

Fruendlich $$q = k_F C^{1/n} \quad (2\text{-}2)$$

Sips $$q = \frac{q_m k C^{1/n}}{1 + kC^{1/n}} \quad (2\text{-}3)$$

The Langmuir isotherm is based on monolayer coverage of surface sites that are energetically identical. The Fruendlich isotherm assumes that adsorption energy increases as the quantity adsorbed increases, but there is no maximum coverage. The SIPS model combines both Langmuir and Fruendlich isotherms to

allow the system to have a maximum coverage and a variable energy of adsorption.

Several recent studies have examined small molecule adsorption on activated carbon [19-31] and on polymer supports[24, 32-34]. Of particular interest is Moon's[28] work on adsorption of sugars on activated carbon. They found that the adsorption could be modeled using either Fruendlich or SIPS isotherms, including binary adsorption using single component parameters. The adsorption of disaccharides was greater than any monosaccharide, with maltose adsorbing to the largest extent.

2.3 Species adsorbed on metal surfaces from liquid phase

The literature is filled with studies of gas adsorption onto metal surfaces, but these are not generally relevant to our work. Several spectroscopic methods exist for the study of adsorption from the liquid phase to active metal surfaces. The most promising is attenuated total internal reflection (ATR-IR), which has been used in our labs but not in this work. A general overview of ATR-IR methods and references applicable to the overall thrust of research on hydrogenolysis is provided but will not be discussed.[35-42] Surface-enhanced Raman scattering (SERS) is also used to examine metal adsorbate interactions. Several good reviews exist but are again outside of the scope of this work.[43-47]

X-ray photoelectron spectroscopy (XPS) is extensively used to study surface composition and has been applied to catalysis but is not as applicable for

in situ measurements, particularly liquids, because it is a high vacuum technique. Several reviews on this method are available.[48-56]

Single crystal surfaces are extensively used in gas phase studies and have also been applied in liquid phase environments. One particularly interesting *in-situ* study stands out.[57] Wang et al. used cyclic voltammetry to oxidize and reduce Ru (001) surface while simultaneously measuring x-ray reflectance. They propose that water is chemisorbed on the metal, possibly as a hydroxide.

2.4 Indirect differential detection

Indirectly detecting quantities adsorbed on solid materials by measuring differences in liquid-phase concentrations under controlled conditions is one of the oldest and simplest methods. Batch reactors are widely used, either with *in situ* monitoring or periodic sampling. Shallow bed adsorption is practical when quantities adsorbed are significant.[16] No literature has been found covering the adsorption of small organic molecules on bulk sponge metals. Only problems with adsorption on exposed metal in HPLC system are mentioned, and these do not look at quantifying the actual species adsorption.

3 NOVEL FLOW MICROREACTOR FOR SPECIES ADSORPTION ON METAL CATALYSTS

3.1 Design strategy

One challenge with measuring species adsorbed on the supported metal catalyst is that the ratio of support area to metal surface area is large. In the case of 5% Ru/C, this ratio is >400:1. This large ratio makes it impossible to distinguish adsorption on the metal from that on the support; for that reason we have to look at adsorption on pure metals only. Reactivity, particle size, and surface area are some of the criteria used in selecting the metal to use. In the case of ruthenium, three forms are commercially available, solid (ingot, bar, foil), sponge metal, and powder (Ru black). Ru black has the largest surface area (~10-15 m^2/g), unfortunately the particle size is too small to be handled easily and would result in metal loss or plugged filters if used in a flow system. This leaves ruthenium sponge metal which has a low surface area (~0.2 m^2/g Ru). This low surface area means that the quantity of substrate adsorbed is extremely small (<1mg/g Ru). Maximizing the metal to solution volume ratio is therefore critical; this and the high cost of Ru metal has led us to develop a reactor system that meets the following design parameters:

1. Low total volume <15 ml
2. Metal capacity up to 20 g
3. Reactor operating temperature range 20 - 200 °C
4. Solid liquid mixing and gas liquid mixing

5. Addition of two different gases at pressures up to 400 psi

6. Online sampling without disturbing the system

7. Option to flush system with different liquids

The reactor system shown in **Figure 3-1** meets these criteria. The system consists of an HPLC pump, tubular reactor, inline sampling system, a "tank" (gas liquid inter-phase), and valving to isolate the reactor.

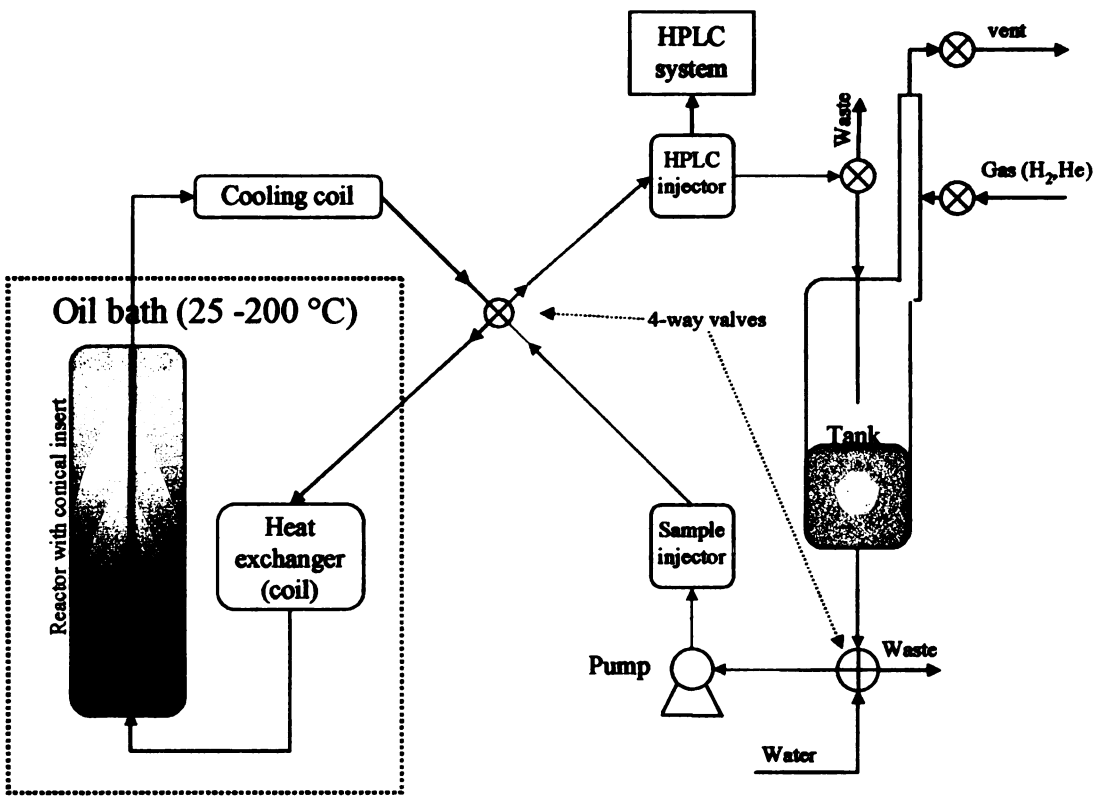

Figure 3-1: Recirculating reactor system

A fluidized bed reactor was chosen to allow large solid to liquid ratio with good mixing. Initially, a simple 10 mm ID column was used. Unfortunately, in this reactor configuration little axial mixing was observed at 3-6 ml/min. The relatively large particles and high density of ruthenium sponge metal prevented fluidization. Calculations showed that at 25 °C the bed should be fluidized at ~2 ml/min while

at 100 °C more than 6 ml/min was needed. The general solution to this problem is a tapered reactor that allows a velocity gradient. Internally tapering a small 316 stainless steel reactor or insert proved to be a technical barrier. Machining a conical insert, on the other hand, was relatively simple, and thus this route was taken to produce the reactor.

3.2 System description

The circulation pump is a Bio-Rad 1350 HPLC pump with the intake modified with a simple t-fitting to decrease the volume and allow operation under pressure. The output from the pump goes through a home-made pressure damper consisting of a coil of flattened 1/16 SS tubing. The pressure damper is needed to prevent excess pressure buildup during valve switching.

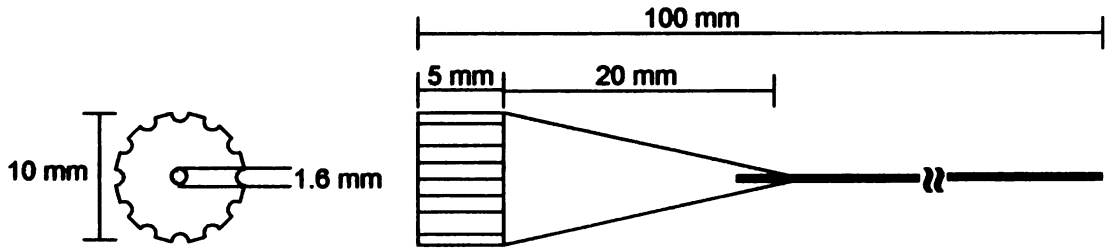

Figure 3-2: Dimensions of 316 stainless steel reactor insert.

The reactor consists of a 10 mm x 100 mm SS HPLC column with 2.0 µm frits at the ends. The machined conical insert (**Figure 3-2**) is placed in the column to create a semi-fluidized bed in the reactor. This was needed for mixing purposes. A coil of SS tubing was placed before the reactor to act as a heat exchanger to preheat the liquid entering the reactor. A water cooled heat exchanger is placed after the reactor to protect the pump and other systems.

The "tank" (where the reactor gas-liquid interface is located) is made from 12mm thick-walled Pyrex. It facilitates dissolution of gases into solution, and acts as a sight glass, allowing the fluid level in the system to be monitored. Valves and fittings are added to allow monitoring and manipulation of the head space gases. It was found that no additional mixing was needed in the tank. An additional HPLC "sample injector" (**Figure 3-1**) valve allows the introduction of substrates to the system.

The in-line sampling system consists of two Rheodyne 7010 HPLC valves configured as shown in **Figure 3-3** so as to allow the sampling loop to be flushed with water and the sample to be injected on a Bio-Rad HPX87-H column followed by two detectors; a Perkin-Elmer LC 90 UV detector (210 nm) and a Waters 410 RI detector. It should be noted that the HPLC system can detect dissolved gases and distinguish between He, H_2, and Ar, with the response being directly proportional to the headspace pressure. The ability to detect dissolved gas could be used to measure hydrogen consumption on a flow through system.

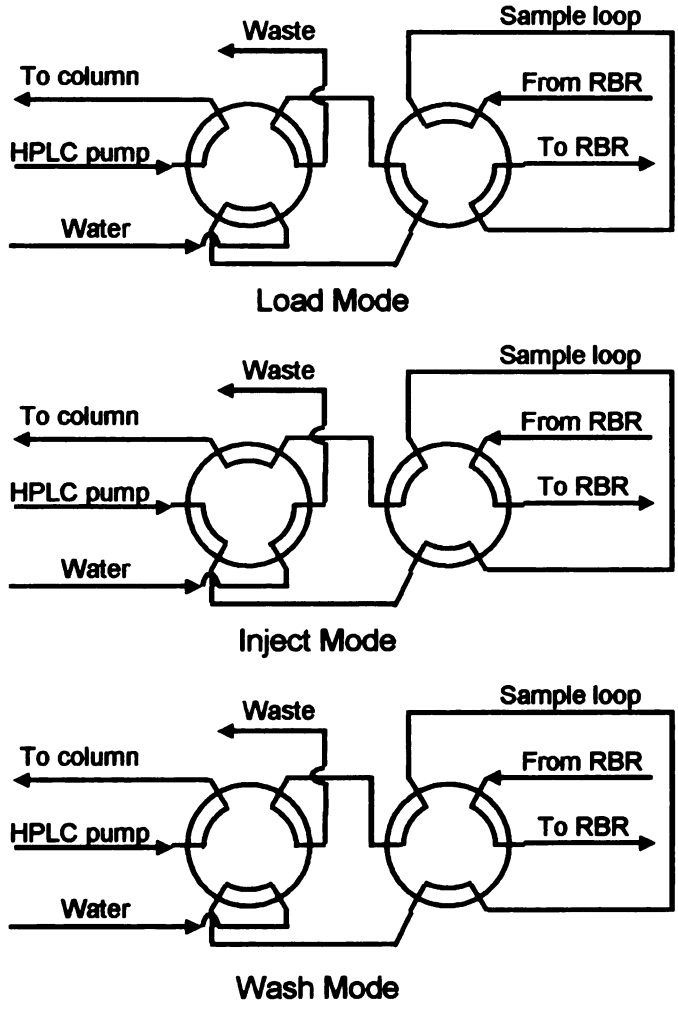

Figure 3-3: Configuration of in-line sampling system

3.3 System evaluation

3.3.1 System mixing

Pulse experiments to evaluate system mixing were performed using lactic acid with the UV detector placed in-line. A 100 µl pulse of 1.0 M lactic acid was

added to the recirculating fluid that was flowing at 6 ml/min. **Figure 3-4** shows that there is sufficient mixing in the system, provided the time scale of sampling once every 30 minutes. Even if the flow rate is set at 3 ml/min, there should be sufficient mixing for uniform sampling.

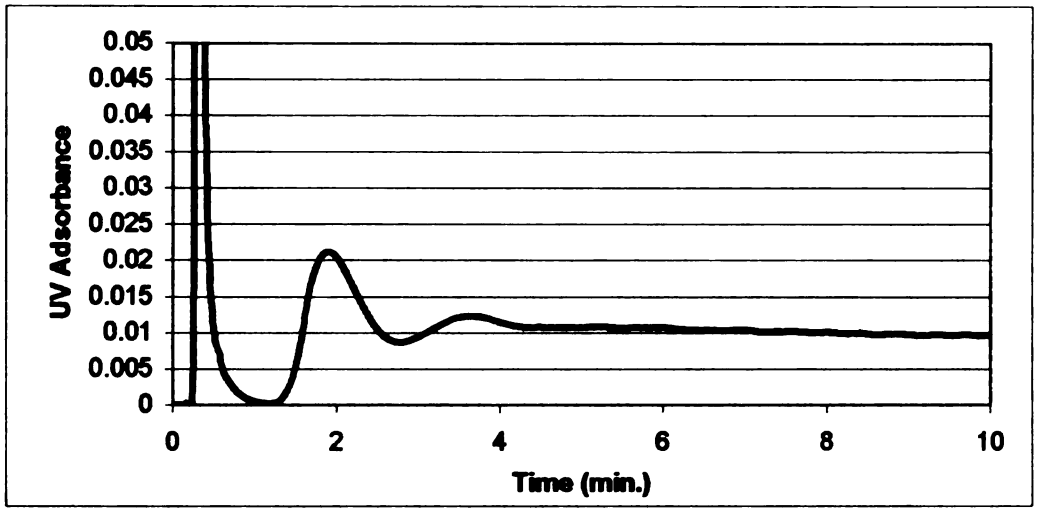

Figure 3-4: Pulse attenuation at 6ml/min for recirculating system.

3.3.2 Volume determination of reactor, tank, loop, and system

A 10 ml syringe was cut lengthwise and clipped around the tank (1/2" Pyrex tube) to help with reading the level in the tank. The reading on this cover was calibrated by adding fixed volumes of water using a 3 ml syringe and recording readings. It was found that a reading of 3 corresponded to 2 ml while a reading of 0 was equivalent to 1 ml in the tank.

The volume of the reactor and loop were determined by first adding 200 µmol GO to the entire system and letting this recirculate overnight to allow GO to saturate the catalyst surface. At this point the system was sampled. Then the recirculating pump was stopped and the tank drained and refilled with 4 ml of HPLC-grade water. The pump was turned on and recirculated for 2 hours while

samples were taken at 30 minute intervals. The reactor was placed out of line and the dilution process was repeated. The system volume was then calculated using $V=4ml\ \frac{C_2}{C_1 - C_2}$; this gave a loop volume of 3.82 ml and a reactor volume of 5.61 ml.

3.3.3 HPLC calibration

HPLC analysis was based on external calibration. Linear response from a Waters 410 differential Refractive Index (RI) detector was verified by running standard solutions containing either alcohols or organic acids at concentrations from 1 to 10 mg/ml. The standard solution of alcohols is referred to as HO-mix and contains: sorbitol (SO), glycerol (GO), ethylene glycol (EG), 1,3-propanediol (1,3-PG), methanol (MeOH), ethanol (EthOH), isopropanol (IPA), and n-propanol (n-prOH), while the standard acid solution referred to as acid-mix contains glycolic acid (GA), formic acid (FA), acetic acid (AA), and propanoic acid (PA). The RI detector response curves for each mixture are shown in **Figure 3-5**; this figure demonstrates the linear relationship between concentration and detector response. Because of this linearity, the response factor (RF) was calculated at each point for each compound. The RF had an uncertainty of ±2% and did not significantly change with time, but did show a dependence on fluctuations in flow rate. Both mixtures were injected using a Waters 717 Autoinjector (10 µl/sample) and also were injected through the reactor system injector to get the correlation between the two. **Figure 3-6** shows a chromatogram of HO-mix (1 mg/ml) run through both the reactor system injector and the 717 Autoinjector. The peak

response ratio between the injectors is 4.7 and was the same for all compounds. This is slightly higher than the expected ratio of 4.0, because the reactor system has a 40 µl loop vs. 10 µl injections from the 717 Autoinjector. Examining the dilution due to sampling of a standard solution in the recirculating reactor, it was found that the actual injection loop was 43 µl. Therefore the actual amount that the 717 Autoinjector injects is less than 10 µl.

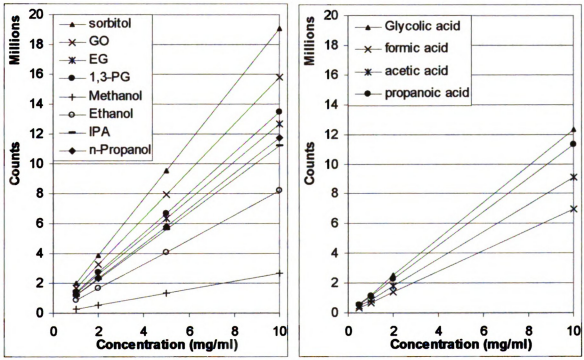

Figure 3-5: Refractive index detector linear response curves for 10 µl injection of HO-mix and acid-mix standard solutions.

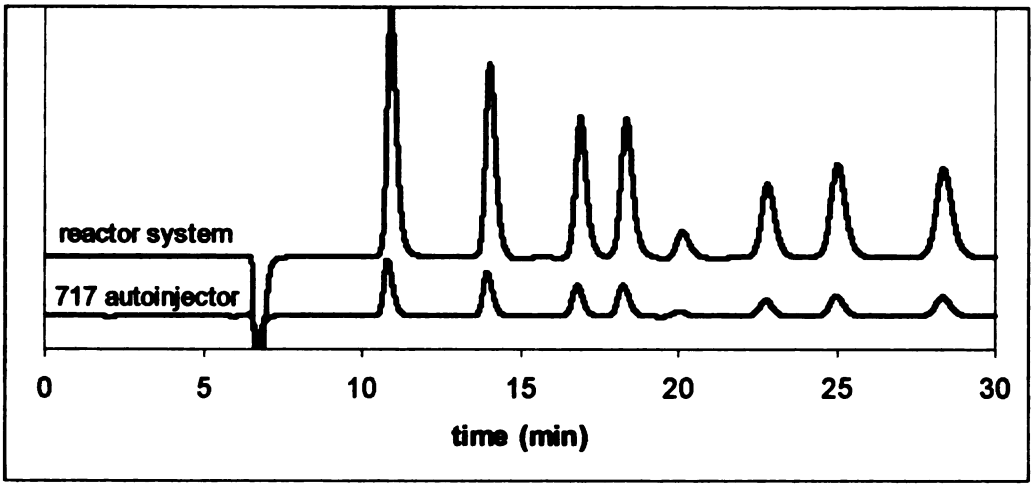

Figure 3-6: Comparison of auto injector vs. reactor system injector with HO-mix (Sorbitol, GO, EG, 1,3-PG, MeOH, EthOH, IPA, n-prOH)

Standards were made at 1% w/w in water and were run using the 717 Autoinjector (10 µl/injection). Relative response factors (RRF), which are constant over all conditions, were calculated and are reported relative to sorbitol on a weight basis (**Table** 3-1); the average organic RRF reported was applied to any unknown peaks. The RRF were used to calculate the RF for each species in the reactor system. With each adsorption reaction, the initial loop concentration of the adsorbing species was used to verify the RF for sorbitol by the RRF for that species.

Table 3-1: Retention times and relative response factors on a weight basis.

Compound	RT at 65 °C	RRF
Oxalic acid	6.55	0.58
Sodium silicate	8.90	0.14
Gluconic acid	9.10	0.92
Glucose	9.22	1.08
Sorbitol	10.43	1.00
Glyceric acid	11.02	0.71
Boric acid	11.39	2.12
Glyceraldehyde	11.55	0.78
Glycolic acid	12.42	0.64
Lactic acid	13.00	0.73
Glycerol	13.59	0.83
Formic acid	14.11	0.36
Acetic acid	15.41	0.46
Ethylene glycol	16.51	0.66
1,2-Propanediol	17.55	0.74
Propionic acid	17.94	0.58
1,3-Propanediol	18.07	0.71
Methanol	19.57	0.14
1,4-Butanediol	21.97	0.83
Acetone	22.00	0.49
Ethanol	22.62	0.43
Isopropanol	24.50	0.59
n-Propanol	28.30	0.61
1-Butanol	35.50	0.56
average organic peak		0.60

3.4 Methods of operation

3.4.1 General description of experiment

For most experiments, the reactor was charged with 10 g ruthenium sponge (-100 mesh, *Aldrich*); this Ru sponge was reused in most experiments. The system was flushed at 3 ml/min with argon purge and degassed HPLC-grade water for at least 10 minutes. This was followed by charging the system with ~12 ml of the same water. The system was set to recirculating mode and placed under 250 psi H_2 to clean and reduce the catalyst metal surface. The reactor was heated to 200 °C for 2-4 hours. During this time the headspace was

exchanged with fresh hydrogen at least three times to remove any methane that was formed during reduction. The reactor was then either cooled to 25 °C while recirculating with H_2 saturated water to generate the "H_2 saturated surface," or was flushed at 200 °C with the argon purge and degassed water for at least one hour, followed by cooling to 25 °C to generate the "H_2 free surface".

With the reactor out of line, the loop was charged with water to 6.1 ml (~1/3 up the sight glass tank). At this point a sample was taken, followed by the introduction of the substrate of interest. After 30 min, the loop was sampled and the reactor placed in-line, followed by automated sampling every 30 min until the experiment was done. UV and RI detector data were collected for 30 minutes and stored for analysis. The level in the sight glass and the headspace pressure was recorded at several times during the experiment.

3.4.2 Data processing

The following variables are using in data processing:

C_n	Concentration of solute in solution at sample n (µmol/ml)
V_{total}	Total system liquid volume (ml)
V_{react}	Volume of reactor and heat exchangers (ml)
V_{loop}	Volume of loop part of reactor system (ml)
V_{tank}	Volume of liquid in tank (ml)
N_0	Moles added to system (µmol)
N_{sol}	Moles in solution (µmol)
$N_{leak\ lost}$	Total moles lost due to leaks (µmol)
$N_{inj\ lost}$	Total moles lost due to injections (µmol)
$N_{ads.}$	Total moles adsorbed (µmol)
Pcount	Corrected peak area counts
$Pcount_{raw}$	Uncorrected peak area counts

RT	Retention time (min)
RT_{avg}	Average retention time (min)
RF	Response factor (counts/(mg/ml))
RRF	Relative response factor

A standard Excel workbook was created and several Visual Basic macros were written to automate the repetitive tasks involved in processing the large amount of data generated with each experiment. The amount adsorbed for a given substrate was calculated using Equation 3-1 and involves the conversion of raw UV and RI detector data into concentration data, finding the system volume, and keeping track of cumulative sampling and leak losses.

Moles of substrate adsorbed	=	Initial moles loaded into the system	-	Moles still in solution	-	Moles lost due to sampling and leaks	(3-1)

Raw UV and RI detector data from chromatograms of each sample were integrated using the Interactive Graphics part of *Varian Star Workstation v6.0 Software.* For each sample, the retention time and area for each identified peak was transferred to a Microsoft Excel worksheet and the areas were corrected for fluctuations in retention times using Equation 3-2.

$$A_{corr} = A\left(1 + \frac{RT_{avg} - RT}{RT_{avg}}\right) \qquad (3\text{-}2)$$

This RT dependent correction of the area was found empirically and is valid for at least 20% deviations in RT. This corrected area was used to calculate solution concentrations using the response factors given in Section 3.3.3. If the measured

concentration deviated by more than 5% from the predicted value in the initial sample with the reactor in loop mode, the RF values were scaled for that experiment to match the measured to the predicted concentration based on the actual amount of species introduced.

For every identified compound in each sample, the number of moles in solution was given by $C_n V_{total}$, where $V_{total} = V_{loop} + V_{react} + V_{tank.}$ and C_n = (HPLC counts) RF_n. In loop mode, V_{react} was omitted. Only a limited number of tank volume data points were recorded for each experiment; linear interpolation was used to find V_{tank} for each sample.

For each sample, the number of moles lost due to sampling for each identified compound was determined as the solution concentration multiplied by the sample loop volume (43 µl). For leak losses, it was assumed that the concentration changed linearly between sampling times; therefore, the average concentration between the current and previous samples multiplied by the change in volume over this same interval gives the number of moles lost due to leakage. These two losses were summed and included in computing the substrate quantities adsorbed from the current sample.

Table 3-2: Calculated values for a hypothetical adsorption experiment on Ru sponge.

Time (h.)	V_{total} (ml)	C_n (mM)	N_{sol} (µmol)	$N_{inj\ lost}$ (µmol)	$N_{leak\ lost}$ (µmol)	N_{ads} (µmol)
0.37	11.26	3.404	38.32	0.15	0.00	7.64
0.88	11.24	3.203	35.99	0.28	0.06	9.77
1.39	11.22	3.128	35.09	0.42	0.12	10.47
1.90	11.20	3.049	34.14	0.55	0.18	11.22
2.40	11.18	2.899	32.41	0.67	0.24	12.78
2.91	11.16	2.852	31.83	0.80	0.30	13.18
3.42	11.14	2.771	30.87	0.92	0.35	13.97
3.93	11.12	2.750	30.59	1.03	0.40	14.08
4.43	11.10	2.742	30.44	1.15	0.45	14.05
4.94	11.08	2.715	30.09	1.27	0.51	14.24
5.45	11.06	2.674	29.58	1.38	0.56	14.58
5.45	11.06	2.674	29.58	1.50	0.56	14.46

$N_{sol}(i) = V_{total}(i)*C_n(i)$; $N_{inj\ lost}(i) = N_{inj\ lost}(i-1) + .043*C_n(i)$;

$N_{leak\ lost}(i) = N_{leak\ lost}(i) + (V_{total}(i-1) - V_{total}(i))*(C_n(i-1) + C_n(i))/2$;

$N_{ads}(i) = N_0 - N_{sol}(i) - N_{inj\ lost}(i) - N_{leak\ lost}(i)$

The total amount adsorbed was based on the number of moles of carbon in each identified compound and reported as equivalent number of moles of the substrate of interest. **Table 3-2** shows calculated values for the adsorption of one

component on Ru sponge to illustrate the calculations described above. It should be noted that for cases where products were formed, a negative adsorption value is reported. This is of course a physical impossibility, but expressing it in this manner simplifies the calculations.

4 CATALYST CHARACTERIZATION

4.1 Methods

For this work, Ru sponge metal (product #267406, Lot# 14021EB) from Sigma-Aldrich was used. Catalysts were characterized on a Micromeritics ASAP 2010 adsorption instrument, either in a standard analysis cell or by attaching the reactor vessel used in the recirculating batch reactor to the ASAP instrument. Experimental details for nitrogen BET surface area measurements of activated carbon are described in Section 7.1.1; the same procedure was used for Ru sponge metal. Attempted N_2 BET measurements of catalyst in the reactor failed, most likely because of flow restrictions through the frit.

General procedures for chemical adsorption experiments consist of pretreatment, initial adsorption analysis, evacuation, and repeat analysis. Pretreatment consisted of reducing the sample at 350 °C under a flow of H_2 for 2 hours, evacuation for 1.5 hours at 360 °C, cooling to 35 °C under vacuum, and evacuation at 35 °C for 10 minutes followed by leak testing. All analyses were run at 35 °C and consisted of dosing known volumes of analysis gas to the sample chamber and recording the volume added vs. pressure. Following this initial adsorption, the sample chamber was evacuated at 35 °C for 60 minutes to remove physically adsorbed analysis gas, and then dosing was repeated as before. The volume vs. pressure data for each dosing was then plotted and the linear region (usually P>100 Torr) was extrapolated to P=0 to give the quantity of

gas adsorbed. The chemically adsorbed quantity of gas is the difference of volume adsorbed in the initial and repeat analysis. The surface area is calculated using the stoichiometry factor (2 for H_2, 1 for CO) and the atomic cross-sectional area of Ru (0.0613 nm^2).

4.2 Results

Surface areas for both physical and chemical adsorption are listed in Table **4-1**. In the table, "fresh" Ru sponge was taken directly from bottle and "used" Ru sponge is a collection of recovered catalyst used in a range of hydrogenolysis experiments with different substrates. Both fresh and used sponges were from the same lot number. Reactors 1 and 2 are mechanically equivalent duplicates used in these studies. Results show a BET surface area (~0.5 m^2/g) that does not change upon using the Ru sponge, this area is consistent with results of prior work by Zhang et al.[2]

Table 4-1: Physical characterization of Ru sponge.

	Fresh Ru	Used Ru	Fresh Ru Reactor 2	Used Ru Reactor 1[(a)]
Total (N_2 BET) surface area (m^2/g)	0.56±0.006	0.527±0.004		-
Metal (H_2) surface Area (m^2/g)	0.23	0.12	0.21	0.15(0.13)
Metal (CO) surface area: (m^2/g)	0.21			

[(a)] Reactor 1 was charged with 8g used and 2g new Ru sponge. Number in parentheses is the amount corrected (by weight fraction) using the new Ru values from Reactor 2.

Unlike the N_2 BET, the surface areas found by H_2 adsorption (0.23, 0.12 m^2/g) show a ~50% decline in the hydrogen active surface area after using the

Ru sponge for reaction. The H_2 area measured for new Ru sponge in Reactor 2 (0.21 m^2/g) is the same within experimental error to that found for new sponge using a standard analysis cell, confirming that using the reactor does not affect the H_2 adsorption measurements. Reactor 1 was charged with some (2 g) new and some (8 g) old Ru sponge; the resulting adsorption area of 0.15 m^2/g is expected based on the weight fractions for this sample. The adsorption of CO on new Ru sponge showed active Ru area of 0.21 m^2/g, the same as found for H_2. CO adsorption was not done on reactors for fear of poisoning the metal surface with CO.

A set of gas adsorption experiments were run with different gases to compare different molecular adsorption properties (**Table 4-2**). Interactions of CO and H_2 on Ru surfaces have been studied,[58-60] but our goal was to see if there might be two different sites, one for CO and one for H. If there are two independent sites, then there should be little dependence on the order of adsorption.

The presence of CO on the surface does not seem to block the adsorption of additional H_2 (Exp A6), while the presence of H_2 partially blocks the adsorption of CO (Exp A3). Blocking of the CO by hydrogen was reported by Peebles[60]. Subsequent addition of H_2 (Exp A4) showed no significant adsorption.

Table 4-2: Gas chemisorption on Ru sponge.

Exp#	Sample	reduction	Volume Adsorbed: (cm^3/g STP)	Surface area:(m^2/g)	umol/g
A1	N_2 BET	no	0.1146	0.4980	
A2	H_2 initial	yes	0.1020	0.3350	4.55
A3	CO after H_2	no	0.1100	0.1820	4.91
A4	H_2 after H_2 and CO	no	0.0190	0.0640	0.85
A5	CO with reduction	yes	0.1940	0.3200	8.66
A6	H_2 after CO	no	0.1040	0.3440	4.64
A7	N_2 with reduction	yes	0.0090	0.0149	0.40
A8	He with reduction	yes	0.0005	0.0008	0.02
A9	Methanol attempt	yes	(~0.05)	---	
A10	H_2 after methanol	no	0.0034	0.0112	0.15
A11	Methane	yes	0.0306	0.0504	1.36
A12	Methane after H_2	yes	0.0016	0.0026	0.07
A13	H_2 after Methane	yes	0.0450	0.1483	2.01

Methane (Exp A11) adsorbed in a smaller amount than H_2; this could be a result of the larger size of methane, or it could be that methane adsorbs with full dissociation. It should be noted that methane did not adsorb on an H_2 saturated surface (Exp A12). The adsorption of H_2 (2.0 μmol/g) after methane (Exp A13) show that there are still sites available. If methane adsorbed with full dissociation, little H_2 adsorption would be expected, while if it were adsorbed as a methyl radical ($H_3C\bullet$) or Methylene (H_2C:), then there should be sites for H_2.

To summarize the characterization of Ru sponge, fresh sponge has the same BET area as used Ru but the fresh sponge H_2 area is twice that of used

sponge. CO adsorption does not affect the adsorption of H_2, but H_2 does affect CO adsorption.

Several analyses were run to evaluate the possibility of measuring H_2 areas after aqueous phase reduction. It was found that a hydrogen-saturated surface flushed with He (to remove water) and then evacuated at 25 °C gave inconsistent results. The adsorbed hydrogen came off the surface during the He flush and evacuation. Measuring gas phase adsorption after liquid phase reduction is not possible.

5 H_2/D_2O EXCHANGE

It has been observed that when H_2 gas and liquid D_2O are placed in a reactor over ruthenium catalyst, D and H atoms are exchanged. This was a problem when we were trying to determine the pathways for aqueous hydrogenolysis of polyols using H-D exchange, as under normal experimental conditions (100-150 °C, 500-1500 psi) the H-D ratios equilibrated on a time scale faster (<30 min.) than our reactions, resulting in a statistical distribution based on the overall H-D pool. At 25 °C and 10-200 psi, this exchange happens over several hours. At this time scale, it is possible to perform experiments to elucidate kinetic parameters for this reaction.

5.1 Experimental

Two different sets of experiments were run. In the first set (Exp #43a-c), a 10 ml pressure vessel was charged with 2 ml of D_2O, 0.1 g dry weight of catalyst, and hydrogen gas (125 psi). The head space was continually sampled through a capillary tube (0.05 mm I.D. x 5 m) into a mass spectrometer. The second set of experiments consisted of H-D exchange using a 70 ml Parr reactor equipped with a magnetic stirring bar, gas connections, and sampling port. This reactor was charged with 10ml D_2O, 0.1 g dry catalyst or 1.0 g Ru sponge, H_2 (50 psi), and D_2 (50 psi). The head space was continually sampled through a capillary tube (0.05 mm I.D. x 5 m) into a mass spectrometer. A pressure drop of ~25 psi was observed during each experiment.

An Ametek Dycor M100M Quadrupole Mass Spectrometer was used for the analysis of the headspace. A HD gas mixture was made by charging a 40 ml pressure vessel with ~0.5 g 5 wt% Ru/C, H_2 (150psi), and D_2 (150psi). After equilibrating this mixture for several days, the H_2:HD:D_2 ratios were assumed to be 1:2:1. Instrument response was examined with H_2, D_2, HD, methane, and Ar. The response ratios were inconsistent and seemed to have some dependence on the degassing and tuning of the instrument.

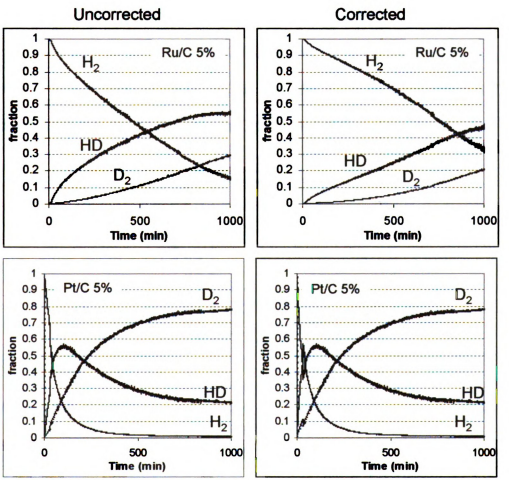

Figure 5-1: Corrected and uncorrected data for H_2 over D_2O with 0.1 g 5% Ru/C (Exp 43B), and H_2 over D_2O with 0.1 g 5% Pt/C (Exp 43C)

After consultation with a technical expert from the mass spectrometer manufacturer, It was concluded that this inconsistency is expected because this instrument is designed and optimized for gases other then hydrogen. Thus no further attempts were made to calibrate and optimize the system. The H-D test mixture was analyzed either before or after each experiment to obtain the relative response factors (RF). The assumption was made that the relative responses were constant with respect to pressure even with a 50 psi pressure drop. Therefore only the ratios of H_2, HD, and D_2 are plotted. Comparison of raw and corrected data for Experiments 43B and 43C are shown in **Figure 5-1**. It can be seen that applying the RF correction has little effect on Experiment 43C, while there were significant changes in Experiment 43B.

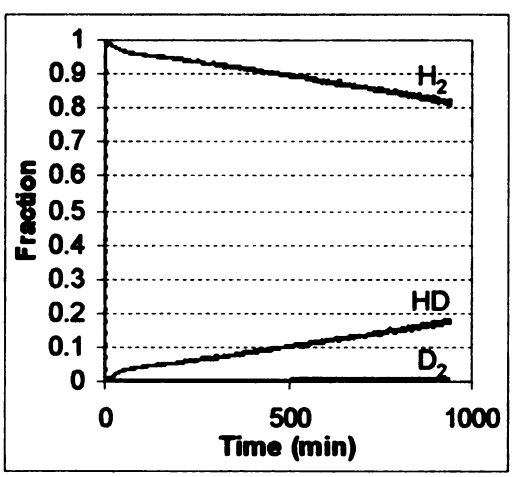

Figure 5-2: Incorporation of deuterium into the gas phase from (DO)ethanol over 0.1 g 5% Ru/C (10 ml reactor 100 psi H_2, Exp 47)

It can be seen in **Figure 5-1** that, over a Pt catalyst surface, deuterium is rapidly incorporated into the gas phase, while over a Ru surface the process is slower, consistent with water strongly dissociating on the Pt surface while little water dissociates on a Ru surface. Dissociation of a O-H bond in the liquid phase

is further confirmed by deuterium incorporation into the gas phase when (DO)ethanol is placed over 5% Ru/C under H_2 gas (Exp 47, **Figure 5-2**). This H-O dissociation is slow, while H_2 and D_2 adsorption\desorption is rapid as seen in Experiment 50 (**Figure 5-3**). Looking at the data in **Figure 5-3,** it appears that deuterium incorporation in the gas phase is a lot slower than seen in Exp 43B (**Figure 5-1**), but this is deceptive because the headspace volume differs by a factor ~10, while the catalyst loadings were the same. The absolute rates should be the same; therefore the apparent rate should be slower with a larger headspace.

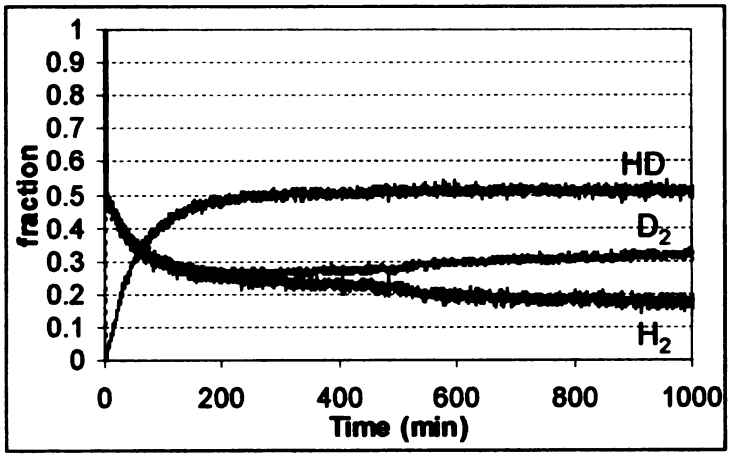

Figure 5-3: H_2 + D_2 over D_2O with 0.1 g 5% Ru/C (50 psi each in 70 ml reactor, Exp 50)

5.2 Modeling

The general approach to this system involved a Langmuir-type adsorption with a pseudo steady state approximation (PSSA). In general, the Langmuir

model looks at adsorption at equilibrium; we wanted to look at the kinetics of adsorption and desorption individually. The model equations are given as follows.

$$XY_{(aq)} + 2M_{(s)} \underset{k2}{\overset{k1}{\rightleftharpoons}} XM_{(s)} + YM_{(s)}$$

$$XYO_{(l)} + 2M_{(s)} \underset{k4}{\overset{k3}{\rightleftharpoons}} XM_{(s)} + YOM_{(s)}$$

$$H_2O_{(l)} + D_2O_{(l)} \underset{k5}{\overset{k5}{\rightleftharpoons}} HDO_{(l)} + DHO_{(l)}$$

combinations of X and Y

X=H	Y=H
X=H	Y=D
X=D	Y=H
X=D	Y=D

Figure 5-4: Proposed reaction model.

The kinetic model proposed is shown in **Figure 5-4.** Several simplifying assumptions were made and are listed in **Table 5-1**. Assumption #1 is somewhat unrealistic, because H or D is involved in all the reactions and it is generally accepted that isotopes should have some effect. Assumption #9 is also somewhat suspect. We have some evidence that there might be two different sites in aqueous phase reactions, one for hydrogen and one for oxygenated species such as water and organics. Some published calculations by Neurock[61] also suggest a two site model.

Table 5-1: Assumptions made for H_2-D_2O exchange model

1. There is no isotope effect.
2. Dissolved gas concentrations are in equilibrium with gas phase.
3. Only dissolved gases react.
4. There are no transport limitations.
5. Dissolved gases can only react with free sites.
6. Liquid species can react with free sites and with other liquid species.
7. Liquid species are in equilibrium with other liquid species.

8. Migration on the metal surface is not considered
9. There is only one type of site on the metal for H-, D-, and O-adsorption.

5.2.1 Approach to solutions

All species involved in this system are shown in **Table 5-2**. Note that HD, DH and HDO, DHO, which physically are identical pairs, are treated as separate species; this was done to not have to take into account the probability of H or a D reacting.

Table 5-2: Species included in H_2, D_2O exchange model

Dissolved Gases:	H_2	HD	D_2		
Species on Metal:	HM	DM	HOM	DOM	M (free sites)
Liquid species:	H_2O	HDO	DHO	D_2O	

To determine the minimum number of reversible independent reactions needed to describe the isotope exchange, a procedure described by J. M. Haile[62] was used. In Haile's method, the formula matrix is generated and the matrix rank is then determined. Then the number of independent reversible reactions needed (Rn) is the number of compounds minus the rank of the formula matrix. **Figure B-2** shows formula matrix and calculation to give Rn=9. The 9 reactions are shown in **Figure 5-5**.

$$H_{2(aq)} + 2M_{(s)} \underset{k2}{\overset{k1}{\rightleftharpoons}} 2HM_{(s)}$$

$$HD_{(aq)} + 2M_{(s)} \underset{k2}{\overset{k1}{\rightleftharpoons}} HM_{(s)} + DM_{(s)}$$

$$DH_{(aq)} + 2M_{(s)} \underset{k2}{\overset{k1}{\rightleftharpoons}} DM_{(s)} + HM_{(s)}$$

$$D_{2(aq)} + 2M_{(s)} \underset{k2}{\overset{k1}{\rightleftharpoons}} 2DM_{(s)}$$

$$H_2O_{(l)} + 2M_{(s)} \underset{k4}{\overset{k3}{\rightleftharpoons}} HM_{(s)} + HOM_{(s)}$$

$$HDO_{(l)} + 2M_{(s)} \underset{k4}{\overset{k3}{\rightleftharpoons}} HM_{(s)} + DOM_{(s)}$$

$$DHO_{(l)} + 2M_{(s)} \underset{k4}{\overset{k3}{\rightleftharpoons}} DM_{(s)} + HOM_{(s)}$$

$$D_2O_{(l)} + 2M_{(s)} \underset{k4}{\overset{k3}{\rightleftharpoons}} DM_{(s)} + DOM_{(s)}$$

$$H_2O_{(l)} + D_2O_{(l)} \underset{k5}{\overset{k5}{\rightleftharpoons}} HDO_{(l)} + DHO_{(l)}$$

Figure 5-5: Reversible reaction model

From these 9 reversible reactions, we get 18 elementary reactions, that are all either 2nd or 3rd order. These reactions will have a rate (velocity) term of the form $r=k[A][B]$ for 2nd order and $r=k[A][B]^2$ for 3rd order. It should be noted that only availability of free metal sites (M) and not their spatial orientation has been included in the model. Because of this, dissociative adsorptions are third order reactions. These terms, when calculated for all 18 reactions, result in 17 unique rate terms shown in **Table B-1** To get the corresponding 13 ODE's, one creates a matrix with the coexistence for each term as need to account for the species balance. This matrix is shown in **Figure B-3.** The vector of ODE's $\frac{d\underset{\sim}{y}}{dt} = \underline{\underline{A}} \bullet \underset{\sim}{r}$ can be used as a function block for matlab's ODE solver. The reason for using this matrix system is that the rate terms are calculated only once in the cycle. If the terms are added as terms in each individual ODE, they would be recalculated each time they are used. This method significantly speeds up the calculations.

The ODE solver used from MATLAB was ODE15S. Initially ODE45, a 4^{th} order Runge-Kutta method, was used, but this problem is too stiff for that solver and tended to diverge.

The initial conditions of the system were calculated from experimental data and were kept constant throughout this modeling exercise. All variables are listed at the top of the Matlab code. Parameters that were adjusted to observe the system behavior were: k1, Kr, Kg, Kl. The reference rate constant was k1, the forward rate of the "gas" side reactions. Kr is equal to k1/k3, the ratio between the "gas" side and "liquid "side forward reactions rates, while Kg = k1/k2 and Kl =k3/k4, the equilibrium constants for the "gas" and "liquid" side reactions, respectively. These values were adjusted to get the model response to be close to experimental. The k1 value of ~1000 ($L^2/mol^2/s$) is within a few orders of magnitude of expected reactions with a surface. Generally, adsorption and desorption reactions are rapid and are not the rate limiting steps in catalytic systems. The value of k5 was set at 1000 (L/mol/s); this was large enough that the proton exchange in the water was close to instantaneous. The value of k5 was varied by a factor of 100 in both directions with no noticeable effect on the model predictions.

5.2.2 Parameter optimization

For the experimental data, the raw data for Experiment 43b (5% Ru/C) and Exp 43c (5% Pt/C) were used. These data were not corrected for the differences in response factors. The only measurable quantities were the compositions in the gas phase. Dissolved gasses are assumed to be in

equilibrium with the head space gas and related by Henry's law. For simplicity, gas phase concentrations were assumed to be the same as dissolved gas concentrations. The actual dissolved gas concentrations in the liquid are lower by a factor ~1000, which if used would raise the corresponding k values.

Initial fitting was done by manually changing *k1, Kr, Kg, and Kl* to approximate the results shown experimentally. The final optimization was done using a random walk approach. For each cycle, one parameter was chose at random and increased or decreased by a random percentage, limited such that no change was greater than 10%. The ODE's were then integrated over the same total time as the experiment, followed by calculation of the overall error using Equation 5-1.

$$\text{Error} = \sum_{0}^{n}((C_{H2}^{exp} - C_{H2}^{cal})^2 + (C_{HD}^{exp} - C_{HD}^{cal})^2 + (C_{DH}^{exp} - C_{DH}^{cal})^2 + (C_{D2}^{exp} - C_{D2}^{cal})^2 \qquad (5\text{-}1)$$

If this error was lower than the previous cycle, the change was kept; if not, the old values were kept and the cycle was repeated. This is a "brute force" method but it is much simpler to implement than some of the gradient methods, and also it tends to avoid local minima if the changes are large. The possibility of an evolutionary model, in which all parameters are changed at once followed by some selection rules as to the direction of the next change, was also examined. This method sounds like it might be a better way of doing the optimization if there are a lot of variables.

The error calculation is simply the summing of all the squares of the individual errors. The one challenge is that ODE15S uses variable time steps so it is necessary to either interpolate the model point to match the experimental

time or the reverse. It was easier to interpolate the experimental data than the model. The experimental data has >5000 points, while the model generally generates 100-200 points depending on the steepness of the curves.

5.2.3 Results and conclusions

Figures 5-7 and **5-8** show the experimental results and the calculated results. The model predicts the shape of the curves nicely. The optimized parameters are shown in Table 5-3. With ruthenium, the gas side reactions are much faster than liquid side, as evident by the large value of Kr. When a molecule of deuterium (D_2) makes it to the surface, is rapidly scrambled with the gas phase. In the case of platinum, the liquid and gas exchange rates are almost the same but the liquid side equilibrium lies a lot more towards the surface bound side. This is consistent with water readily dissociating upon adsorbing on Pt as described in the literature[63-65]

Table 5-3: Optimized parameters for experiment 43B and 43C

Exp 43B k1=50586; Kr=129.54; Kg=6.9848; Kl=8.6846; k5=10000;
Exp 43C k1=31093; Kr=2.0048; Kg=5.3232; Kl=94.379; k5=10000

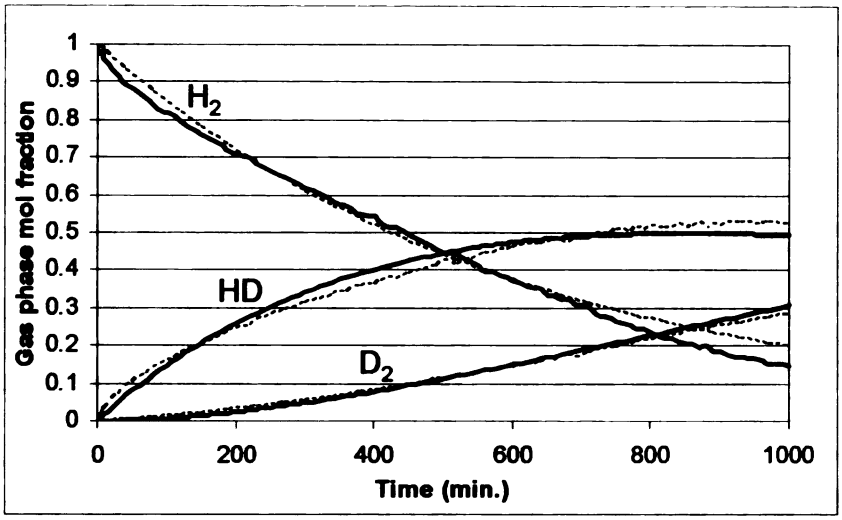

Figure 5-6: Model fit to experimental data for 5% Ru/C (Exp 43B). Dotted lines are predicted values.

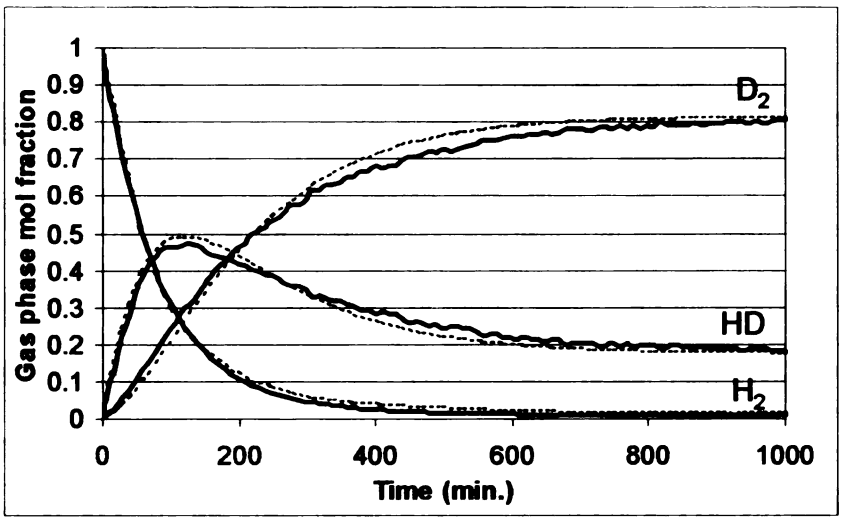

Figure 5-7: Model fit to experimental data for 5% Pt/C (Exp 43C). Dotted lines are predicted values.

6 AQUEOUS PHASE ADSORPTION ON RUTHENIUM SPONGE

All experiments were performed in the recirculating batch reactor (RBR) using previously described experimental procedures (Section 3.4.1). A summary of all experimental conditions can be found in the master experiment list (Appendix A). Data processing and calculations are explained in Section 3.4.2. Unless noted differently, in the figures used to display data generated with the RBR, the left graph displays solution concentration while the right displays quantity adsorbed.

6.1 Sorbitol, glucose and gluconic acid adsorption

Previous work in our lab has looked at transformations of sorbitol (SO) to either propylene glycol (PG)[5] or isosorbide[66]. It has been proposed that the first step in conversion of SO to PG involves the dehydrogenation of SO at the C1 position to form an "aldehyde" intermediate. To get some mechanistic insight into this first step, information on the adsorption of SO on Ru metal would be helpful. Initial adsorption work on ruthenium sponge was done by Schafer. He looked at SO adsorption on hydrogen-saturated metal in a 300 ml Parr reactor with 20 g Ru sponge. No significant adsorption was seen until the temperature was raised above 80 °C. Above 100 °C, ~5-10 mg SO/g Ru was unaccounted for and was assumed to be adsorbed. This is significantly higher than the 0.2-0.5 mg SO/g Ru predicted for the measured metal surface area of ~0.2 m^2/g-sponge and an area of ~30 $Å^2$ per sorbitol molecule. The appearance of activation with

temperature is possibly due to the desorption of hydrogen from the metal surface at ~80 °C, as mentioned in the characterization of the catalyst. The apparent over-adsorption of SO is probably due to the degradation of sorbitol into a large range of products that were not analyzable by HPLC or were below the detection limits in Shafer's system.

The RBR was used to look at sorbitol, glucose, and gluconic acid adsorption at 25 °C on Ru sponge metal. Preliminary experiments with sorbitol (SO) showed that on a hydrogen-saturated Ru surface there was no significant adsorption, while on a hydrogen-free surface sorbitol adsorbed and degraded into a large range of products.

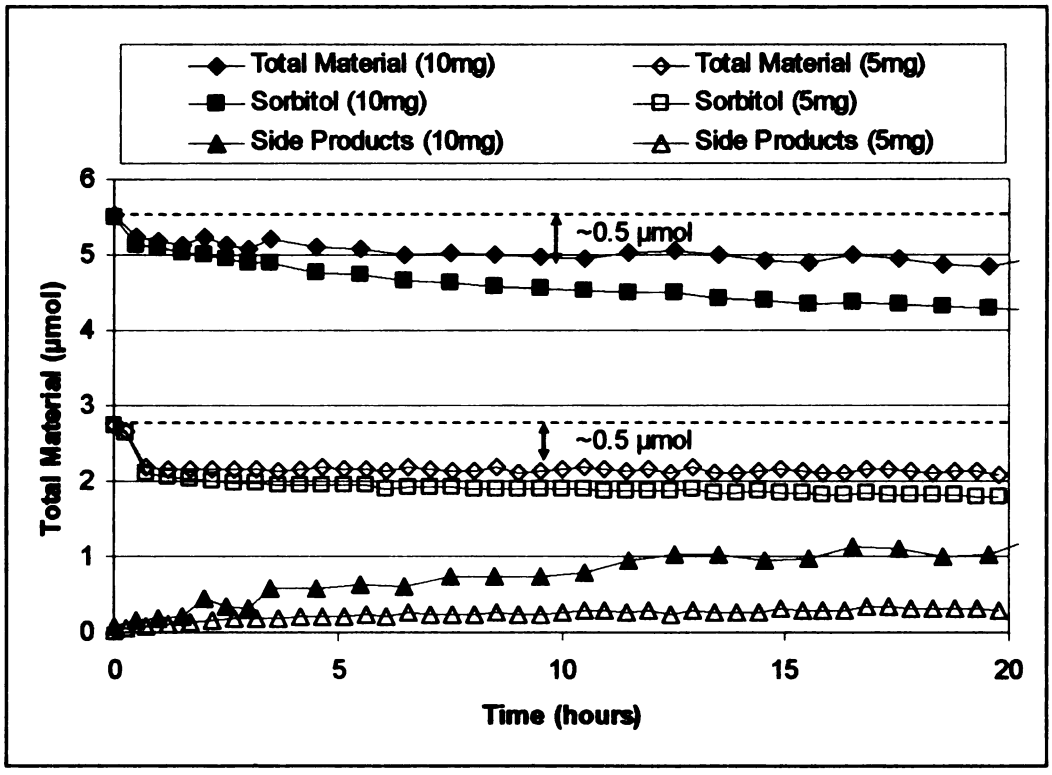

Figure 6-1: Adsorption of sorbitol on 10 g H_2-free Ru sponge at 25 °C. Initial loading of 5 mg (27.5 µmol) and 10 mg (55 µmol).

Figure 6-1 shows that at a high SO concentration (2-5 mM) the metal is saturated in a relatively short time (1-2 hours), while at lower concentrations adsorption is slower as seen in stepwise additions (**Figure 6-2**). The presence of a large range of products makes it hard to give an accurate accounting of the amount adsorbed. Using an average response factor and average molecular weight (100 g/mol), each of these experiments show an adsorption of ~0.1 mg/g Ru (0.55 µmol/g). It should be noted that no glucose is seen in adsorption experiments with sorbitol. Control experiments were run to see if this apparent amount of adsorption was really due to the Ru metal and not a result of calculation error or system behavior. First, an empty column (Exp 11) was used but this had a significantly larger volume then a Ru sponge filled column. To keep the volume constant with minimal increase in surface area, 150 µm glass beads (Exp 21) were used. To give a larger surface, a third experiment (Exp22) used Controlled-Pore Glass ® (product# CPG03000D, lot#11D011) with a total surface area of ~15 m^2. All three of these experiments showed no adsorption of SO.

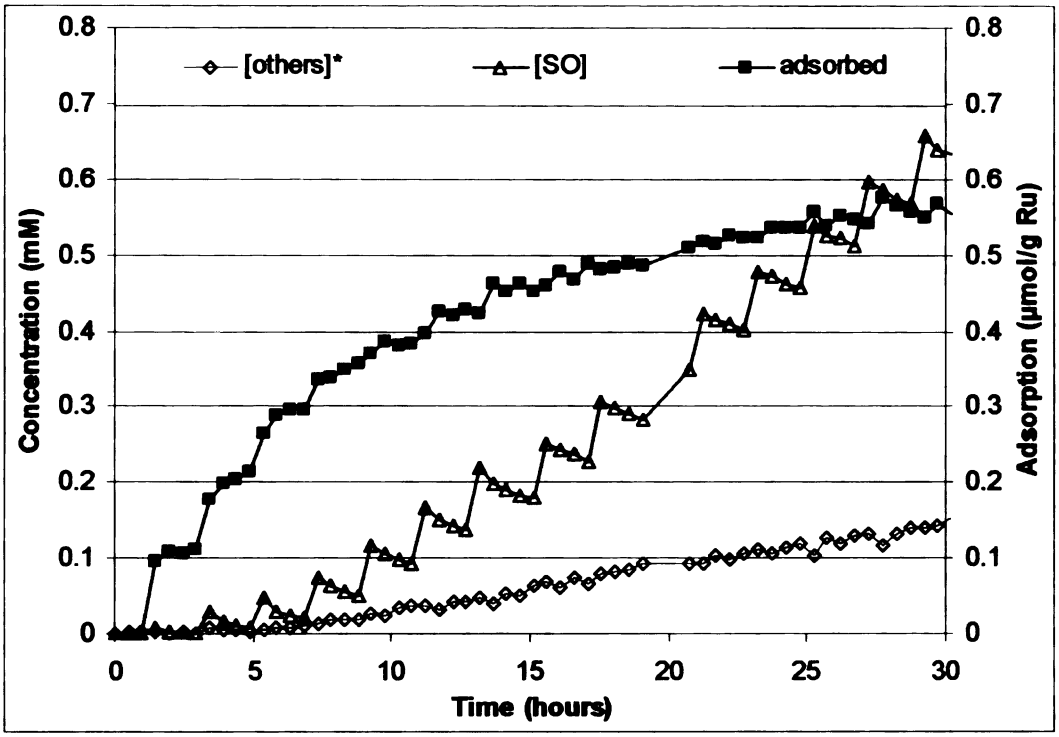

Figure 6-2: Adsorption of sorbitol at 25 °C on 10 g Ru sponge using stepwise dosing (Exp 20). Concentration of other species is in sorbitol equivalents.

When sorbitol was adsorbed in the presence of 5 mM H_2SO_4 (Exp 14), only one main product was formed at 10.8 minutes retention time on the HPLC. In the presence of acid, it is well known that sorbitol can cyclize by dehydration to form 1,4-anhydro-D-glucitol (sorbitan) and 1,4-3,6 dianhydro-D-glucitol (isosorbide).[67] These species were identified by comparing their retention times with those determined by Dozeman[67] on the same Bio-Rad column. The formation of sorbitan at 25 °C with dilute acid only in the presences of Ru sponge metal gives some evidence of the activation of the C1 position.

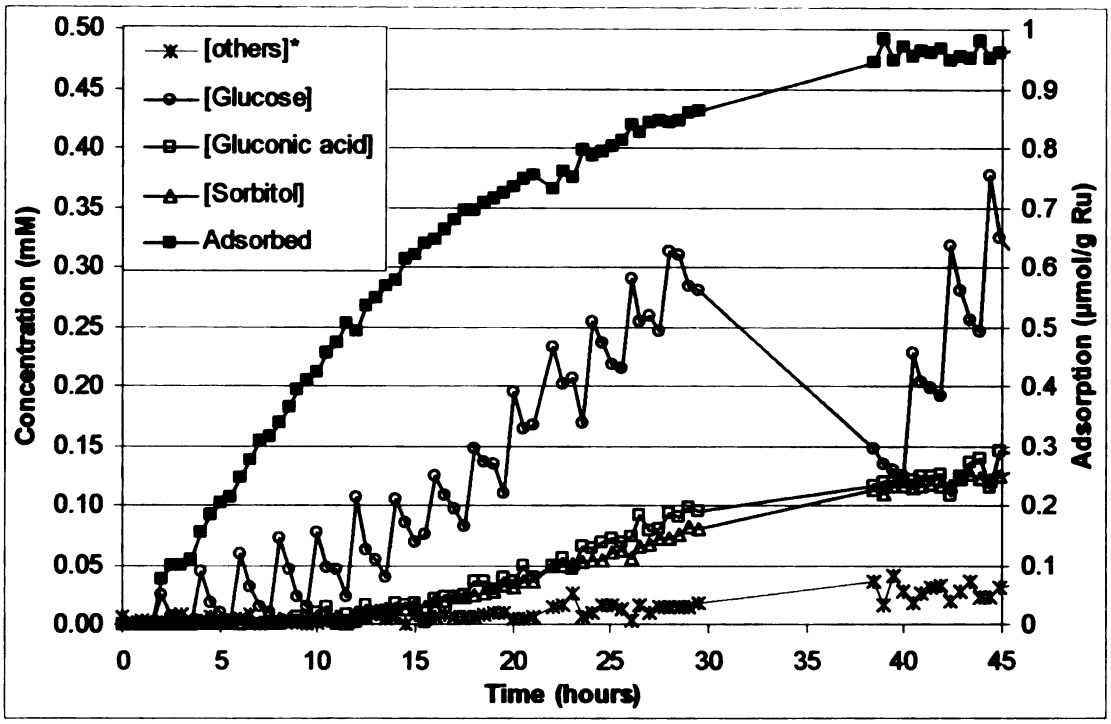

Figure 6-3: Adsorption of glucose at 25 °C on 10 g Ru sponge using stepwise dosing (Exp 23). Concentration of other species is in glucose equivalents.

Adsorption of glucose at 25 °C on Ru sponge using stepwise dosing (Exp 23) is shown in **Figure 6-3.** The total adsorbed material is 0.88 µmol/g Ru, which is similar to glycerol under the same conditions but more than sorbitol (0.55 µmol/g Ru). The only products detected to any extent are sorbitol and gluconic acid. Both these products are formed to the same extent, suggesting a Cannizzaro-type disproportionation. It should be noted that in the presence of air, gluconic acid is the main product. After stopping the stepwise addition of glucose, the system was left to equilibrate overnight, sampling was started, and then 500 psi H_2 was added to the headspace. **Figure 6-4** shows that the concentration of gluconic acid jumped up followed by a slow conversion to sorbitol. This is a real change, because gluconic acid is measured by UV

detection and not refractive index (RI) detection. Because of glucose and gluconic acid peak overlap in RI, the glucose concentration is subject to error. This shows that some form of adsorbed acid can be removed by adding H_2.

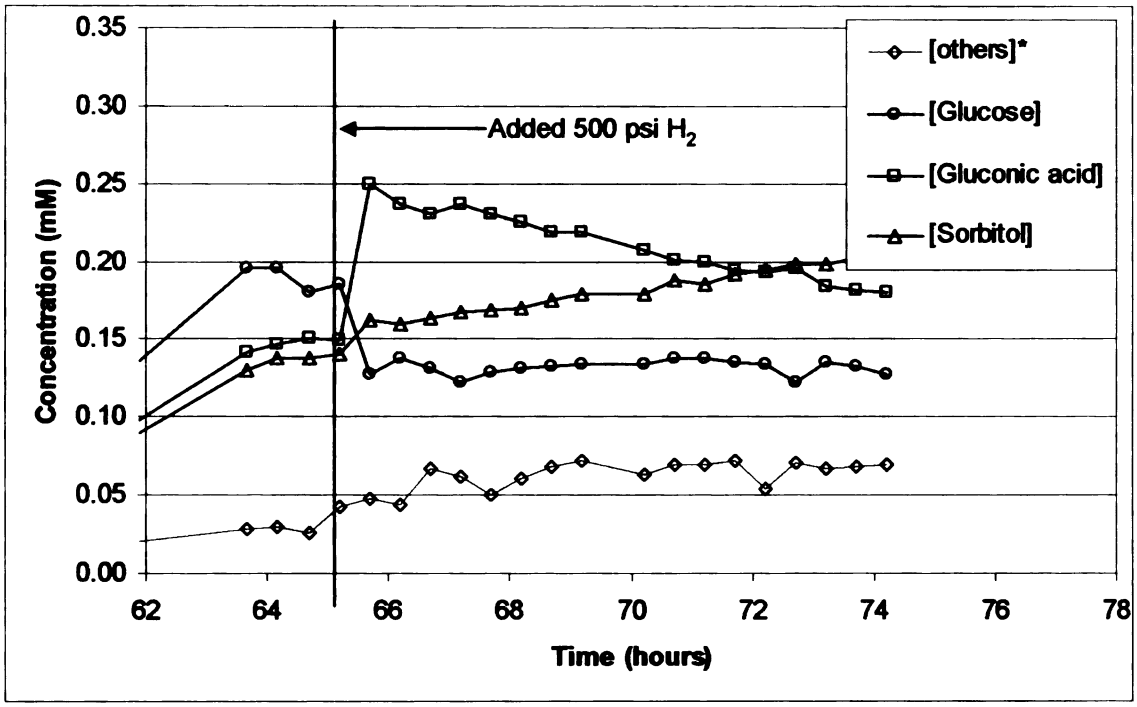

Figure 6-4: Effects of H_2 addition on adsorbed glucose at 25 °C on 10 g Ru sponge after stepwise dosing (Exp 23)

Adsorption of gluconic acid on a hydrogen-free surface shows no formation of side products. **Figure 6-5** shows the adsorption of gluconic acid at 25 °C on Ru sponge (Exp 25); the leveling off and slight decrease seen between 10-23 hours is mainly due to a small leak in the system that was not accounted for in the calculations; the actual amount adsorbed should be ~0.8 mg (0.42 μmol/g Ru). The addition of H_2 shows a slight increase the solution concentration of gluconic acid. This increase and the increase seen in Exp 23 (**Figure 6-4**) are taken as evidence that some gluconic acid adsorption is reversible. It should be noted that the observed increase is with in the uncertainty of the data.

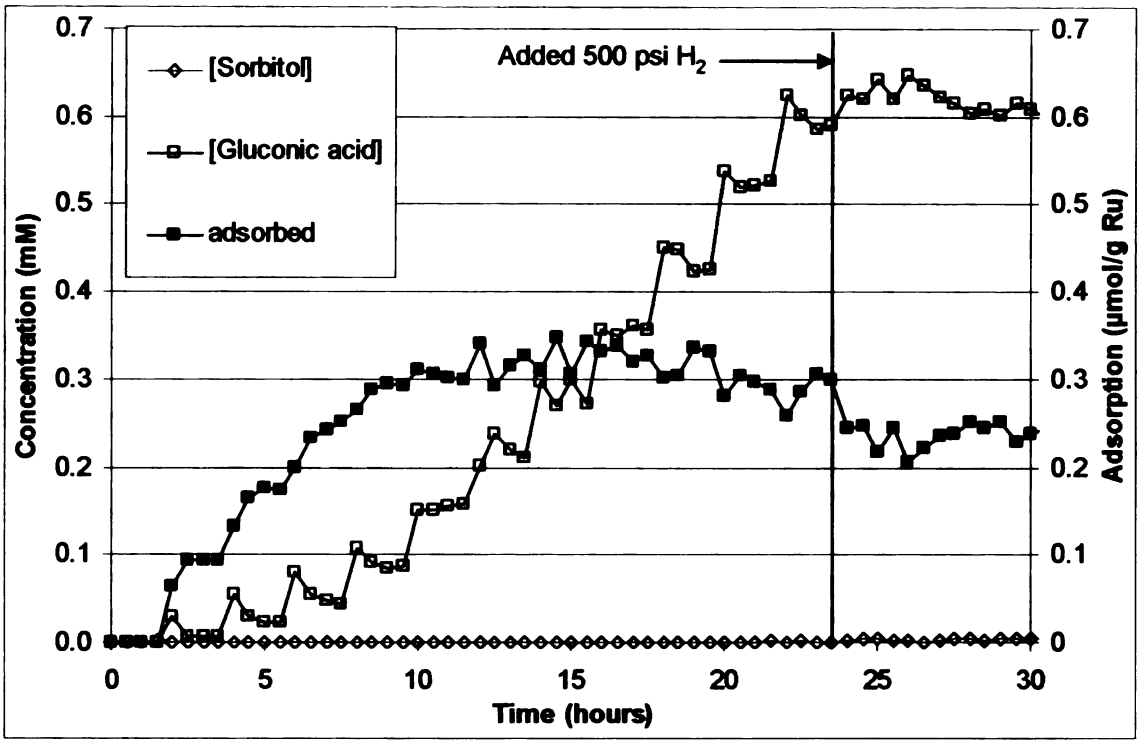

Figure 6-5: Adsorption of gluconic acid at 25 °C on 10 g Ru sponge using stepwise dosing (Exp 25)

The stepwise addition of sorbitol and glucose both show a lag time before products appear. This lag seems to be related to the oxidation state of the substrate: it is 5 hours for sorbitol and 10 hours for glucose. Comparing the total material adsorbed shows that glucose (0.88 µmol/g Ru) is significantly higher than sorbitol (0.55 µmol/g Ru) and gluconic acid (0.42 µmol/g Ru). Unfortunately, because of product formation and the large molecule size, this system is too complex to draw meaningful mechanistic conclusions. Therefore, we changed to a smaller substrate, glycerol, as discussed below.

6.2 Glycerol Adsorption

The adsorption of glycerol was studied by itself and in combination with propylene glycol. The effects of concentration, hydrogen saturation, and temperature were looked at with the hope of gaining mechanistic insight into the adsorption process. Experiments were done to look for evidence that the adsorption is reversible.

6.2.1 Concentration dependence

Initial glycerol (GO) adsorption studies were performed at 25 °C using stepwise addition (Exp 24) and a fixed dose of 4.3 µmol (Exp 26) of GO. **Figure 6-6** clearly shows that in both experiments adsorption plateaus at ~0.3 µmol/g Ru even though concentrations are 2.6 and 0.05 mM respectively.

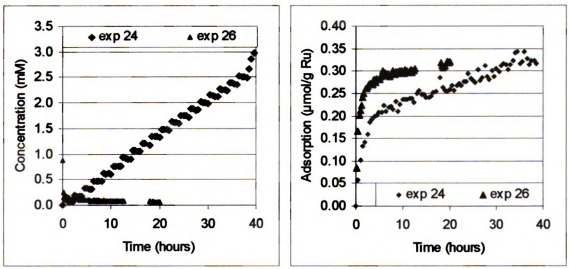

Figure 6-6: Adsorption of glycerol at 25 °C on 10 g Ru sponge comparing stepwise (Exp 24) and fixed dosing (Exp 26).
Left solution concentration; *right* quantity adsorbed.

This result and the results from sorbitol adsorption mentioned before led us to assume that the total quantity adsorbed was independent of concentration. Most subsequent experiments were run based on this assumption, but it was only after examining all experiments at 25 °C that this assumption was validated.

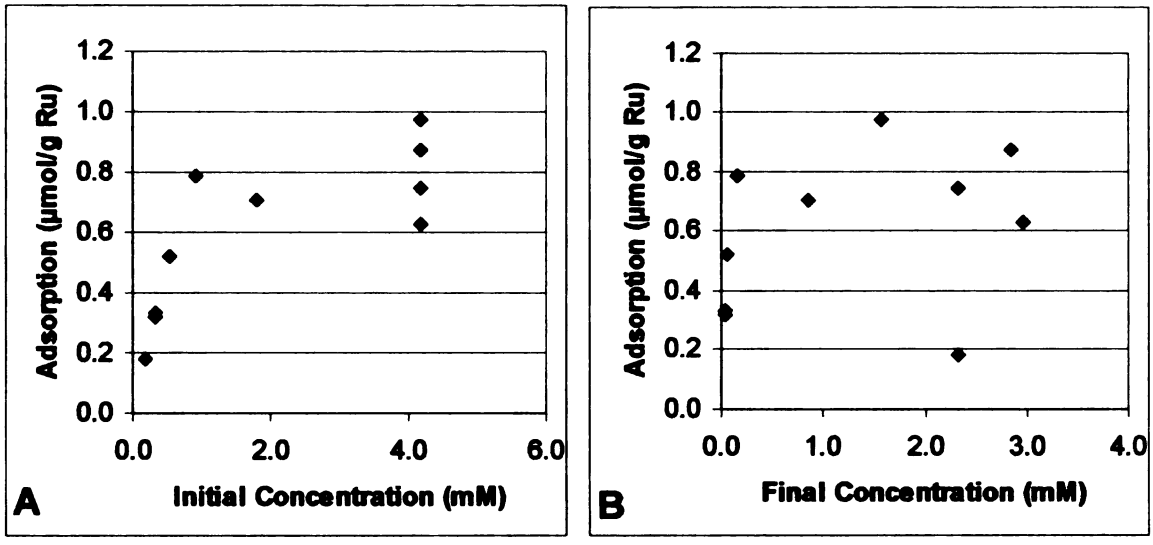

Figure 6-7: Adsorption of GO at 25 °C using (**A**) fixed dosing: maximum initial concentration vs. total adsorbed, and (**B**) final solution concentration vs. amount adsorbed.

Figure 6-7 shows maximum initial concentration vs. total adsorbed (A) and also the final solution concentration vs. amount adsorbed (B) after ~18 hours. Maximum initial concentration is the concentration in the loop before the reactor is put inline. It should also be noted that this data has both 10 and 20 gram loadings of ruthenium sponge while the total volume of the system is about the same (11-13 ml). As long as there is enough GO in the system, the adsorption peaks at ~0.8 ± 0.2 µmol/g Ru. The uncertainty is based on four nearly identical experiments at 7.5 mM initial concentration. The quantity adsorbed, 0.8 µmol/g Ru, is only about 10% of the quantity of CO adsorbed via chemisorption (~9 µmol CO/g Ru). Yet the value is close to that predicted (1-1.2

μmol/g Ru) by assuming end-on GO adsorption with a 30 $Å^2$ per molecule surface area. Most experiments were run for at least 18 hours and adsorption curves seem to level off after ~10-20 hours. This behavior was also observed in stepwise addition of GO (Exp 24). It does not appear that exposure of H_2-free Ru surface to water for an extended time changes the adsorption behavior, but even small amounts of polyol decomposition could deactivate the surface.

Some noted exceptions to the above behavior are Experiment 67 and 68 (**Figure 6-8** and **Figure 6-9**) which showed that the initial 5 μmol GO added adsorbed completely in the first 15 hours; the subsequent addition of 5 more μmol GO still adsorbed readily. Reduction conditions were not the same as for most experiments. In Experiment 67, the metal was washed with degassed water for 2 days (over the weekend); this was ~2-3 L of water that might have oxidized some metal.

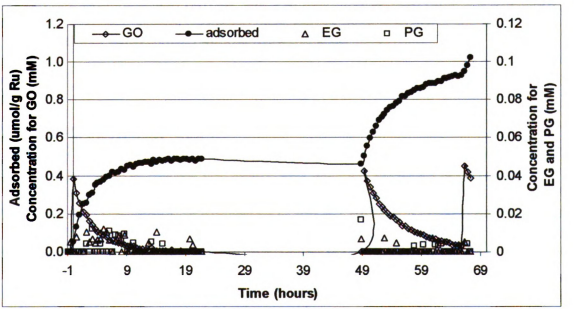

Figure 6-8: Adsorption of GO at 25 °C (Exp 67) on Ru sponge prepared with excess water. For clarity EG and PG concentrations are plotted at 10X.

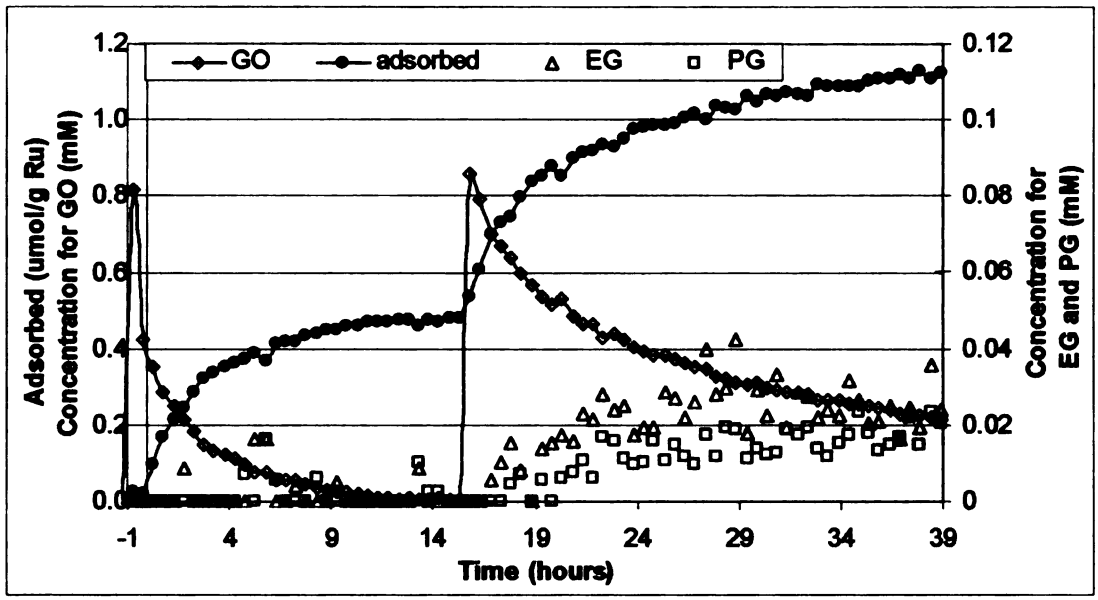

Figure 6-9: Adsorption of GO at 25 °C (Exp 68) on Ru sponge prepared by reduction on the Micromeritics ASAP 2010 instrument. For clarity EG and PG concentrations are plotted at 10X.

For Experiment 68, the Ru sponge was dry reduced on the ASAP instrument and flushed only with 10-20 ml degassed water. It is interesting to note that EG and PG did not form initially in Exp 68, while in Exp 67 and most other experiments these products were formed almost from the start.

6.2.2 Hydrogen saturation

Generation of the "H_2 saturated" and "H_2 free" surfaces is described in Section 3.4.1. Discussion of the nature of the Ru surface is presented in Chapter 4 and 5. **Figure 6-10** shows adsorption of GO on both H_2-saturated (Exp 28) and H_2-free (Exp 39) surfaces at 25 °C. The H_2-saturated metal shows limited adsorption of ~0.05-0.1 μmol GO/g Ru, while ~0.3 μmol GO/g Ru is adsorbed on hydrogen free metal surface with the formation of trace amounts of EG and PG.

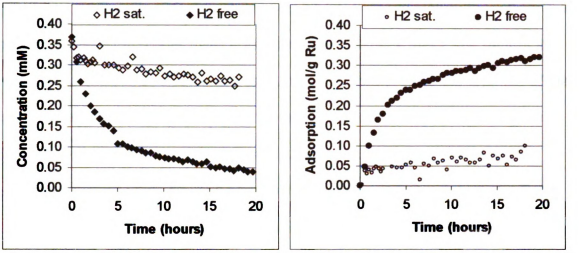

Figure 6-10: Comparison of adsorption of GO at 25 °C on H_2-saturated (Exp 28) and H_2-free (Exp 39) Ru sponge (10 g).

After some minor repairs and the addition of 10g more Ru sponge into the reactor, the effect of H_2 saturation was rechecked (**Figure 6-11**). Total GO added was 50 µmol (7.5 mM max) for each reaction. Unlike Exp 28 and 29, where the headspace gas was H_2, both Experiments 93 and 100 used Ar in the headspace.

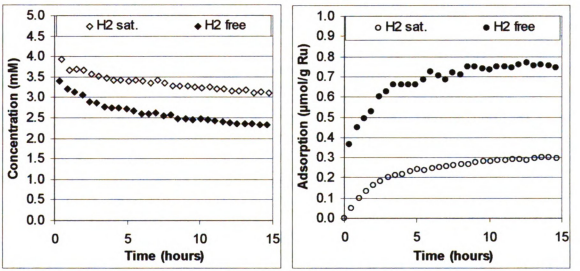

Figure 6-11: Effects of higher GO loading on adsorption at 25 °C on H_2-saturated (Exp 100) and H_2-free (Exp 93) Ru sponge (20 g).

GO adsorption (0.3 μmol/g Ru) was higher than expected in Exp 100; this might be due to the higher initial concentration of GO or it might just be that the headspace gas composition is critical. Unfortunately, no direct comparison of the effects of the headspace gas during the adsorption run was done, but **Figure 6-12** shows adsorption of GO (4.5 μmol loading) at 50 °C under Ar on a H_2-saturated surface (Exp 30). The observed adsorption of GO (~0.3 μmol/g Ru) is comparable to GO adsorption seen on a H_2-free surface at the same loading (Exp 39), except that the adsorption rate is a lot slower. The higher adsorption under Ar could be explained by desorption of H_2 from the Ru surface, freeing up sites for GO to adsorb. At 25 °C, the rate of H_2 desorption is practically zero while at 50 °C it is significant.

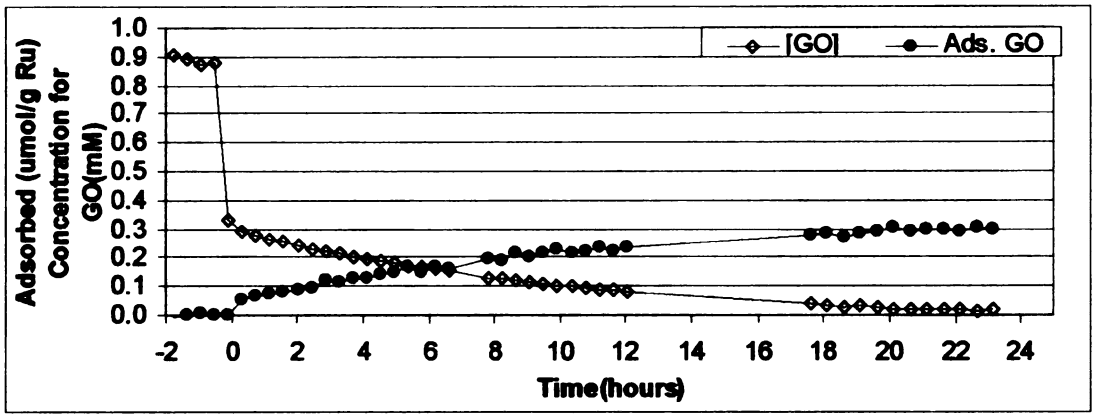

Figure 6-12: Adsorption of GO on H_2-saturated Ru sponge (10 g) under argon at 50 °C (Exp 30).

The effects of adding hydrogen to the headspace after GO adsorption on a H_2-free metal surface will be discussed in Section 6.2.3. Heating of the H_2-saturated system to 100 °C (end of Exp 28 not shown) resulted in rapid decomposition of glycerol with the formation of methane, PG, EG, and trace

amounts of CO. It should be mentioned that at 25 °C the addition of H_2 (250 psi) appears to stop any further decomposition reactions.

6.2.3 Temperature effects on GO adsorption

Experiments were run at 25, 40, 60, and 80 °C under identical conditions (50 µmol GO, 20 g Ru sponge, and standard metal preparation). Gas analysis was not performed on all experiments; those that had no actual analysis done but were corrected with assumed methane production are labeled "exp#*".

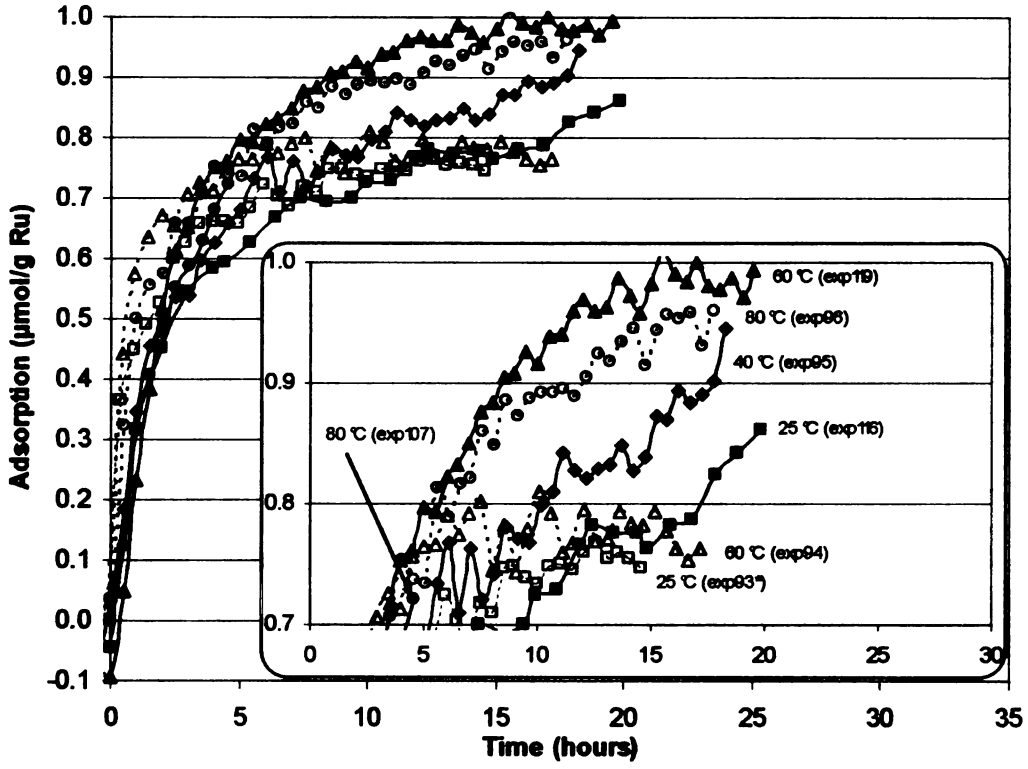

Figure 6-13: Temperature dependence of GO adsorption. (50 µmol GO loading, 20 g Ru sponge). Inset shows magnification of upper region of graph.

Figure 6-13 shows that adsorption does not significantly change at different temperatures and is ~0.8 - 1.0 µmol/g Ru. Multiple experiments at the same temperature were added to the graph to show that experimental variations have

a greater effect than temperature. Looking at the products formed as a function of temperature (**Figure 6-14),** it can clearly be seen that GO decomposition goes through a maximum at 60 °C.

Scheme 6-1

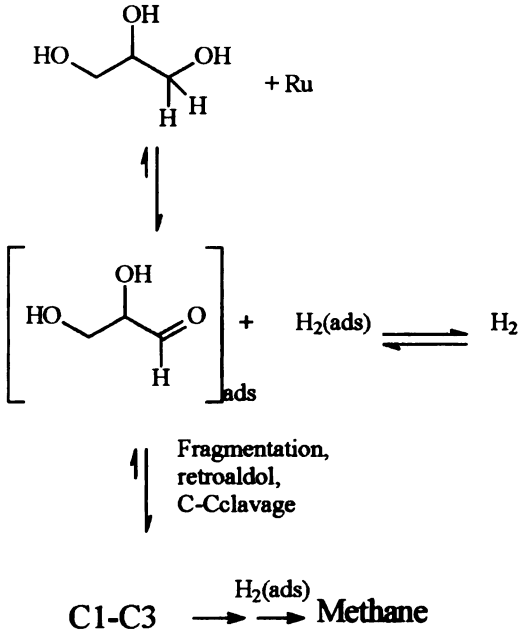

Scheme 6-1 can be used to explain the observed behavior. As the temperature increases, so does the fragmentation of GO, but hydrogen is needed to react with these fragments to remove them from the surface. Surface bound H_2 is produced by the adsorption of GO, but can come off into solution at elevated temperatures. This H_2 desorption starts to be significant at 60-80 °C. This release of H_2 has the effect of oxidizing the metal surface.

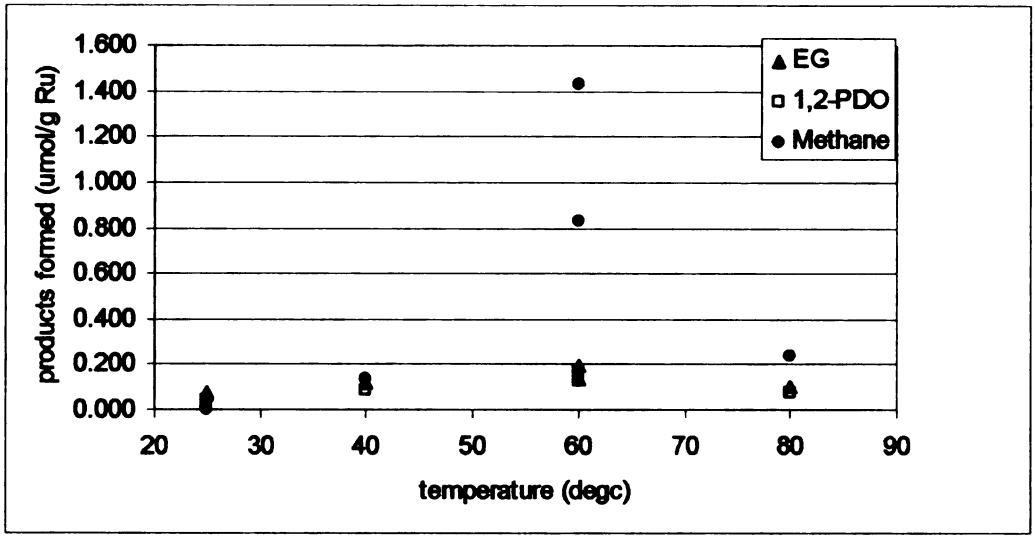

Figure 6-14: Glycerol decomposition products vs temperature. Multiple experiments are included at 25 and 60 °C.

As shown previously, hydrogen saturation inhibits the adsorption of glycerol at 25 °C. Adding H_2 to the headspace at 25 °C only stopped the adsorption of GO, but at 80 °C (Exp 96) the result is the conversion of adsorbed GO to methane without adsorption of additional GO (**Figure 6-15**). It should be noted that adding H_2 and increasing the temperature to 200 °C results in quantitatively converting all carbon species to methane.

Some additional temperature effect experiments were run (Exp 30, 31, 32). Experiment 32 is run stepwise at 80 °C and includes the addition of EG and PG. Data from these experiments were unreliable due to fact that changes in temperature were made may days after the start of the experiment.

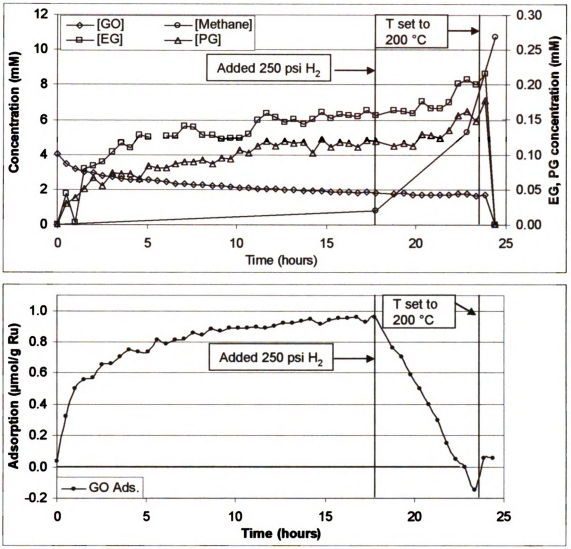

Figure 6-15: Adsorption of GO (50 µmol loading) at 80 °C on 20 g Ru sponge (Exp 96) showing the effect of adding H_2 and increasing temperature to 200 °C. Quantity GO adsorbed shown on lower graph, solution concentrations on upper graph. Concentrations of EG and PG are plotted on right axis.

6.2.4 Propylene glycol (PG), ethylene glycol (EG), and 1,3-propanediol (1,3-PDO) adsorption

Propylene glycol adsorption experiments were run at 25 °C with 6.5 and 66 µmol PG loading. **Figure 6-16** shows PG adsorption of ~0.18 µmol/g Ru at low loading (Exp 42) and ~0.75 µmol/g Ru at high loading (Exp 41). The amount

of PG adsorbed at the high loading is similar to that found for glycerol. This would indicate that the surface is saturated. Comparing adsorption at lower concentrations suggests that PG binds less strongly than GO.

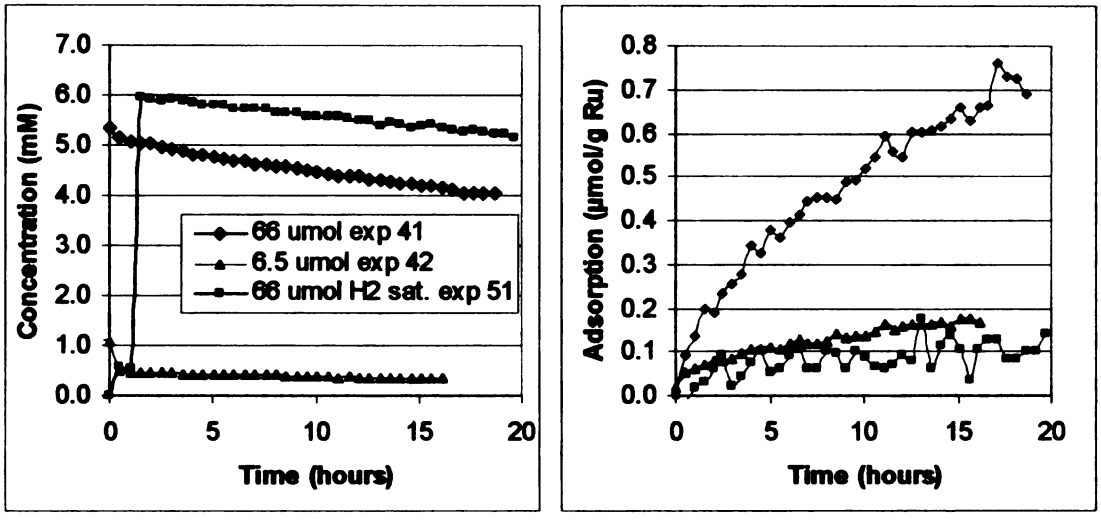

Figure 6-16: Adsorption of PG at 25 °C on 10 g Ru sponge comparing loading and H_2 saturation.

As with GO, the pre-saturation of Ru with H_2 inhibited the adsorption of PG (**Figure 6-16,** Exp 51). This finding is consistent with the concept that an initial dehydrogenation step as proposed for glycerol also applies to propylene glycol. The cyclic nature of the noise in Experiment 51 probably stems from the HPLC system, but no satisfactory cause was ever found. Lactic acid and an unidentified peak were the main products and were only seen in the high concentration run with no hydrogen (Exp 41). The area response (RI) for these two peaks is almost the same, suggesting that they might be related.

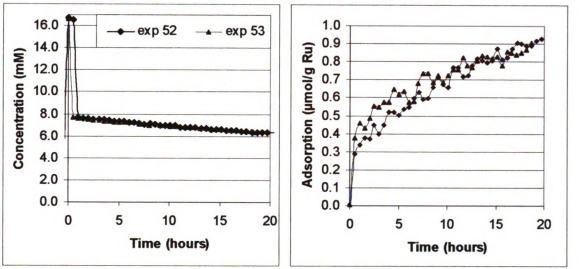

Figure 6-17: Adsorption of EG (80.6 µmol) on 10 g Ru sponge at 25 °C.

Ethylene glycol was run only at 81 µmol EG loading (Exp 52, 53) and showed an extent of adsorption of ~0.8 - 0.9 µmol/g Ru (**Figure 6-17**), again similar to GO. H_2 saturation effects were not checked.

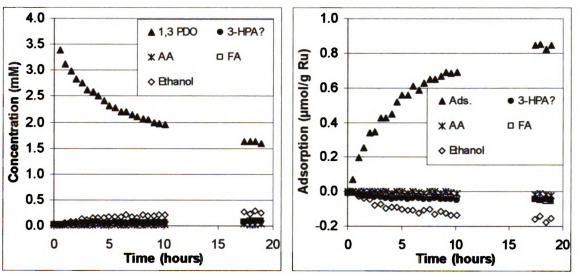

Figure 6-18: Adsorption of 1,3-PDO (50 µmol) on 20 g Ru sponge at 25 °C.

Adsorption of 1,3-Propanediol (1,3-PDO) on 20 g Ru sponge at 25 °C (Exp 113) gave an extent of adsorption of ~0.8 µmol/g Ru (**Figure 6-18).** This is similar to other polyols. It should be noted that 1,3-PDO showed a range of

decomposition products including ethanol, formic acid (FA), acetic acid (AA), and 3-hydroxypropanoic acid (3-HPA).

6.2.5 Binary adsorption (GO, PG)

To examine the difference in binding energies of glycerol (GO) and propylene glycol (PG) on Ru, experiments were run with both species simultaneously. In one run, PG was added first followed by GO, in another run, GO followed by PG, and in third run both were added at the same time. These experiments were all run at 25 °C with 10 g Ru sponge.

Initial adsorption of PG after 16-20 hours was ~0.18 µmol PG/g Ru for a loading of 6.6 µmol (Exp 42). At a higher loading of 66 µmol (Exp 44), this increased to ~0.6 µmol PG/g Ru. In each experiment, 4.34 µmol of GO was then added and allowed to adsorb for 20 hours (**Figure 6-19**). In both cases, GO adsorbed after PG in the amount of ~0.2 (Exp 42) and ~0.1 (Exp 41) µmol/g Ru, respectively. The total amount adsorbed is similar to the amount GO adsorbed at similar loadings (Exp 39 and 93).

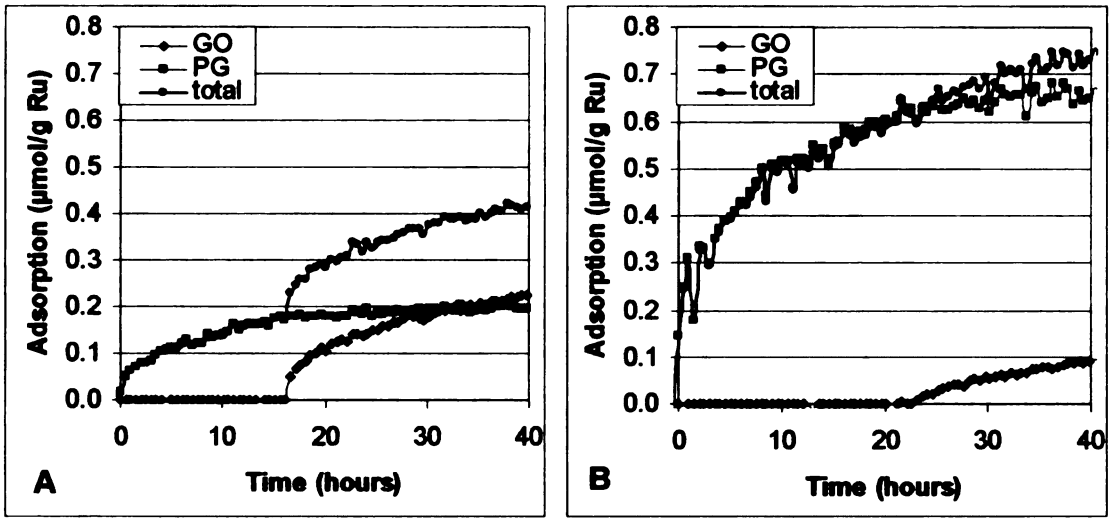

Figure 6-19: Adsorption of PG followed by GO on 10 g Ru sponge at 25°C. **A**: Exp 42, initial PG loading of 6.6 µmol; and **B**: Exp 44, initial PG loading of 66 µmol. GO loading of 4.34 µmol follows PG loading.

When the order is reversed (**Figure 6-20**) with initial addition of GO (6.5 µmol) followed by PG (6.6 µmol), there is no adsorption of PG. The amount of GO adsorbed was ~0.27 µmol/g Ru before the addition of PG and ~0.32 µmol/g Ru at the end of the experiments. It is clear that adsorbed GO inhibits the adsorption of PG, while adsorption of PG leaves sites available for GO to adsorb on.

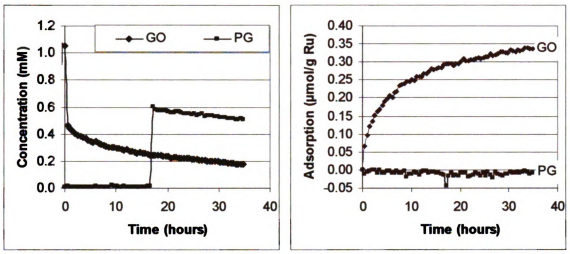

Figure 6-20: Experiment 45, adsorption of GO (6.5 µmol) followed by PG (6.5 µmol) at 25 °C on 10 g Ru sponge.

The simultaneous adsorption of GO and PG (2.2 GO, 3.3 PG µmol) is shown in **Figure 6-21.** These results show behavior that is consistent with a GO preference over PG for Ru and an irreversible interaction with the Ru.

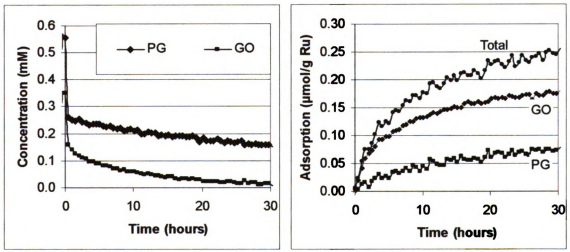

Figure 6-21: Experiment 49, adsorption of GO (2.2 µmol) and PG (3.3 µmol) at 25 °C on 10 g Ru sponge.

6.3 Isopropanol and acetone adsorption

Glycerol and PG are C3 species with multiple hydroxyl groups; each shows adsorption on Ru sponge metal. It is logical to next look at C3 compounds with one hydroxyl group, namely isopropanol (IPA), n-propanol (n-prOH), and ethanol. **Figure 6-22** shows the adsorption of isopropanol (IPA) on 20 g Ru sponge at 25 °C. It should be noted that a negative adsorption value seen in figures means that a compound is formed. It can be seen in **Figure 6-22** that acetone is formed. This is expected if IPA undergoes dehydrogenation and if acetone is not strongly adsorbed. The addition of hydrogen at 20 hours converts all the acetone formed to IPA.

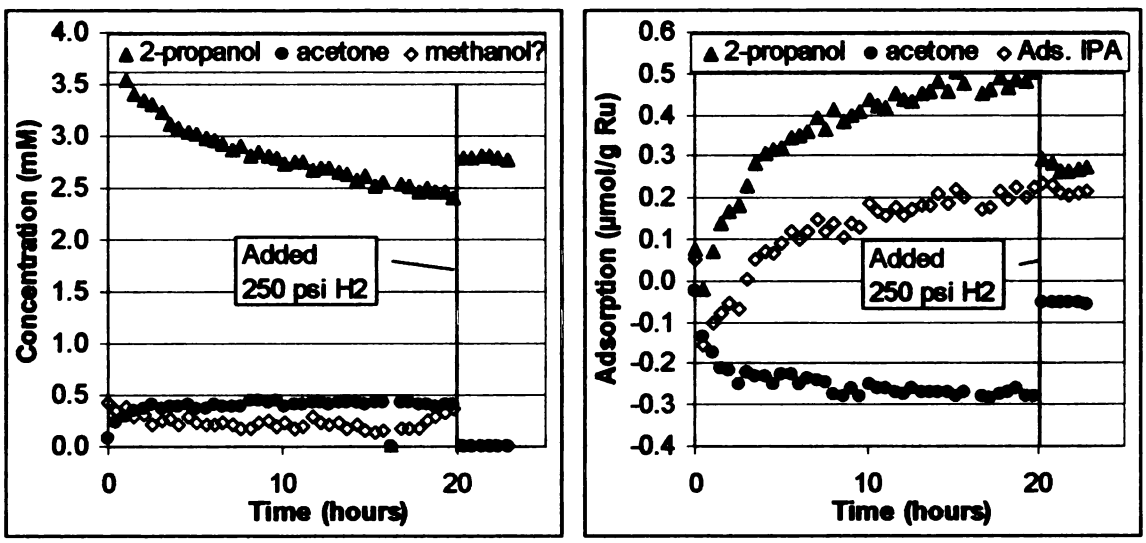

Figure 6-22: Adsorption of IPA (50 µmol) at 25 °C on 20 g Ru sponge (Exp 109) showing effect of addition of H_2.

It would be expected that if IPA were adsorbed on a H_2-saturated surface, we would see no acetone. **Figure 6-23** show that this is the case. Also, no additional products are seen. It is uncertain why a small amount of IPA adsorbs, but clearly no dehydrogenation occurs when the surface is first saturated with hydrogen.

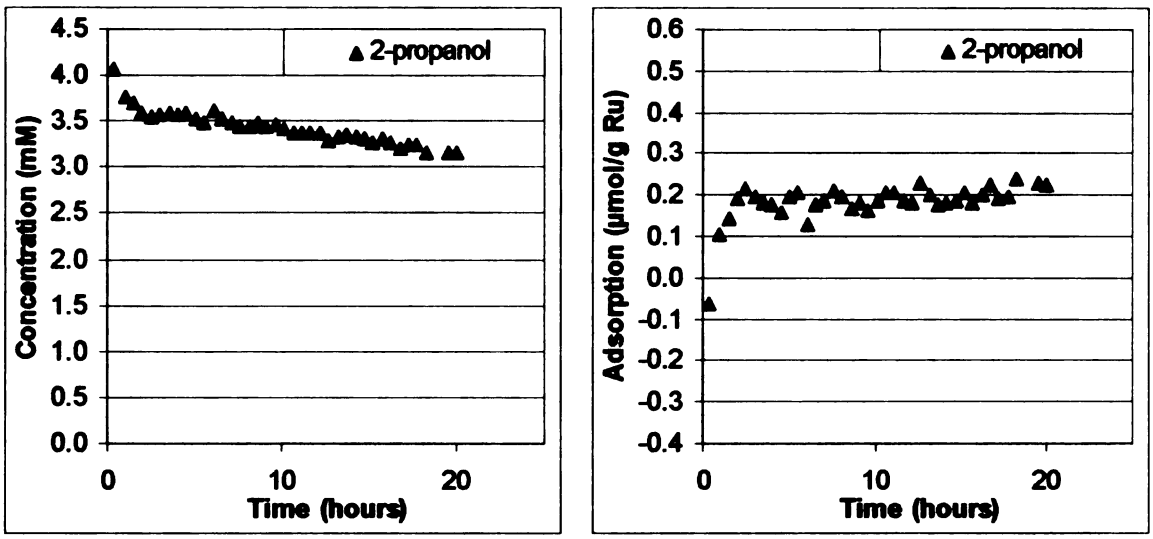

Figure 6-23: Adsorption of IPA (50 µmol) at 25 °C on 20 g H_2 saturated Ru sponge (Exp 111) under 20 psi H_2.

Figure 6-22 shows a peak that was tentatively labeled as methanol, but this was an impurity that was there at the start of the experiment. It is curious that it disappeared when H_2 was introduced, which suggests that it might have been a dissolved gas or a carbonyl species. If it was a carbonyl, we would expect to see a peak in the UV, but none was seen. Unfortunately, no UV peak (210 nm) was seen for acetone either at these low concentrations, so we cannot rule out the possibility that this peak is an unsaturated compound. For now, the "methanol" peak is assumed to be an inert molecule of some sort and is ignored.

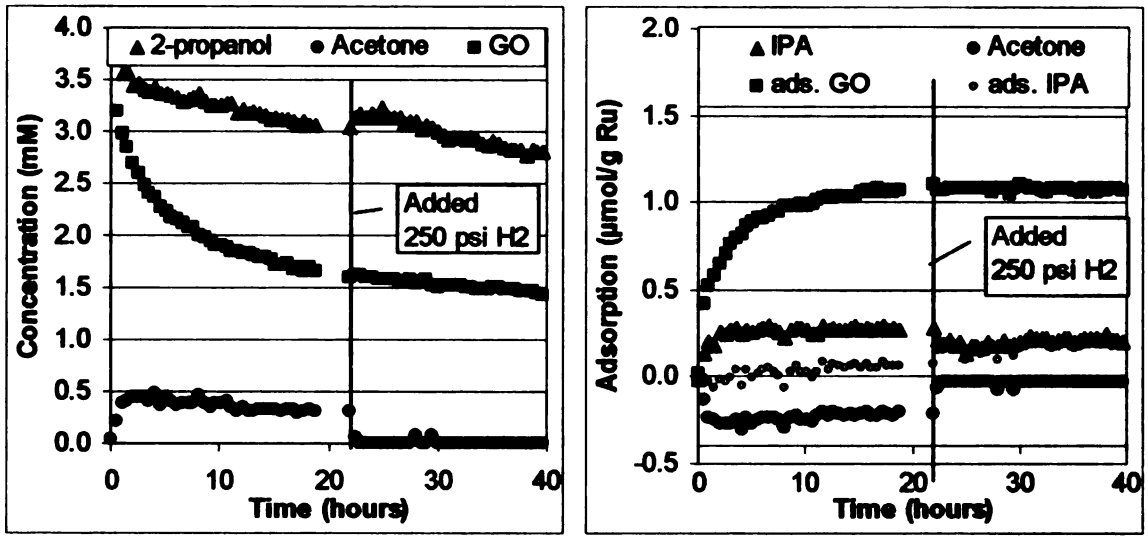

Figure 6-24: Competitive adsorption of GO and IPA (50 µmol each) at 25 °C on 20 g Ru sponge (Exp 112) showing the effect of adding H_2.

During the adsorption of IPA, acetone is formed in the first 5 hours and then its concentration stays constant. When IPA is adsorbed in the presence of GO (**Figure 6-24**), the maximum amount of acetone (~0.5 µmol/g Ru) is formed in about the same time frame as in the adsorption of IPA alone. In the presence of GO, the acetone that was formed slowly converts back to IPA. Presumably the hydrogen liberated from adsorbing GO reduces the acetone back to IPA.

The next logical experiment was the adsorption of acetone. **Figure 6-25** show adsorption of acetone at 25 °C on 20 g of H_2-free Ru sponge. It clearly shows that IPA is formed.

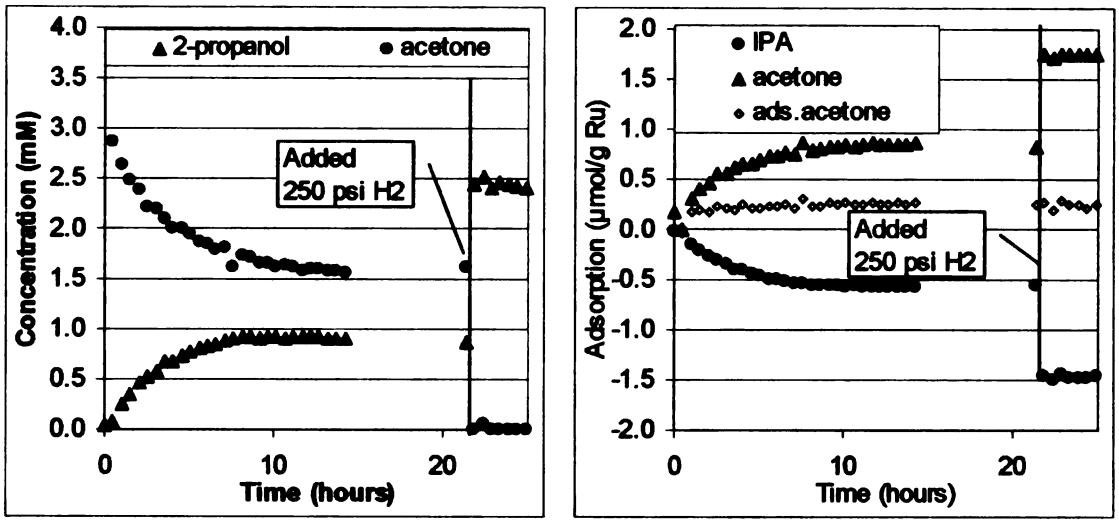

Figure 6-25: Adsorption of acetone (50 µmol) at 25 °C on 20 g Ru sponge (Exp 115) showing effect of addition of H_2.

The observation of acetone hydrogenation with no H_2 available can possibly be explained by the dissociation of water on the Ru surface to supply the H_2. Another possibility is that when an acetone molecule adsorbs, it dissociates completely (Scheme 6-2) to liberate six H-M. This is sufficient hydrogen to convert three molecules of acetone to IPA. So if the hydrogen comes only from acetone, then the amount of IPA formed cannot exceed three-fourths that of amount of acetone adsorbed.

Scheme 6-2

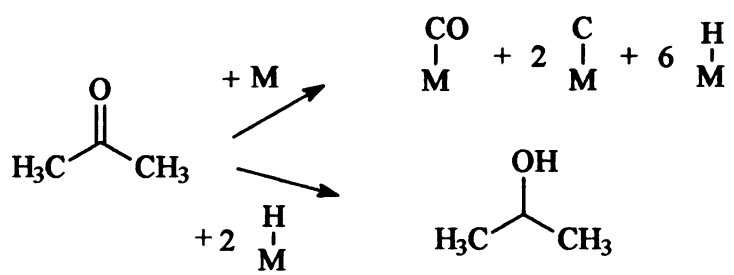

It might be possible to take the carbon all the way to CO_2 by a water shift type reaction (Scheme 6-2) which could generate 10 more H's. But there is no evidence of CO_2 liberation and the ~¾ ratio of ~0.5 μmol IPA formed to ~0.8 μmol acetone adsorbed per gram of Ru sponge might suggests that the hydrogen comes from the acetone. The subsequent addition of H_2 results in the rapid conversion of all acetone to IPA.

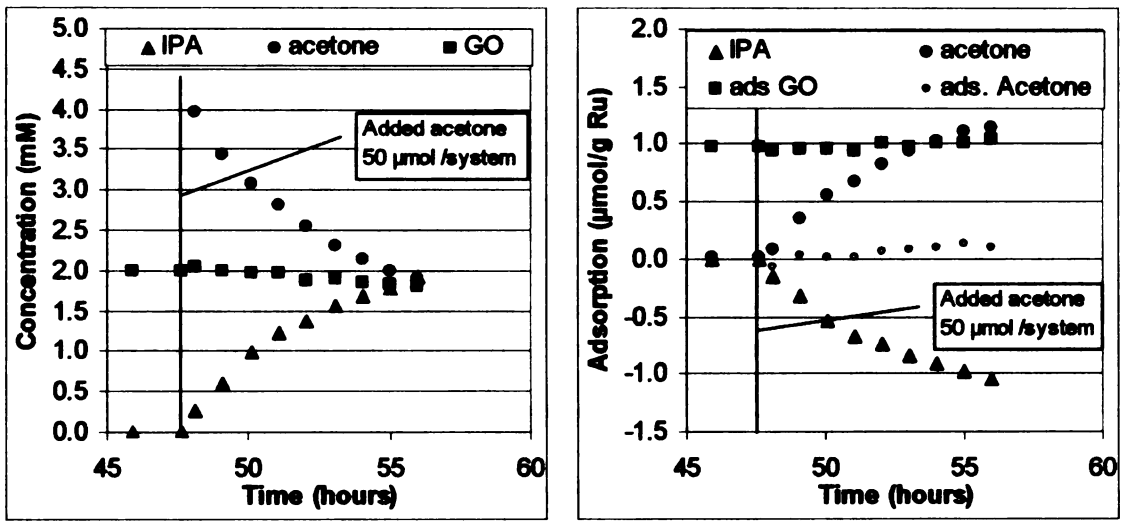

Figure 6-26: Adsorption (50 μmol each) of acetone after GO adsorption at 25 °C on 20 g Ru sponge (Exp 116) showing the formation of IPA.

It is possible to convert more acetone to IPA if GO is adsorbed on the Ru surface first. Doing this should make more H_2 available. **Figure 6-26** shows adsorption of acetone after the saturation of Ru sponge with GO. The quantity of IPA produced is >1.0 μmol after 7 hours; this is twice as much IPA as is produced from acetone by itself. **Figure 6-27** shows the direct comparison of these two cases. Because the initial quantities of acetone are not the same, we can only reach the qualitative conclusion that more IPA is produced from acetone

in the presence of some hydrogen donating species such as GO than from acetone alone.

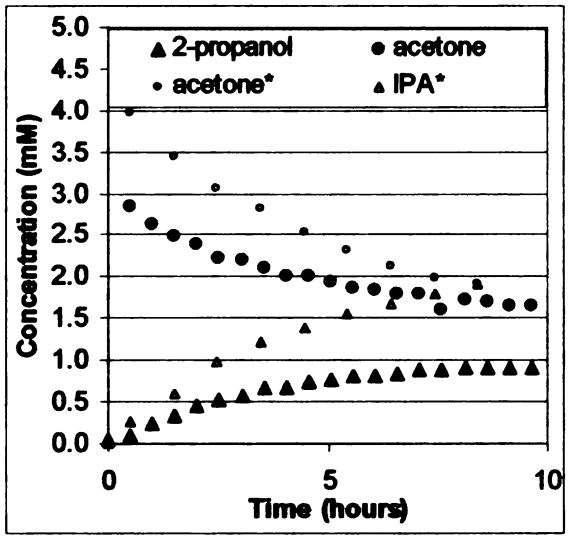

Figure 6-27: Comparison of acetone adsorption (50 µmol) at 25 °C on 20 g Ru sponge (Exp 116, 115) Showing the effects of pre-saturation with GO. Open symbols are from presaturated experiment.

The total quantity adsorbed in IPA/acetone system is ~0.2 µmol/g Ru. This is independent of hydrogen saturation or which substrate is used first. It is interesting that this is about the same amount as seen in GO adsorption on a hydrogen-saturated Ru surface. It is possible that there are other adsorption mechanisms at work.

6.4 n-Propanol and ethanol

The interaction of two primary alcohols, n-propanol (n-prOH) and ethanol, with H_2-free Ru surface was looked at. Both ethanol and 1-propanol adsorbed to he same extent, as seen in **Figure 6-28**. Both produced the corresponding acids. There was production of methane in both cases but more appeared to form from ethanol than from n-propanol.

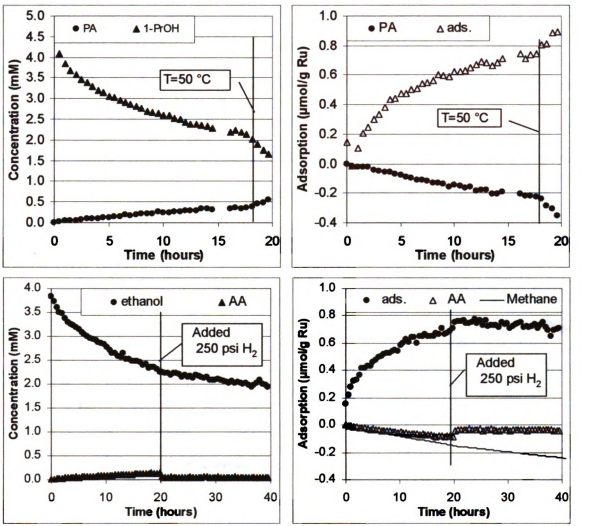

Figure 6-28: Adsorption (50 µmol loading) of n-propanol (Exp 121) and ethanol (Exp 114) at 25 °C on 20 g Ru sponge. Acetic acid (AA) and PA are formed.

During Experiment 121, adsorption of n-prOH (**Figure 6-29**), the temperature was increased to 50 °C after 18 hours with the following three results: conversion of n-prOH to PA, increased production of methane, and an increase in total quantity n-prOH adsorbed. It might be possible that at higher temperatures water acts as an oxidant of the Ru, releasing hydrogen and providing oxygen for oxidation of n-prOH to PA. It is also possible that the

adsorbed intermediate "propionaldehyde" undergoes disproportionation to form n-prOH and PA.

It has been observed that upon addition of H_2 the solution concentration of the acids produced drops sharply followed by a steady conversion to the corresponding alcohol. This sharp drop suggests adsorption of PA on the newly reduced surface. It is unlikely that PA reduction takes place, because reduction of the acids is very slow at 25 °C. This same behavior was also seen in the adsorption of gluconic acid.

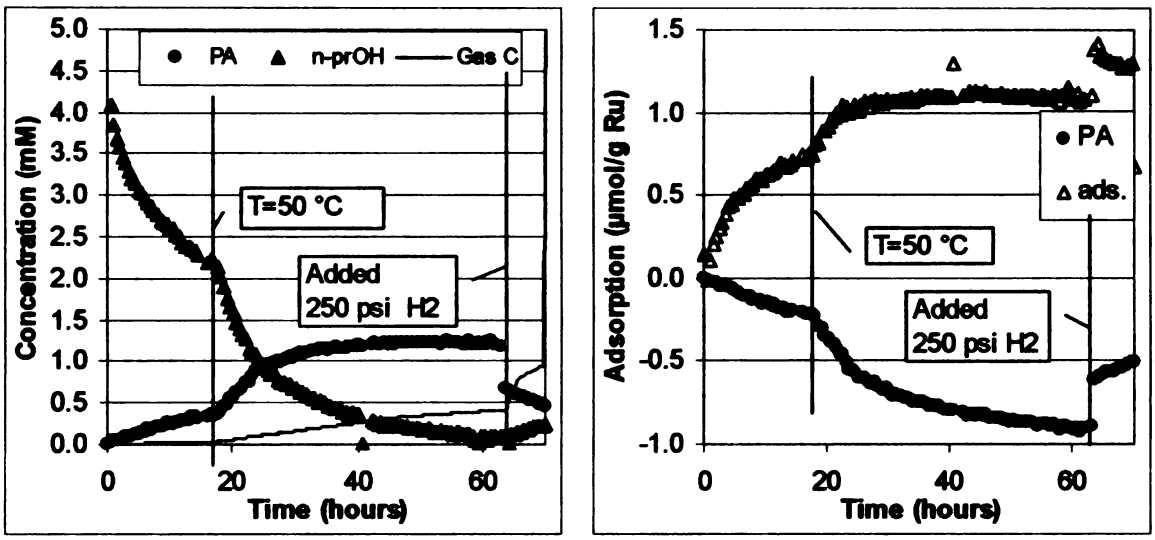

Figure 6-29: Adsorption of n-prOH (50 µmol/system) at 25 °C on 20g Ru sponge (Exp 121) showing effect of addition of H_2 and increase in temperature to 50 °C. Gas C in legend refers to total gaseous carbon.

6.5 Organic acid adsorption

Adsorption of LA was conducted at 25 °C on both H_2-free and H_2-saturated Ru sponge metal. Initial loadings ranged from 5-190 µmol. Adsorption of equimolar mixtures of LA and PA were also examined.

Figure 6-30 shows concentration dependent adsorption of LA at 25 °C on 10 g of H_2-free Ru sponge surface. In each case the adsorption levels off after ~4-6 hours. There were no products seen. The amount of LA adsorbed seems directly proportional to the initial loading. At 5 μmol loading, the adsorption is ~0.15 μmol/g Ru, while at 50 μmol/system the adsorption is 1.3 μmol/g Ru. At 190 μmol, the adsorption is 4.3 μmol/g Ru, which is several times the adsorption seen with polyols.

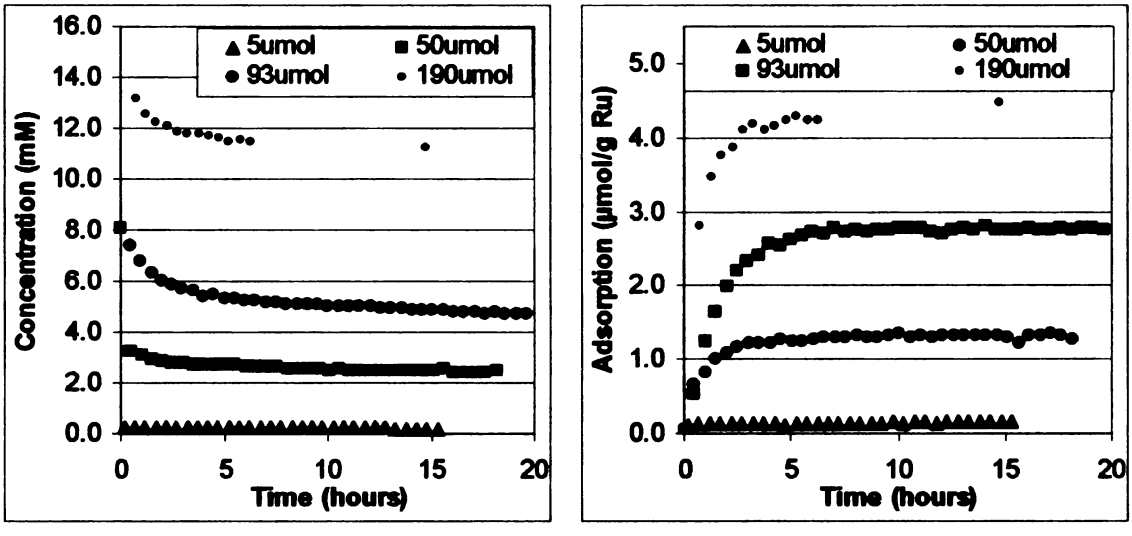

Figure 6-30: Concentration dependence of LA adsorption at 25 °C on H_2 free Ru surface for different initial loadings. (Exp 54, 56, 57, 58)

The gas phase was not analyzed, but if there was production of significant amounts of methane it would have shown up in the HPLC analysis; no methane was detected. If we compare the maximum amount of LA adsorbed (4.3 μmol/g Ru) to the gas phase H_2 and CO adsorption (~4.5 and 9 μmol/g Ru), LA can occupy about two metal sites at the highest concentration examined. Control runs of LA with no Ru present showed no adsorption, but in the presence of air in

a control run lactic acid was oxidized to pyruvic acid, presumably by the tube walls.

The effects of H_2 saturation on adsorption of LA at 25 °C on 10 g of Ru sponge is shown in **Figure 6-31.** Unlike the adsorption of polyols, the adsorption of LA is not limited by H_2 saturation. This is not unexpected, because there is no need to dehydrogenate LA on the surface in order to adsorb a molecule of LA. Clearly the mode of adsorption is different than is seen for polyols.

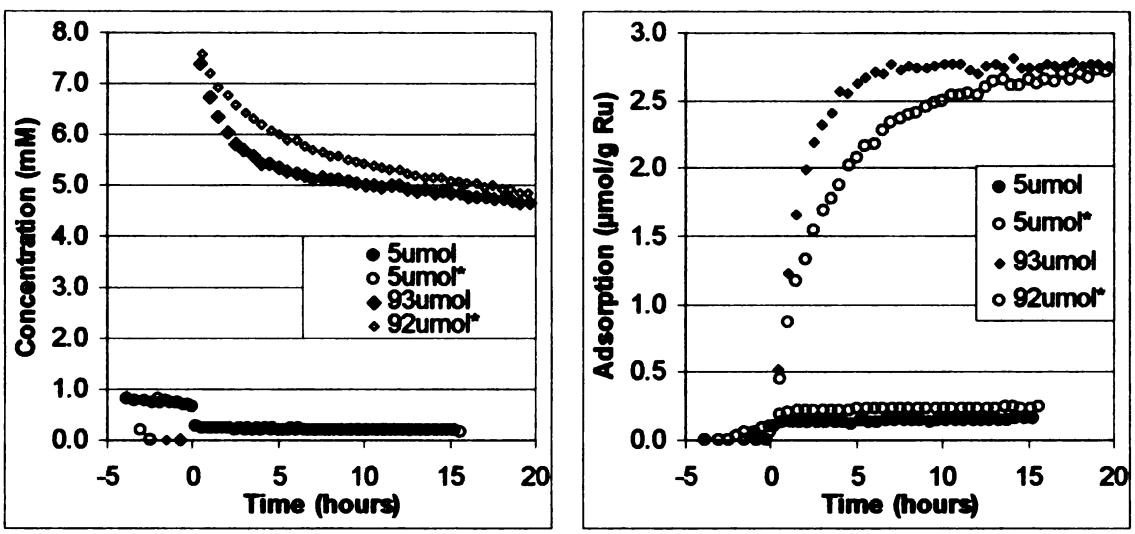

Figure 6-31: H_2 saturation effects on adsorption of LA at 25 °C on 10 g Ru sponge metal (Exp 54,55*,56,60*). **denotes experiments on hydrogen saturated surface.*

The pH was checked after LA adsorption for Exp 54, 57, and 58 and appeared to be higher than would be expected based on the LA concentration. **Figure 6-32** shows measured and calculated pH vs initial concentration. Calculated pH is based on simple weak acid dissolving in water. The model curve is based on the assumption that when a molecule of LA adsorbs, it also generates one molecule of base.

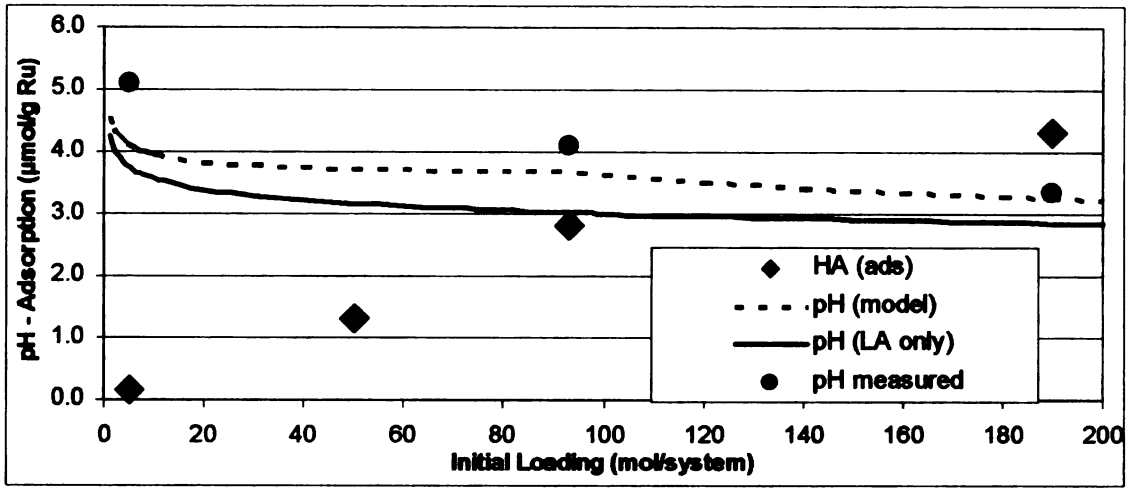

Figure 6-32: Predicted vs. experimental pH as function of initial loading (µmol).

Only one experiment was run with the adsorption of PA and that was the competitive adsorption of LA and PA (120 µmol loading each, **Figure 6-33**). PA seems to have a slightly lower adsorption (2.5 µmol/g Ru) than LA (3.0 µmol/g Ru). These quantities are the same as found for LA by itself at similar loading. If we look at the total loading of 240 µmol, we see an adsorption of 5.5 µmol/g Ru. This is what would be expected if adsorption is directly proportional to initial concentration, so it is apparent that LA and PA are not competing for surface sites in adsorption and that the surface is not saturated under these conditions.

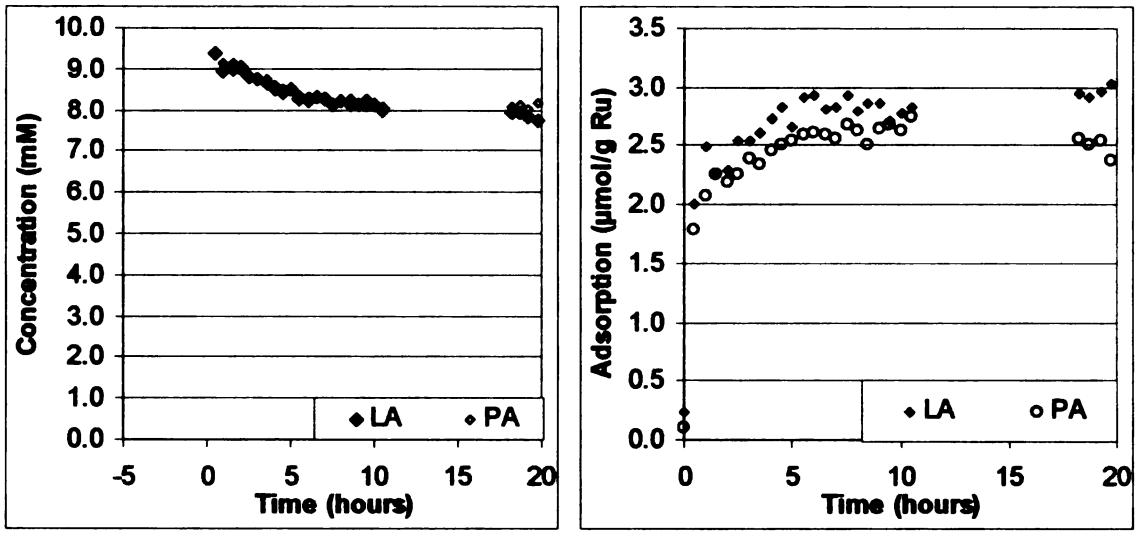

Figure 6-33: Adsorption of equimolar mixture of LA and PA (120 µmol/system) at 25 °C on 20 g of H_2-free Ru sponge. (Exp 70)

6.6 Comparisons and conclusions

The differences in adsorption properties of the various organic substrates on Ru sponge metal are contrasted in **Table 6-1.** The total quantities adsorbed for acids is ~4 µmol/g Ru, while that of all polyols, except sorbitol and isopropanol, is ~0.8 µmol/g Ru. These results suggest that there two different methods of adsorption. The molecular size does not vary significantly between LA and C3 polyols, ruling out simple steric effects as an explanation for the differences observed.

For polyol adsorption, a minimum of one terminal hydroxyl group is needed; this is supported by the lack of adsorption in the case of IPA. The inhibition of adsorption of polyols by hydrogen pre-saturation of the Ru surface is evidence supporting dehydrogenation as the first step hydrogenolysis of polyols.

Table 6-1: Contrasting adsorption properties on Ru sponge of organic acid and polyol.

Organic Acids	C3 polyols
Adsorption ~4 μmol/g Ru	Adsorption ~0.8 μmol/g Ru
No H_2 influence	Strong H_2 influence
Consistent with H_2 adsorption (2 Ru atoms/ acid molecule)	Consistent with ~30Å^2/ molecule (~10 atoms/molecule)
No degradation	Dissociative with degradation

7 AQUEOUS PHASE ADSORPTION ON ACTIVATED CARBON

7.1 Experimental methods

7.1.1 Carbon characterization

The carbons used in this study were a 0.8 mm extrudate activated carbon (ROX 0.8, lot #520020, Norit Americas, Marshall, TX) and a powder activated carbon (designation 3310, lot #28850, Johnson Matthey, Sevierville, TN). Both of these carbons have served as support materials for catalysts we have used in GO hydrogenolysis, and lactic acid hydrogenation studies. The total surface area of each carbon was characterized by BET nitrogen physisorption at 78 K over a relative pressure of P/P_0 from 0.0 to 0.2 in a Micromeritics ASAP 2010 (Micromeritics Instrument, Norcross, GA). Surface area was calculated from the BET equation; micropore volume was determined using the t-plot method and total pore volume was characterized as volume adsorbed at the maximum relative pressure of 0.99. A summary of the carbon characterization results is given in **Table 7-1**.

Table 7-1: Carbon characterization by N_2 adsorption at 78 K.

Carbon Type	3310	ROX
BET Surface Area (m^2/g)	715.6	833.6
Micropore Area (m^2/g)	374.8	585.8
Total Pore Volume (cm^3/g)	0.654	0.536
Micropore Volume (cm^3/g)	0.173	0.272

7.1.2 Isothermal adsorption measurements

The quantity of material adsorbed onto activated carbon in this study was determined by the difference in initial and final species concentration in solution, which were measured prior to and following exposure to activated carbon catalyst supports, respectively.

$$C_{AS} = \frac{(C_{Ao} - C_A) \cdot V_{solution}}{m_{carbon}} \tag{7-1}$$

Isothermal adsorption experiments at 25°C were performed using 8.5 mL glass vials with Teflon-lined plastic lids. The vials were initially washed in HPLC-grade water, air-dried, and weighed in preparation for experiments. Carbon was weighed and added to the vials based on the total concentration of the solute(s) to be studied (0.1g carbon ≤ 0.1 M < 0.5g carbon ≤ 0.750 M < 1.0g carbon ≤ 2.0 M) in order to maintain at least a 15% change in solution concentration before and after adsorption. A quantity of solution of known concentration was then added to the vials to give approximately 7mL total solution + carbon in the vial. The final vial weight was then recorded for analysis following reaction. The vials

were capped and rotated end-over-end on a rotator overnight to ensure thorough mixing and equilibration. Upon removal from the rotator, the vials were either centrifuged or left standing for approximately 30 minutes to allow the suspended carbon in the sample to settle. One milliliter samples were then taken and analyzed via HPLC using the method described below.

7.1.3 Elevated temperature adsorption experiments

Adsorption measurements were performed at elevated temperatures (40°C – 160°C) using a Parr 5000 multireactor system (Parr Instrument Company, Moline, IL). This system has six 75mL stainless steel reactors with internal stirring, independent temperature control, and continuous pressure monitoring. For these experiments, the reactors were cleaned and air-dried, and then carbon was added to the reactors according to the solution concentration to be examined: one gram of carbon was used for 0.05 M and 0.2 M concentrations of GO or PG, and four grams were used for a 0.5 M concentration. A Teflon stir-bar and 60mL of solution were added to the reactor. All starting, intermediate, and final weights were recorded. The desired temperature was set and the reactor contents were held for at least two hours at the desired temperature, after which a liquid-phase sample was taken. (The two-hour equilibration time was verified by room temperature experiments in vials for different time periods from 0.5 to 24 hr.) Sampling consisted of removing 1.5mL of waste to clean the sampling line, followed by removal of 1.0 mL as a sample. Typically, multiple temperatures between 40 and 160°C were examined in each experiment. All

waste aliquots and samples were collected and weighed at the conclusion of the experiment to check for mass loss via system leaks. Samples were analyzed using the HPLC method described below.

7.1.4 Analysis

All samples from adsorption experiments were analyzed using a high pressure liquid chromatography system consisting of a Waters 717 Plus autosampler (Waters Corporation, Milford, MA), a Perkin Elmer pump (Perkin Elmer, Wellesley, MA), a Waters 410 differential refractometer, and a Perkin Elmer LC 90 UV spectrophotometric detector. The system used a Bio-Rad HPX87H column (Bio-Rad Laboratories, Hercules, CA) with 5mM sulfuric acid solution as the mobile phase. The column was operated isocratically at 50°C and a mobile phase flow rate of 0.6 ml/min.

A sample injection size of five microliters was used for samples above 0.1 M concentration; ten microliter injections were used for samples below or at 0.1 M. Samples with a concentration above 0.5 M were diluted by a factor of four to maintain an injected concentration between 0.1 M and 0.5 M. A three-point calibration curve was used to determine response factors – no internal standards were thus used in determining species concentrations.

7.1.5 Adsorption modeling

The remainder of this chapter will discuss modeling of single component and multi-component adsorption; therefore the general method for fitting

experimental data to Langmuir and Freundlich adsorption models is discussed in this section. Unless noted, the notations used for modeling are give in **Table 7-2**.

All data from single component vial adsorption experiments at 25°C were modeled using both the Freundlich and Langmuir isotherms to obtain adsorption constants at room temperature.

Freundlich: $$C_{AS} = K_F \, C_A^{\,n} \tag{7-2}$$

Langmuir: $$C_{AS} = \frac{K_A \, C_A \, C_{TA}}{1 + K_A \, C_A} \tag{7-3}$$

Goodness of Fit: $$X^2 = \frac{\sum_{i=1}^{n} (C_{ASi}^{exp} - C_{ASi}^{cal})^2}{n} \tag{7-4}$$

For the Freundlich isotherm, the coefficients K_F and n were found by a least-squares fitting of experimental data as C_{AS} vs C_A with predicted C_{AS} using solver in Microsoft Excel. Goodness of fit (χ^2) is the average residuals squared. The coefficients for the Langmuir isotherm (K_A, C_{TA}) were found using the same procedure. Our published adsorption of GO and PG on activated carbon uses the more traditional method, where the Freundlich isotherm coefficients, K_F and n were found by a least-squares linear regression of experimental data as $ln(C_{As})$ vs. $ln(C_A)$ to give slope n and intercept $ln(K_F)$. Goodness of fit (R^2) is given by Microsoft Excel. For the Langmuir isotherm, a plot of experimental data as (C_A/C_{As}) vs. C_A gives a slope $1/C_{TA}$ and an intercept ($1/K_AC_{TA}$). The traditional method was more cumbersome to use and also tended to weigh small quantities adsorbed more heavily.

Table 7-2: General notation used for modeling adsorption on activated carbon

C_A	Observed solution concentration of species A in equilibrium with carbon (M)
C_{Ao}	Initial solution concentration of species A prior to adsorption (M)
C_{AS}	Concentration of solute A in activated carbon adsorbent (mol/kg carbon)
C_{TA}	Maximum concentration of A in activated carbon adsorbent (mol/kg carbon)
ΔH_A	Heat of adsorption (kJ/mol)
K_0	Van't Hoff constant (M^{-1})
K_A	Langmuir adsorption model equilibrium constant for adsorption of solute A (M^{-1})
K_F	Constant in Freundlich isotherm model ($mol/M^n/kg$)
m_{carbon}	mass of carbon in solution (kg)
n	Exponent in Freundlich isotherm model equation
R	Ideal gas constant (8.31 J/mol/K)
T	Temperature (K)
$V_{solution}$	Volume of solution (liter)
Subscript A,B	Denotes component, either glycerol or propylene glycol

7.1.6 Summary of experiments performed

In our lab, the catalyst used for most hydrogenation/hydrogenolysis work is 5% Ru/C (PMC 3310). For this reason, the majority of adsorption experiments are on 3310 carbon, the support used on the Ru/C catalyst obtained directly from the manufacturer. The substrates were selected to match with Chen's[68] hydrogenation experiments and include organic acids, primary alcohols, diols, and glycerol. Examination of an additional carbon, Norit ROX, was included to help with our mechanistic investigations of glycerol hydrogenolysis; on that support only GO and PG were studied. **Table 7-3** summarizes adsorption experiments covered in this work.

Table 7-3: Summary of experiments preformed during the study of aqueous phase adsorption on activated carbon.

Compound	3310 carbon	ROX carbon	Reduced Catalyst (5%Ru/C 3310)
Formic acid (FA)	I		
Acetic acid (AA)	I		
Glycolic Acid (GA)	I		
Propanoic acid (PA)	I,V		V
Lactic acid (LA)	I,V		V
Ethanol (EtOH)	I		
n-propanol (n-prOH)	I,V		V
Ethylene glycol (EG)	I,V		
Propylene glycol (PG)	I,V	I,V	
1,3-propane diol (1,3-PD)	I		
Glycerol (GO)	I,V	I,V	
LA&PA	EI,xV		
LA&PG	EI, xV		
LA&n-prOH	EI, xV		
PA&PG	xV		
PA&n-prOH	EI,xV		
GO&PG	xI,xV	xI,xV	
EG&PG	EI		

I=isothermal adsorption; EI= equimolar isothermal adsorption; xI=variable mole fraction isothermal adsorption; V=variable temperature adsorption; EV= equimolar variable temperature adsorption; xV=variable mole fraction variable temperature adsorption.

Single component adsorptions on 3310 carbon were done with organic acids, primary alcohols, diols, and glycerol. Adsorption of equimolar mixtures of LA&PA, LA&PG, PA&PG, GO&PG, and EG&PG were examined. Variable temperature (40°C – 160°C) adsorption measurements of LA, PA, n-PROP, EG, PG, GO, LA&PA, and GO&PG were done on 3310 carbon.

Control experiments were carried out in vials or in the reactor without addition of carbon. No degradation or loss of PG or GO was observed at any temperature. Experiments in which total vial or reactor weight after experiment differed from initial weight by more than ± 2%, indicative of a leaking vessel, were discarded.

7.2 Glycerol and propylene glycol

7.2.1 Isothermal adsorption of GO+PG on ROX activated carbon

Adsorption experiments were conducted at room temperature (25°C) in glass vials for substrate solution concentrations ranging from 0.01 M to 2.0 M. **Figure 7-1** compares the experimental quantities adsorbed with those predicted by the Freundlich and Langmuir isotherm models for individual adsorption of GO and PG on ROX activated carbon. A summary of the calculated parameters at room temperature for each adsorption isotherm is given in **Table 7-4**. As can be seen, the Langmuir isotherm gives the best fit of GO adsorption over the entire concentration range studied.

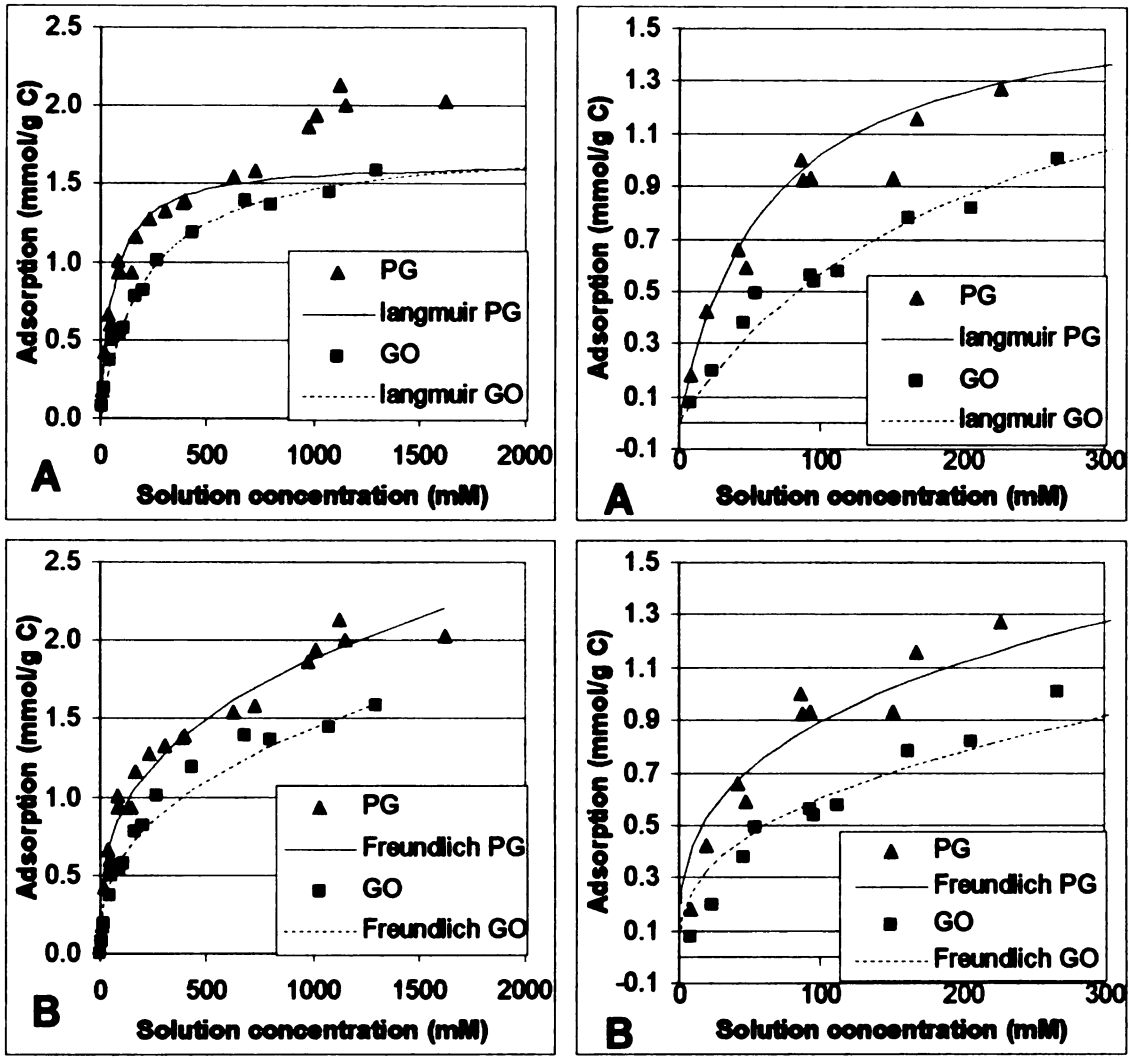

Figure 7-1: Experimental and predicted a) Langmuir and b) Freundlich adsorption isotherms for PG and GO at 25°C on ROX carbon.

For PG, the Langmuir model gives the best fit below 0.75 M, but the Freundlich model better describes the data at concentrations above 0.75 M. The observed isotherm for PG suggests that the quantity adsorbed reaches a plateau at the Langmuir maximum of C_{TA} ~1.64 mol/kg at about 0.75 M in solution and then adsorbs by another mechanism at higher concentration. In Section 7.5 a new adsorption model is proposed that takes in to account two different modes of adsorption, micropore filling, and surface adsorption. In micropore filling the

adsorption energy is significantly higher than that found for surface adsorption. Micropore filling dominates at low concentrations, while at high concentrations both modes contribute to the observed adsorption. Filling of the micropores has a relatively constant energy of adsorption and is best represented by the Langmuir isotherm. In the Fruendlich adsorption isotherm, adsorption energies are dependent on coverage, making it better able to predict adsorption at higher concentrations where both adsorption modes are active.

Table 7-4: Langmuir and Freundlich isotherm coefficients for GO and PG on ROX carbon.

	GO	PG		GO	PG
Langmuir			**Freudlich**		
CTA (mol/kg)	1.77	1.64	K_F	0.105	0.202
$K_{A,298K}$ (M^{-1})	4.75E-03	1.63E-02	n	0.379	0.323
R^2 Fit	0.983	0.997	R^2 Fit	0.946	0.916

Glycerol shows no tendency to adsorb beyond its Langmuir maximum of C_{TA} = 1.77 mol/kg. While the reported value of the Langmuir C_{TA} for GO is ~8% larger than that for PG, we do not believe that the difference in the two values is significant. Because GO and PG have nearly identical molar volumes of 73.0 mL/mol, the volume of species adsorbed according to the Langmuir model is likewise similar. It is significant, however, that the molar quantity of PG adsorbed is greater than that of GO at any concentration below the Langmuir maximum; this is reflected by the fact that the calculated adsorption equilibrium constant for PG is approximately three times that for GO. Interestingly, the mass of GO and

PG adsorbed at any concentration is nearly identical (**Figure 7-2**); we assume this is coincidental but worth noting.

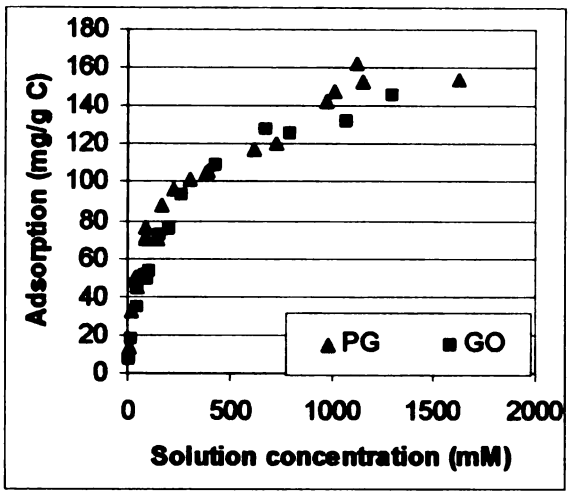

Figure 7-2: Adsorption of PG and GO on ROX carbon on a mass basis.

Using the measured ROX carbon micropore volume of 0.27 cm^3/g, the micropore concentrations of PG and GO corresponding to C_{TA} at room temperature can be calculated to be 6.07 M and 6.55 M, respectively. This is 44% and 48%, respectively, of the pure component molar concentration of 13.7 M for both PG (1.04 g/cm^3) and GO (1.26 g/cm^3). Assuming that the density of PG/water and GO/water varies linearly with mass concentration, the remaining micropore volume is filled with water (the only other species present) at a concentration of 29.0 M for GO and 31.0 M for PG. This approximate 5:1 molar ratio of water to GO or PG is similar to the result reported by Parsons *et al.* [69] in their analysis of glycerol aqueous solutions – they report that all water is associated with glycerol and solution behavior changes significantly at a glycerol mole fraction of ~0.15 (5.6:1 molar ratio). Thus it appears that glycerol retains water associated by hydrogen bonding when adsorbed into the carbon. On the other hand, the continued adsorption of PG beyond the Langmuir model value of

C_{TA} may be because PG is less hydrophilic than PG and thus sheds solvating water to reach a higher concentration in the pore as PG solution concentration is increased above 1.0 M. A second paper by Parsons and Koga [70] on PG-water solutions supports this interpretation of lower PG hydrophilicity in solution. The less hydrophilic nature of PG also accounts for its larger adsorption equilibrium constant relative to GO; PG favors residence in the carbon pores rather than in bulk solution.

7.2.2 Isothermal adsorption of GO+PG on 3310 activated carbon

Isothermal adsorption on the Johnson-Matthey 3310 powder activated carbon, as with the ROX carbon, follows the Langmuir isotherm model closely for PG and GO solution concentrations up to 0.75 M. A summary and comparison of the results for the ROX and 3310 carbons fit to the Langmuir isotherm are found in **Table 7-5**. As can be seen, the values of C_T for GO and PG are similar on the 3310 carbon, in agreement with the results found for the ROX carbon. If the 3310 carbon micropore volume of 0.17 cm^3/g is used, the concentrations of species in the micropores at the maximum Langmuir concentration C_{TA} are 6.35 M and 7.0 M for GO and PG, respectively. These values are very close to the values of 6.5 M and 6.1 M obtained on the ROX carbon, indicating that adsorption is strongly associated with the micropore volume of each carbon. Further, if the additional PG adsorption (up to 2.0 mol/kg) on the ROX carbon is considered, the micropore concentration for PG on the ROX carbon becomes 7.35 M, very close to the PG value of 7.0 M for the 3310 carbon. Thus the absolute and relative quantities of PG and GO adsorbed in the micropores of the

two carbons are similar; this is supported by the ratio of adsorption constants (K_{PG}/K_{GO}) at 298 K (**Table 7-5**), which are 3.6 and 3.4 for the 3310 carbon and the ROX carbon, respectively. However, the affinity of PG and GO for the 3310 carbon is greater than that for the ROX carbon, as the ratio (3310/ROX) of adsorption constants (K_A) at 25°C for GO and PG is 1.32 and 1.39, respectively. The greater adsorption affinity for the 3310 carbon may result from differences in surface functionality or in micropore structure, considering the two carbons come from different sources.

Table 7-5: Comparison of Langmuir isotherm coefficients for ROX carbon and 3310 carbon.

Carbon Type		C_{TA} (mol/kg)	$K_{A,25\,C}$ (M^{-1})
GO	ROX	1.77	4.75E-03
	3310	1.10	6.25E-03
PG	ROX	1.64	1.63E-02
	3310	1.22	2.28E-02

7.2.3 Elevated temperature adsorption

Quantities of GO and PG adsorbed onto ROX and 3310 carbon were determined at concentrations from 0.1 to 0.5 M and temperatures from 313 to 433 K. At each temperature, the equilibrium constant (K_A) for the Langmuir model was calculated using C_{TA} determined from isothermal adsorption experiments at 298 K. The equilibrium constant is assumed to vary with temperature based on

the Van't Hoff equation, as the Langmuir model assumes all adsorption sites have equal binding energies and thus the heat of adsorption (ΔH) is constant.

$$\ln(K_A) = -\frac{\Delta H}{R} * \frac{1}{T} + \ln(K_0) \qquad (7\text{-}5)$$

For each species, the plot of ln (K_A) vs. 1/T (absolute) from experiments was fitted with a straight line via least squares linear regression to give the heat of adsorption (ΔH) from the slope (-ΔH/R) and the preexponential constant (K_o) from the intercept ln(K_o). The plots for GO and PG on ROX and 3310 are seen in **Figure 7-3** and the calculated heats of adsorption and preexponential factors are given in **Table 7-6.**

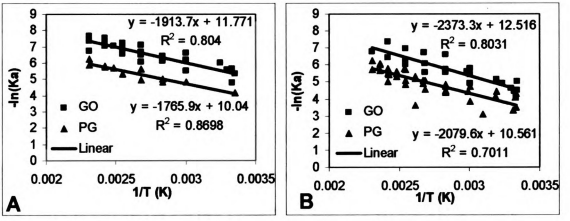

Figure 7-3: Temperature dependence of Langmuir equilibrium constant K_A for GO and PG on ROX (**A**) and 3310 (**B**) carbon.

It is seen that the data follow the Langmuir model well over the measured temperature range of 298 K – 433 K for both carbons. The heats of adsorption of GO and PG are both approximately 15 kJ/mol (3.6 kcal/mol) on ROX carbon, while on 3310 carbon GO is 14 kJ/mol and PG is some what higher at 22 kJ/mol. This is indicative of similar van der Waal's type forces and weak hydrogen bonding responsible for adsorption of each species.

Table 7-6: Langmuir isotherm coefficients for GO and PG on ROX carbon

	ROX		3310	
	GO	PG	GO	PG
Langmuir				
C_{TA} (mol/kg)	1.77	1.64	1.10	1.22
$K_{A,296K}$ (M^{-1})	4.75E-03	1.63E-02	6.25E-03	2.28E-02
ΔH (kJ/mol)	-15.91	-14.68	-14.02	-22.32
K_0 (M^{-1})	7.73E-06	4.36E-05	1.95E-05	4.36E-06
R^2 Fit				

7.2.4 Two component adsorption studies

Aqueous solutions of PG and GO at total species concentrations ranging from 0.05 to 0.5 M and species fractions of PG and GO ranging from 0 to 1.0 were conducted at room temperature on ROX carbon and at elevated temperatures on both ROX and 3310 carbon. The extended Langmuir model (Eq. (7-6) and (7-7)) has been applied as the model of choice for mixed solute adsorption; the denominator of the extended Langmuir model accounts for competitive adsorption of the two species (A=GO; B=PG) into the activated carbon micropores.

$$C_{AS} = \frac{K_A C_A C_{TA}}{1 + K_A C_A + K_B C_B} \tag{7-6}$$

$$C_{BS} = \frac{K_B C_B C_{TB}}{1 + K_A C_A + K_B C_B} \tag{7-7}$$

All coefficients (C_{TA}, C_{TB}, ΔH_A, ΔH_B, K_{Ao}, K_{Bo}) required in the extended Langmuir model were taken from the single component results reported in **Table 7-6**.

Figure 7-5 shows the predicted dual component adsorption isotherms on ROX carbon at 25 °C and total initial concentrations of 0.05 M, 0.3 M, and 0.5 M. The abscissa in **Figure 7-5** is the fraction of glycerol in the total solute present (GO/(GO+PG)) – not mole fraction in solution. The data are reported in this fashion to show comparison of model with experiment and accentuate the different adsorption behavior of GO and PG. It is seen that the extended Langmuir model accurately predicts the adsorption of propylene glycol and glycerol over the studied concentration range. The preference for PG adsorption is clear; in fact, at equimolar concentrations the quantity of PG adsorbed is approximately three times that of GO, in accordance with the ratio of equilibrium constants determined in single component experiments. The adsorption on 3310 shows similar behavior as ROX only with higher adsorption quantities. Predicted and experimental isotherms for GO and PG on 3310 can be found in Appendix B (**Figure B-1**). It should be noted that predicted GO values are higher then experimentally found but the experimental data has a lot of scatter.

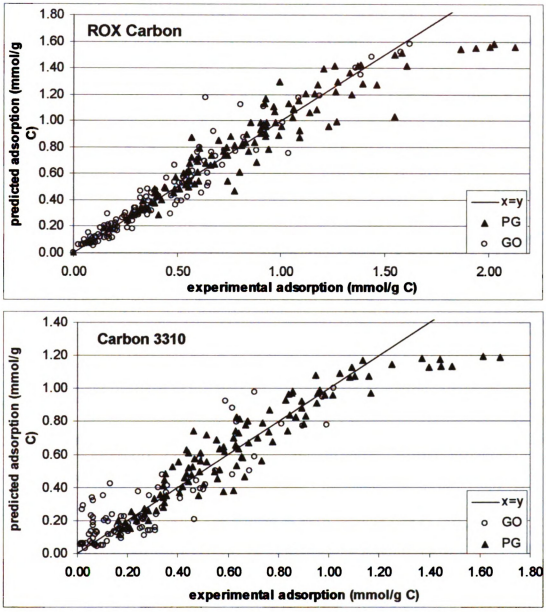

Figure 7-4: Experimental vs predicted adsorption of PG and GO on ROX carbon and 3310 carbon for all data.

Performance of the extended Langmuir model for GO and PG on ROX carbon and 3310 is shown in **Figure 7-4,** which compares experimental to predicted values. All data are included (single and dual component isothermal and variable temperature data)

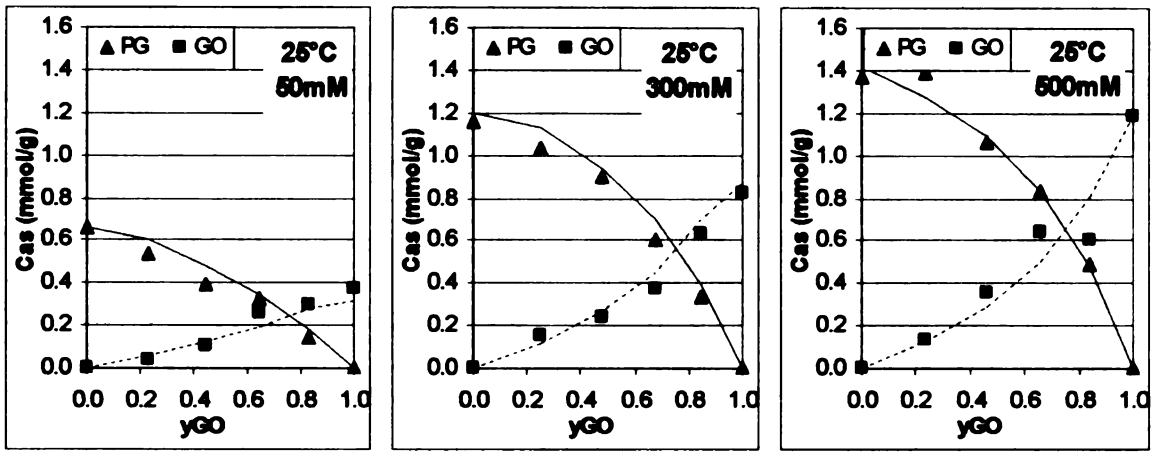

Figure 7-5: Experimental and predicted Langmuir isotherms for mixtures of GO and PG on ROX carbon at 25 °C and 0.05 M, 0.3 M and 0.5 M total species concentration. Abscissa is fraction of GO in the total species (GO + PG) present. Lines are the predicted isotherms.

Figure 7-6 shows the predicted isotherms at a total initial concentration of 0.5 M and temperatures of 80 °C, 120 °C, and 160 °C. The predicted values again show good agreement with experimental data, and validate the assumption of constant heat of adsorption over the range of concentrations and temperatures investigated.

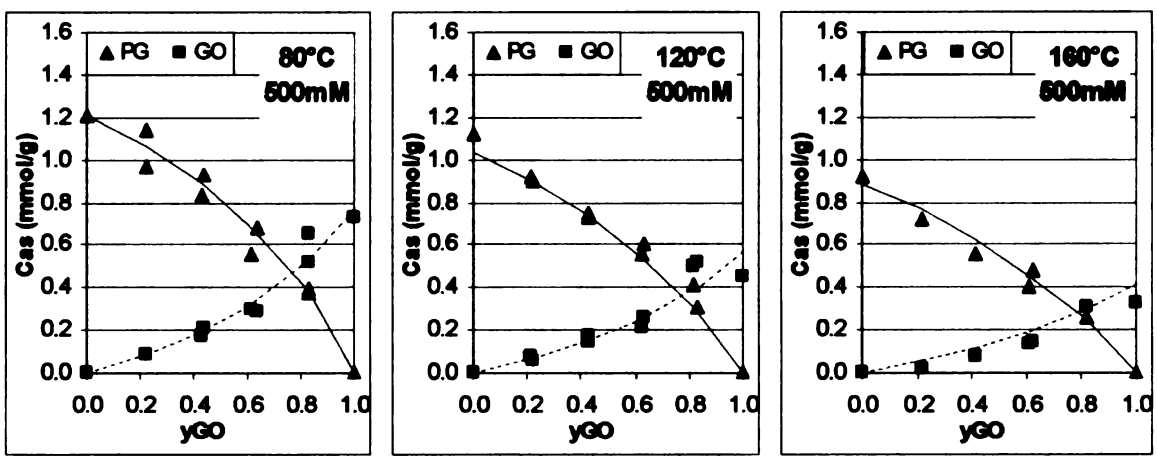

Figure 7-6: Experimental and predicted Langmuir isotherms for mixture of GO and PG on ROX carbon at 0.5 M total species concentration and 80 °C, 120 °C, and 160 °C. Abscissa is fraction of GO in the total species (GO + PG) present. Lines are the predicted isotherms.

The adsorption data clearly show that PG and GO concentrations in the carbon pore structure are significantly different than those in bulk solution. This obviously affects the interpretation and kinetic modeling of reactions taking place over activated carbon catalysts. **Figure 7-7** shows the extended Langmuir model predictions of GO and PG pore concentrations, based on the measured micropore volume, in ROX activated carbon at a temperature of 180°C for different bulk GO and PG concentrations. GO pore concentration is only modestly different than GO solution concentration at this temperature, while PG pore concentration is approximately five-fold larger than its corresponding solution concentration.

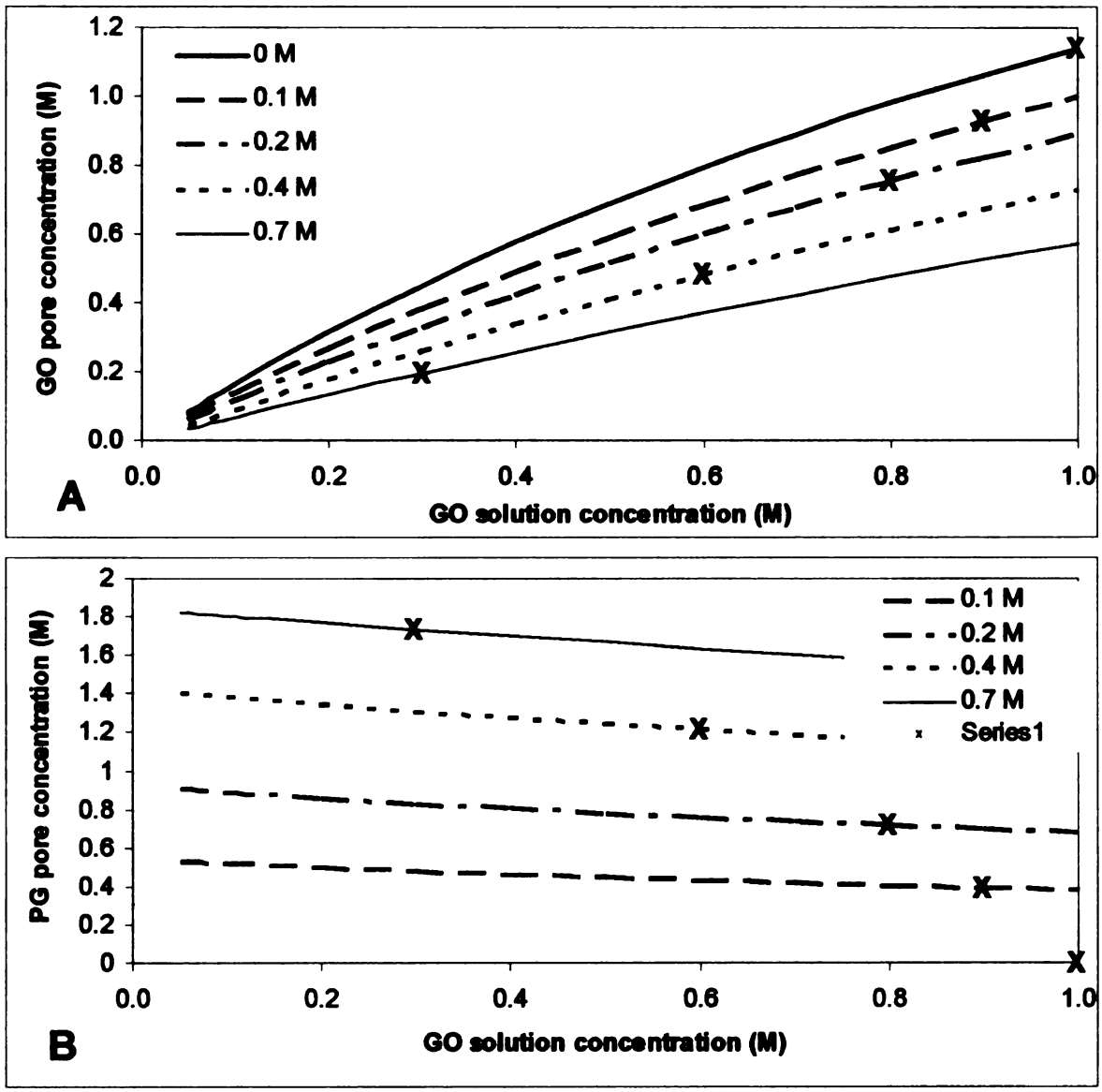

Figure 7-7: Extended Langmuir model predictions of a) GO and b) PG pore concentrations in ROX carbon at 180 °C. Symbols represent trajectory of 1.0 M GO conversion to PG.

The presence of PG lowers GO pore concentration significantly, while the presence of GO only affects PG pore concentration slightly. The "x" symbols in **Figure 7-7** represent an idealized (100% selective) reaction trajectory of GO hydrogenolysis to PG starting with 1.0 M GO solution. During reaction, GO pore concentration declines more rapidly than does solution concentration – converting 70% of GO to PG, which lowers solution GO concentration from 1.0 M

to 0.3 M, reduces the corresponding GO pore concentration from 1.15 M to 0.19 M, a six-fold decrease. At the same time, PG concentration increases from zero to 0.7 M in solution, and to nearly 1.8 M in the pore. These differences deviate from bulk solution concentrations to a significant enough extent that they must be accounted for in accurate kinetic modeling of GO hydrogenolysis over activated carbon catalysts. Moreover, the local concentrations may depend on the particular carbon support in use, so that any comparisons between carbon catalysts must include comparison of the adsorption properties of reactants and products.

7.2.5 Conclusion

The adsorption of propylene glycol and glycerol over two activated carbon supports has been examined over a broad range of concentrations (0.005 M to 1.5 M) and temperature (298 – 433 K). Adsorption of individual species is well-represented by the Langmuir isotherm, and simultaneous adsorption of the two species is described by an extended Langmuir model that uses the single-component adsorption constants and accounts for competitive adsorption between the two species. The overall quantities of PG and GO adsorbed are comparable and are closely related to the carbon micropore volume. Propylene glycol exhibits an enhanced affinity for adsorption relative to glycerol, with its equilibrium constant approximately 3.5 times that for glycerol. This enhanced adsorption is attributed to the less hydrophilic nature of PG, which favors its presence in the carbon micropores vs. the bulk solution, and also accounts for

the lower extent of solvation of PG via hydrogen bonding. The adsorption model shows that pore concentrations in liquid phase reactions using activated carbon catalysts can be significantly different than the corresponding concentrations in the surrounding solution.

7.3 Ethanol, n-propanol, EG, and 1,3-PDO adsorption

Adsorption of ethanol, n-propanol (n-prOH), ethylene glycol (EG), and 1,3-propanediol (1,3-PDO) are compared in **Figure 7-8** and include the Langmuir and Fruendlich predicted adsorption. It should be noted that both models were fit over the entire concentration range. The Fruendlich model predicts the observed adsorption better for all species at concentration >200 mM. The predicted concentration needed to adsorb 1 mmol of substrate per gram carbon is 734 mM for EG (0.017), 213 mM for 1,3-PDO (0.091), 162 mM for ethanol (0.49), and 34 mM for n-prOH (1.78), this is consistent with the order of the K_{ow} value given in parenthesis. K_{ow} is the distribution coefficient between octanol and water as defined in the literature.[71]

On 3310 carbon both the Langmuir and Fruendlich adsorption models perform worse than on ROX carbon, which could be due to the large micropore volume found in ROX. In Section 7.5, a new adsorption model is proposed that gives better performance for organic acids, PG, and n-prOH. It is expected that it would also perform better for ethanol, EG, and 1,3-PDO but it was not tested on these compounds.

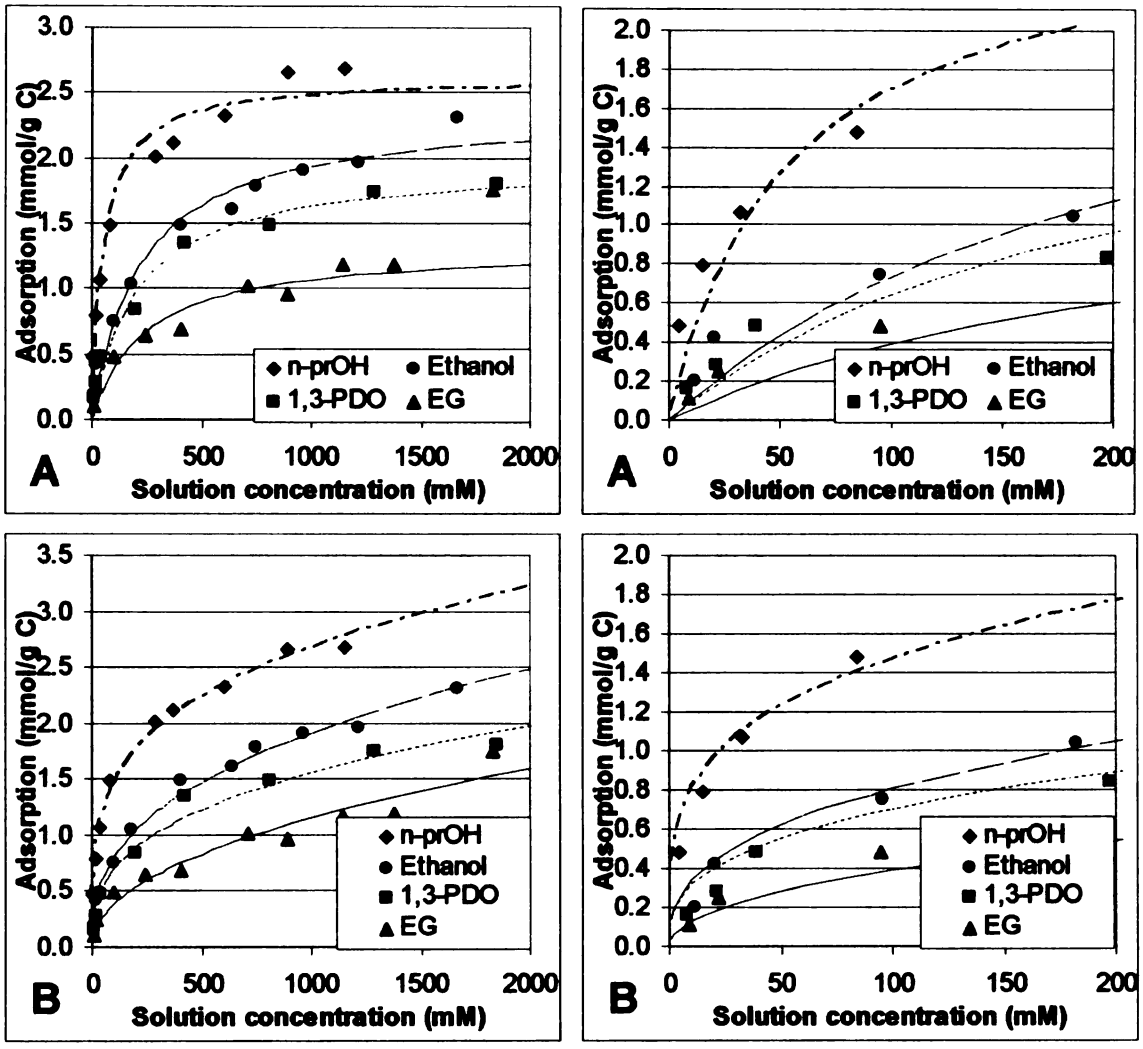

Figure 7-8: Experimental and best fit data for isothermal adsorption of n-propanol (n-prOH), ethanol, 1,3-propanediol (1,3-PDO), and ethylene glycol (EG) on 3310 carbon at 25 °C. (**A**-Langmuir, **B**-Fruendlich)

7.4 Organic acids

The effect of chain length was examined in the adsorption of formic acid (FA), acetic acid (AA), and propanoic acid (PA). **Figure 7-9** compares the experimental quantities adsorbed with those predicted by the Freundlich and

Langmuir isotherm models for individual adsorption of FA, AA, and PA on 3310 carbon.

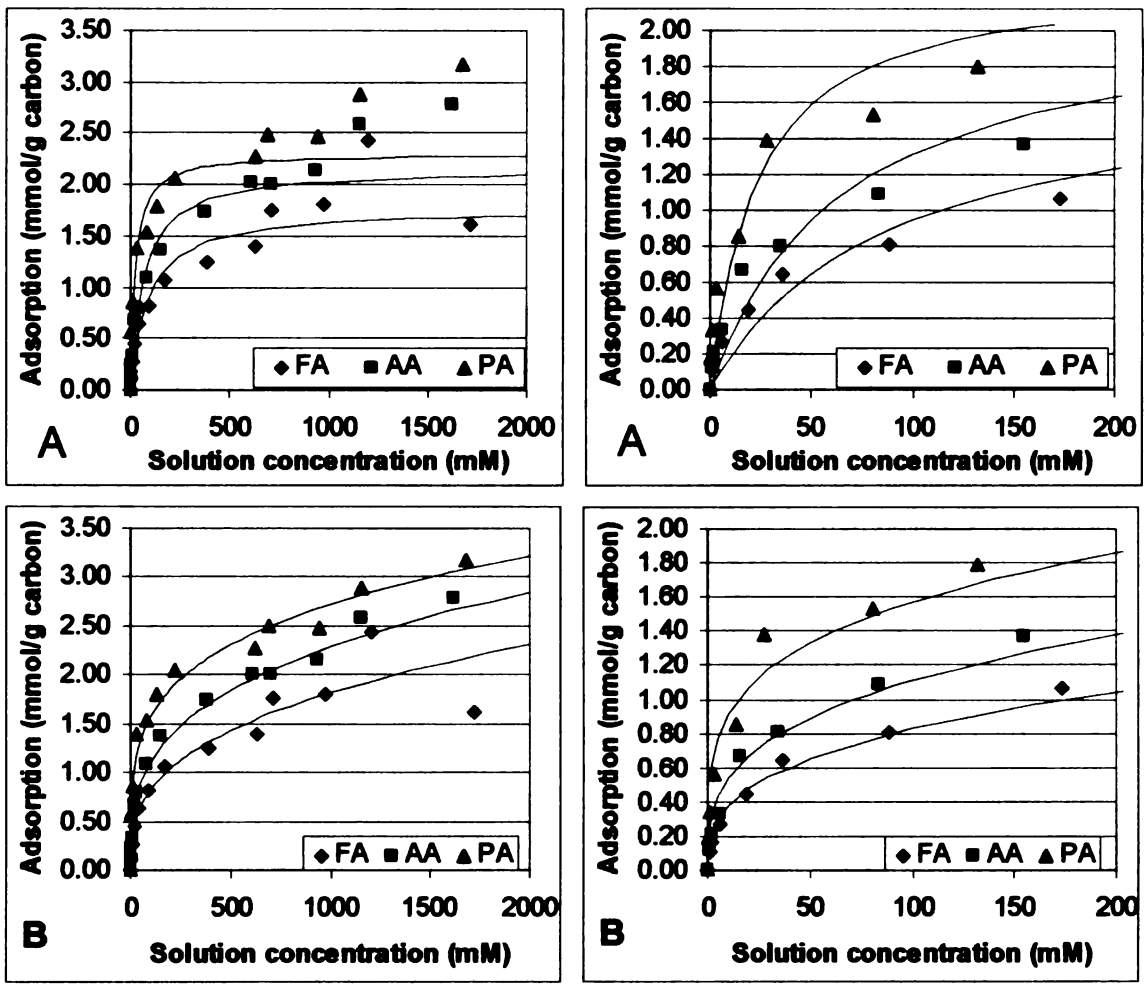

Figure 7-9: Experimental and best fit data for isothermal adsorption of formic, acetic, and propanoic acid on 3310 carbon at 25 °C. (**A**-Langmuir, **B**-Fruendlich)

As can be seen, the Freundlich isotherm gives a better fit for all three acids over the entire concentration range studied. Examining the adsorption at high concentration, we see that AA and PA adsorb ~3 mmol/g C while the FA is closer to 2.2 mmol/g C. The last two data points for the FA do not fit the Freundlich model. Including these points in fitting the Freundlich model results in decreasing adsorption (~2 mmol/g C) while overestimating the adsorption at low

concentrations. Looking at the predicted concentration needed to adsorb 1 mmol of acid, PA (16 mM) is adsorbed much more strongly than AA (72 mM) which is stronger then FA (176mM). This behavior could simply be explained by the increased organic character from FA<AA<PA. A similar trend can be seen in the octanol-water distribution coefficient (K_{ow}) for each acid; 0.58, 0.84, 1.39.

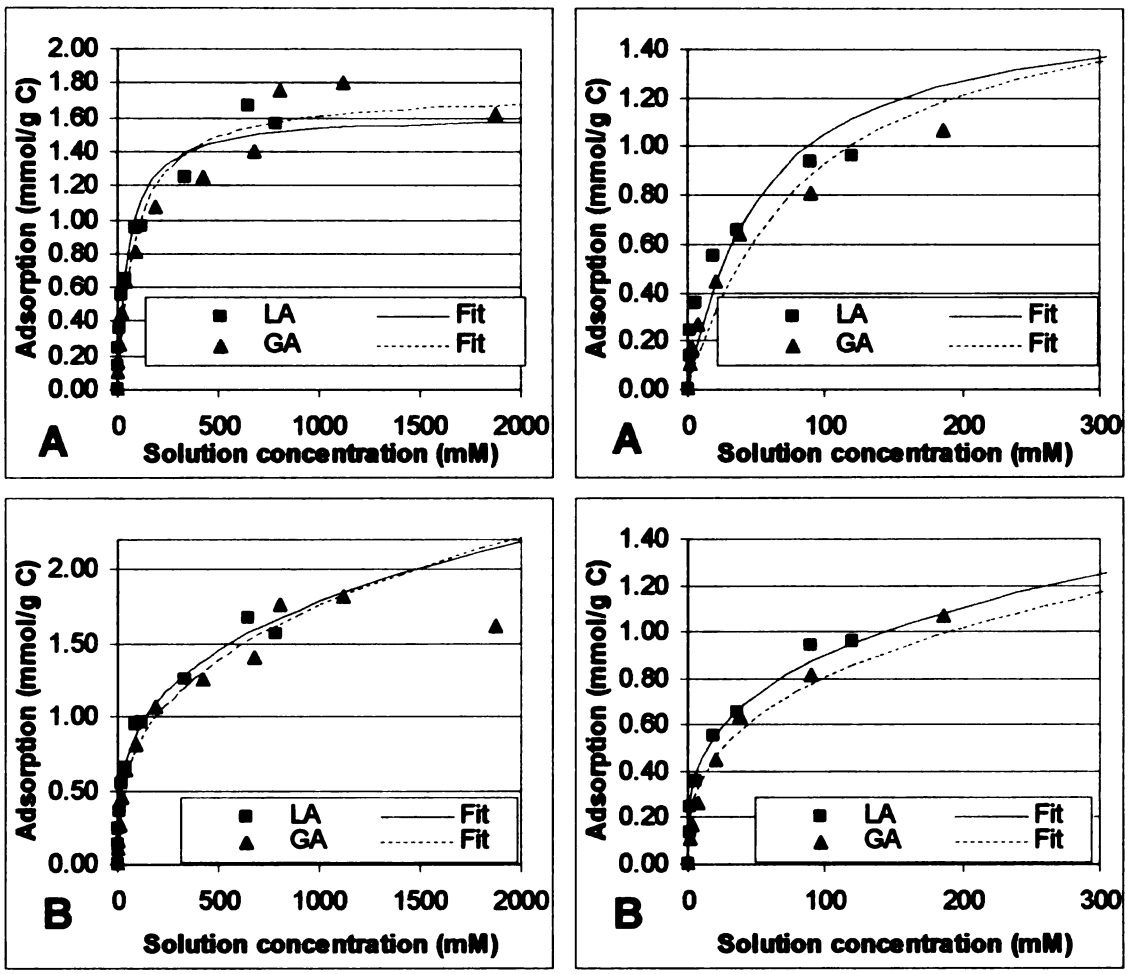

Figure 7-10: Experimental and best fit data for isothermal adsorption of glycolic and lactic acid on 3310 carbon at 25 °C. (**A**-Langmuir, **B**-Fruendlich)

Glycolic acid and lactic acid are compared in **Figure 7-10** and show almost identical adsorption behavior. It should be noted that LA data only goes to 800 mM; this was done to prevent any dimer adsorption. Again, the Fruendlich

model nicely predicts the observed adsorption of ~2 mmol/g C. The adsorption of GA appears lower than LA, but this is well within experimental error. The predicted concentration needed to adsorb 1 mmol of acid is 190 mM for GA and 142 mM for LA; this puts it in the same range as FA (176 mM). LA appears to adsorb to a slightly higher extent than FA, which is counter to the behavior predicted from the K_{ow} values LA(0.49) and FA(0.58). GA has the lowest K_{ow} value of 0.33, and is also the least adsorbed.

Figure 7-11 shows the adsorption of equimolar mixtures of PA+LA and PA+PG on 3310 carbon at 25 °C. The Fruendlich isotherm prediction of adsorbed pure PA is shown for reference. Solution concentrations and the amounts adsorbed were each summed for PA and LA and plotted as PA+LA. PA adsorption in the mixture is less than the pure component adsorption, indicating that LA competes with PA. When we look at the mixture of PA+PG, this is not the case. This result suggests that PG does not compete with PA and is excluded from the carbon. It should be noted that at higher total concentration (>500 mM) the adsorbed amount of PA appears less than that for pure PA, but this is merely the result of defining total solution concentration as the sum of the PA and PG concentrations.

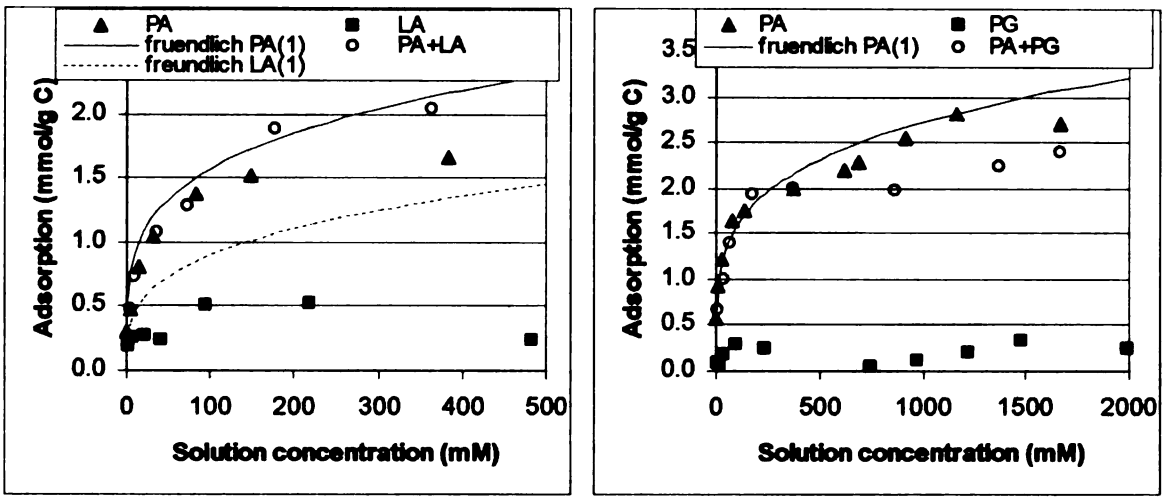

Figure 7-11: Isothermal adsorption of equimolar mixtures of PA+LA (**A**) and PA+PG (**B**) on 3310 carbon at 25 °C.

Adsorption of equimolar mixtures of PA+PG and LA+PG is shown in **Figure 7-12**. PG appears not to inhibit adsorption of LA to any significant extent, while LA inhibits the adsorption of PG. The temperature dependence of organic acid adsorption was only examined for LA and PA and will be discussed in the multi-component modeling section.

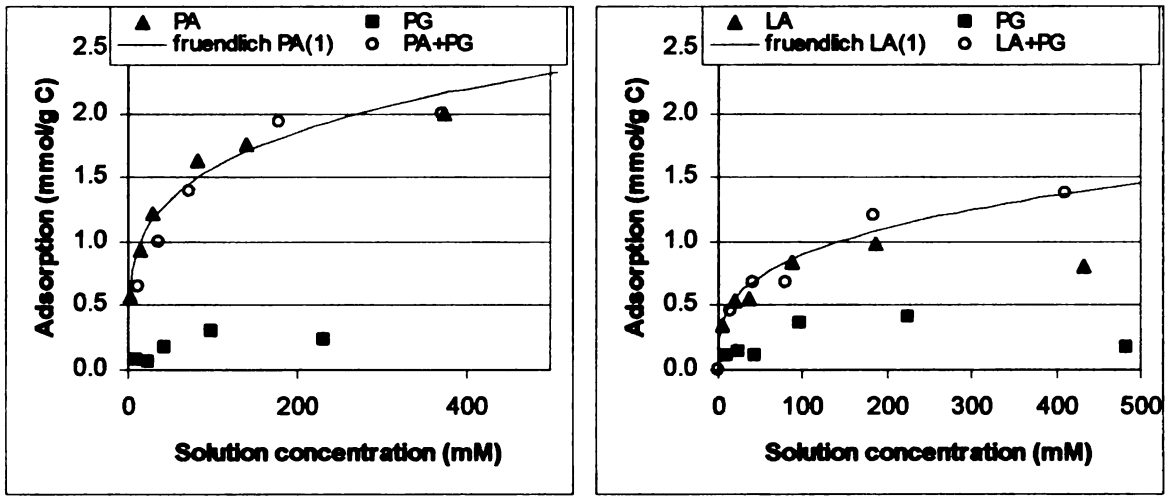

Figure 7-12: Isothermal Adsorption of equimolar mixtures of PA+PG (**A**) and LA+PG (**B**) on 3310 carbon at 25 °C.

7.5 Multi component adsorption studies relevant to hydrogenation of LA and PA to PG and n-prOH

As previously mentioned, a goal of this work is to have a comprehensive model for predicting pore concentrations of reactive species from single component data to be used in kinetic models for hydrogenation reactions of LA and PA to PG and n-prOH. Single compound isothermal and variable temperature data were collected for each species and variable temperature data were collected for combinations of LA + PA, LA + n-prOH, LA + PG(limited), PA + PG and, PA + n-prOH. Data for these experiments will be presented and discussed together with the modeling of this system.

Initial attempts to use the extended Langmuir model failed to predict the competitive nature of the adsorption, even though the Langmuir model gave a reasonable fit for single compound adsorptions. It was thought that large differences in the maximum Langmuir concentration C_{TA} for PA (2.3mmol/g) and LA (1.6mmol/g) were overestimating the effect of LA, so we adjusted the extended Langmuir model with "weighting factors" α_{AB} and α_{BA}. The adsorption is then defined by Equation 7-8 and 7-9, where $\alpha_{AB} = \frac{C_{TB}}{C_{TA}}$ and $\alpha_{BA} = \frac{1}{\alpha_{AB}}$.

$$C_{AS} = \frac{K_A C_A C_{TA}}{1 + K_A C_A + \alpha_{AB} K_B C_B} \tag{7-8}$$

$$C_{BS} = \frac{K_B C_B C_{TB}}{1 + K_A C_A + \alpha_{BA} K_B C_B} \tag{7-9}$$

This model is referred as Weighted Extended Langmuir or WEL and is also applied to PG-GO system, where it showed no significant changes ($\alpha_{AB} \approx \alpha_{BA} \approx 1$) and therefore was not used in that system. This correction did not significantly improve our model's performance in the LA-PA system.

A closer look at single compound data showed that at low concentrations (<100 mM), the adsorption of LA, PA, and n-prOH is much stronger (**Figure 7-13**).

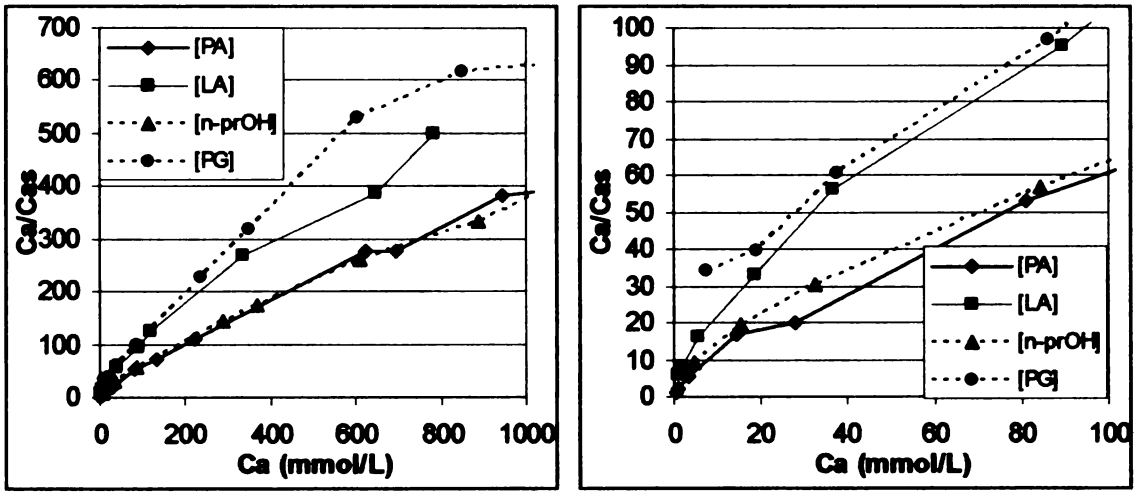

Figure 7-13 : Low concentration adsorption deviation from Langmuir isotherm at low concentration for LA, PA, PG, and n-prOH on 3310 carbon at 25°C.

We therefore propose that there are two different modes of adsorption: the filling of micro-pores, and adsorption on macro-pore surfaces. In the filling of the micro-pores, interactions of the substrate with the walls are much more pronounced compared with planar surface interactions. Each adsorption mode is assumed to follow the weighted extended Langmuir model, and the adsorption is simply the sum of both. This adsorption model will be referred to as **Dual Weighted Langmuir (DWL)**. This approach of using two part adsorption modeling

is not new; some of the literature[22, 72, 73] shows models where part of the adsorption is competitive and some is independent.

The generalized form of the DWL adsorption isotherm for *n* competing species is shown in Eq. 7-10. The labeling of constants and concentrations follows the same approach used earlier in this work, where the first subscript refers to the compound (except numbers are used in place of letters (i.e. A and B are now 1 and 2), and the last subscript designates the adsorption mode.

$$C_{ns} = \frac{C_{nt1} K_{n1} C_n}{1 + \frac{1}{C_{nt1}} \sum_{i=1}^{nt} C_{it1} K_{i1} C_i} + \frac{C_{nt2} K_{n2} C_n}{1 + \frac{1}{C_{nt2}} \sum_{i=1}^{nt} C_{it2} K_{i2} C_i} \qquad (7\text{-}10)$$

$$C_{ns} = \frac{C_{nt1} K_{n1} C_n}{1 + K_{n1} C_n} + \frac{C_{nt2} K_{n2} C_n}{1 + K_{n2} C_n} \qquad (7\text{-}11)$$

For single component adsorption, Equation 7-10 simplifies to Equation 7-11. The adsorption now depends of four parameters: C_{nt1},K_{n1} and C_{nt2},K_{n2}. C_{nt1} is limited by the micropore volume (V_{mp}), and molar volume (V_m) of the species adsorbing cannot exceed V_{mp}/V_m. C_{nt2} is the maximum adsorption on macro-pore surfaces and using a Langmuir model should theoretically be limited to a monolayer coverage. This restriction was not applied because of the difficulty of calculating a monolayer coverage and also the possibility that there is multilayer adsorption.

All single component isothermal adsorption data on 3310 carbon and ROX carbon were fitted with the Dual Weighted Langmuir model. Optimization was

done using Microsoft Excel Solver to minimize the sum of the square of the residuals. It should be noted that in some cases there was no stable solution and it was necessary to assign a fixed value to C_{1t2} (maximum adsorption second adsorption mode). Optimized parameters can be found in **Table 7-7**

Table 7-7: Optimized isothermal adsorption parameters for the DWL model.

	PA	LA	n-prOH	PG
K_{n1} (M^{-1})	1.22E+00	1.22E-01	1.20E-01	5.45E-02
C_{nt1} (M)	8.00E-01	8.39E-01	1.18E+00	1.00E+00
K_{n2} (M^{-1})	5.59E-03	3.44E-04	2.39E-03	1.62E-04
C_{nt2} (M)	2.25	4.00	2.08	4.00

Extending the DWL model to variable temperature data requires that the temperature dependence of the equilibrium constants K_{n1} and K_{n2} be known.

$$K = K_0 e^{\left(-\frac{\Delta H}{R}\cdot\frac{1}{T}\right)} \qquad (7\text{-}12)$$

Equation 7-12 shows that K(T) depends on two constants, K_o and $\Delta H/R$ (H for short). For single component data, this means that we are trying to optimize six parameters (C_{nt1}, K_{n1o}, H_{n1}, C_{nt2}, K_{n2o}, H_{n2}), which is too many degrees of freedom. Langmuir adsorption isotherms have an implied assumption that C_{nt} is independent of temperature; therefore C_{nt1} and C_{nt2} were found using isothermal data. The same least square fitting method describe previously was used to find K_{n1o}, H_{n1}, K_{n2o}, H_{n2}, with the additional constraint that the calculated K's at 298 °K must equal those found in the isothermal fitting. (**Table 7-7**) The optimized values are showing in **Table 7-8**. Generally, the optimization converged on a single

solution, except for n-propanol. With n-propanol, the initial guess for these parameters did have some effect on the final optimized values found using Excel Solver.

Table 7-8: Optimized isothermal adsorption parameters for the DWL model.

	PA	LA	n-prOH	PG
K_{n1o} (M^{-1})	2.46E-05	2.33E-05	1.25E-04	1.18E-05
$\frac{\Delta H_{n1}}{R}$ (K)	-3.22E+03	-2.55E+03	-2.07E+03	-2.52E+03
K_{n2o} (M^{-1})	1.91E-05	8.87E-06	6.66E-05	1.34E-06
$\frac{\Delta H_{n2}}{R}$ (K)	-1.69E+03	-1.09E+03	-1.12E+03	-1.43E+03

A simple program was written that would randomly change one of the initial values for K_{n1o}, H_{n1}, K_{n2o}, H_{n2} by a random amount not exceeding ±50%. The system was then solved using Microsoft Solver and the final parameters saved. These final parameters were used as the input for the next cycle. The program was set to run overnight but stopped after 13944 cycles when there was a combination that did not converge. The value of the objective function (sum of the square of residuals) was examined and it was found that 82% of all solutions were within 0.5% of the lowest value found. The range of solutions that were within 0.5% of the optimum value are listed in **Table 7-9** and varied by more than ±7%. These results emphasize the importance of checking the stability of the solutions found using numerical optimization and making sure a global minimum has been found.

Table 7-9: Percentage range of optimized parameters whose objective function is within 0.5% of the "best fit".

H_{c1}	$\ln(K_{0c1})$	H_{c2}	$\ln(K_{0c2})$	fit
7.79%	5.90%	-3.74%	-1.48%	0.49%
-7.51%	-5.69%	7.04%	2.79%	0.50%
0.00%	0.00%	0.00%	0.00%	0.00%
-6.63%	-5.02%	7.09%	2.81%	0.44%
7.28%	5.51%	-7.25%	-2.88%	0.49%

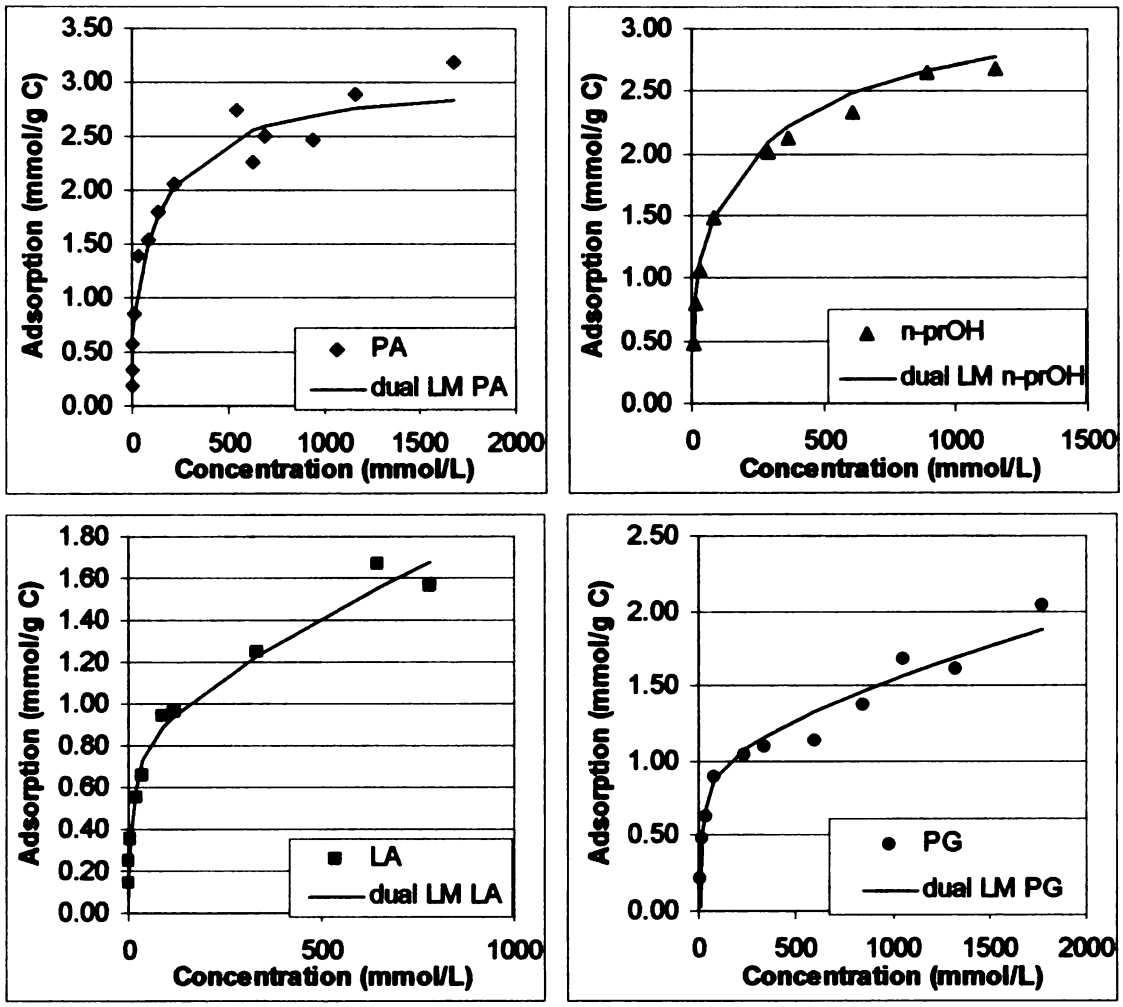

Figure 7-14: Experimental data and WDL fit for the isothermal adsorption of PA, LA, n-prOH and, PG on 3310 carbon at 25 °C

An Excel sheet that expands Equation 7-10 and 7-12 to model the competitive adsorption of up to 4 compounds has also been developed. Isothermal adsorption data for LA, PA, PG and, n-prOH on 3310 carbon at 25 °C

is shown in **Figure 7-14** and includes the DWL fit. The model accurately predicts the experimental data.

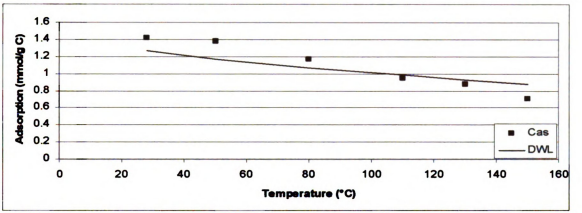

Figure 7-15: Variable temperature adsorption of 1000 mM LA on 3310 carbon.

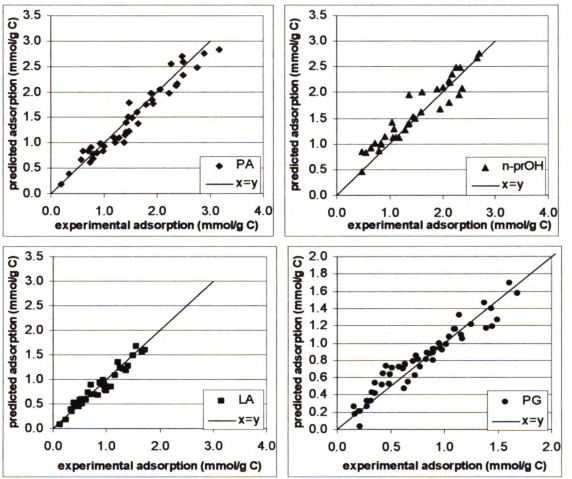

Figure 7-16: Experimental vs predicted single component variable temperature adsorption PA, LA, n-prOH and, PG on 3310 carbon from 25-160°C

The variable temperature data were obtained as described above. Adsorption data for a typical single variable temperature experiment are shown in **Figure 7-15**. The parity plots are shown in **Figure 7-16** for single compound system; the DWL reasonably predicts the adsorption on 3310 carbon over a wide temperature range. **Figure 7-17** shows the predicted isotherms for LA+PA at a total initial concentration of 0.5 M and temperatures of 25 °C, 80 °C, and 150 °C. The predicted values again show good agreement with experimental data, and validate the assumption of constant heat of adsorption over the range of concentrations and temperatures investigated. PA is preferentially adsorbed on 3310 carbon.

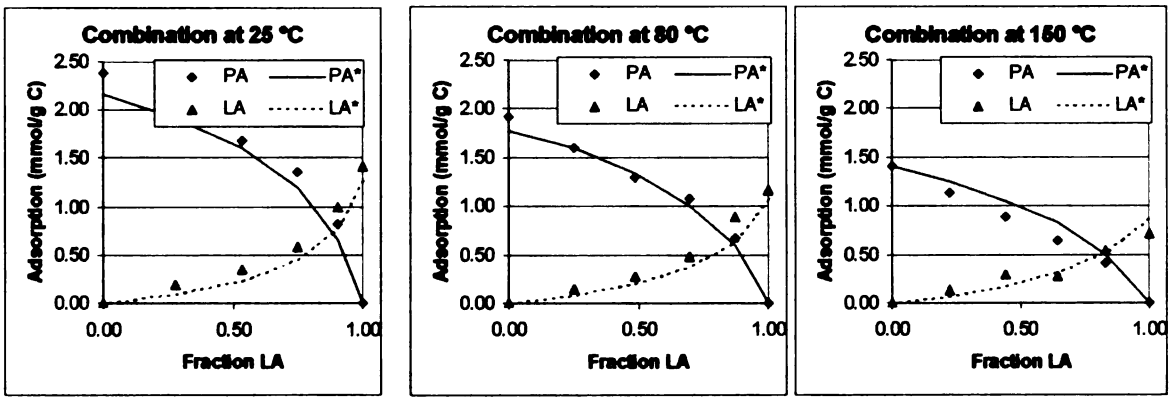

Figure 7-17: Experimental and predicted DWL isotherms for mixture of LA and PA on 3310 carbon at 0.5 M total species concentration and 25 °C, 80 °C, and 150 °C. Abscissa is fraction of LA in the total species (LA + PA) present. Lines are the predicted isotherms.

Figure 7-18 shows the predicted adsorption isotherms for an equimolar mixture of LA+PG at total initial concentrations from 10 to 500 mM and temperatures of 25 °C to 150 °C. It can be seen that the DWL model overpredicts the adsorption of PG relative to LA. If we compare the low concentration fit of DWL for LA and PG, it can be seen in **Figure 7-19** that LA is underpredicted

while PG is slightly overpredicted. This imperfect fitting may be due to the difficulties of obtaining reliable adsorption data at very low concentrations. Gathering more data to improve the model is possible, but likely not worth it because experimentally it was found that PG generally does not inhibit the hydrogenation of LA to a significant extent, so it would be simpler to leave out PG and any non-adsorbed species in the final model.

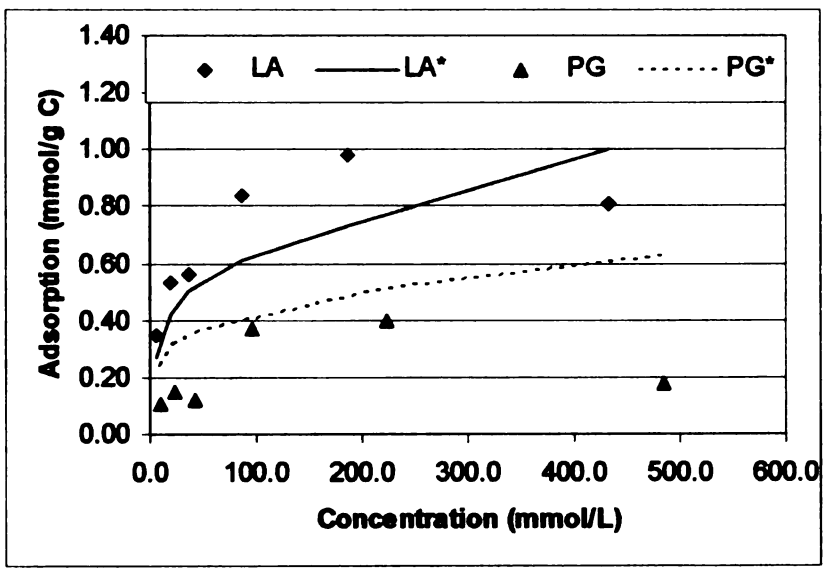

Figure 7-18: Adsorption isotherm for equimolar mixture of LA and PG on 3310 carbon at 25 °C

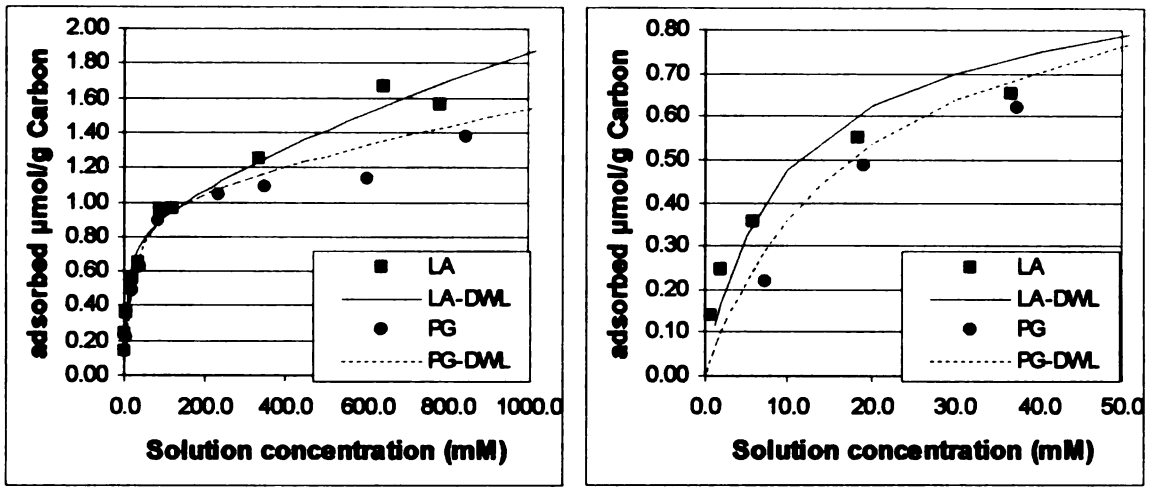

Figure 7-19: Adsorption isotherm for LA and PG on 3310 carbon at 25 °C

Figure 7-20 shows the predicted isotherms for LA+n-prOH at a total initial concentration of 0.5 M and temperatures of 30 °C, 80 °C, and 150 °C. The predicted values for LA show good agreement with experimental data while the n-prOH is underpredicted at low temperatures. This deviation is probably due to the difficulties encountered in fitting the n-prOH data as described later in this chapter.

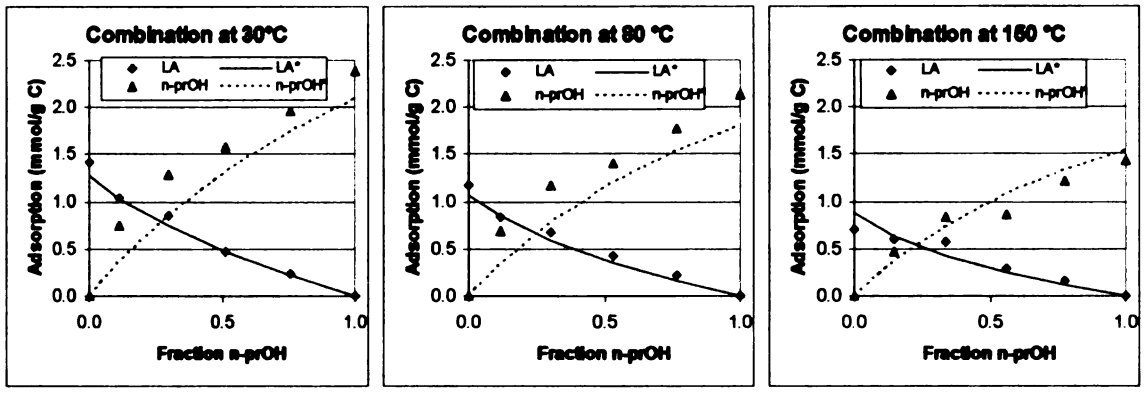

Figure 7-20: Experimental and predicted DWL isotherms for mixture of LA and n-prOH on 3310 carbon at 0.5 M total species concentration and 30 °C, 80 °C, and 150 °C. Abscissa is fraction of n-prOH in the total species (LA + n-prOH) present. Lines are the predicted isotherms.

Figure 7-21 shows the predicted isotherms for PA+n-prOH at a total initial concentration of 0.5 M and temperatures of 30 °C, 80 °C, and 150 °C. The

predicted values for PA show good agreement with experimental data while the n-prOH is underpredicted at low temperatures. This difficulty of n-prOH adsorption is similar to what was seen in LA + n-prOH and will be discussed later in this chapter. Experimental data show that PA and n-prOH compete for the same sites and adsorb in very similar quantities. Therefore, n-prOH should show inhibition on the reaction rate of hydrogenation of PA.

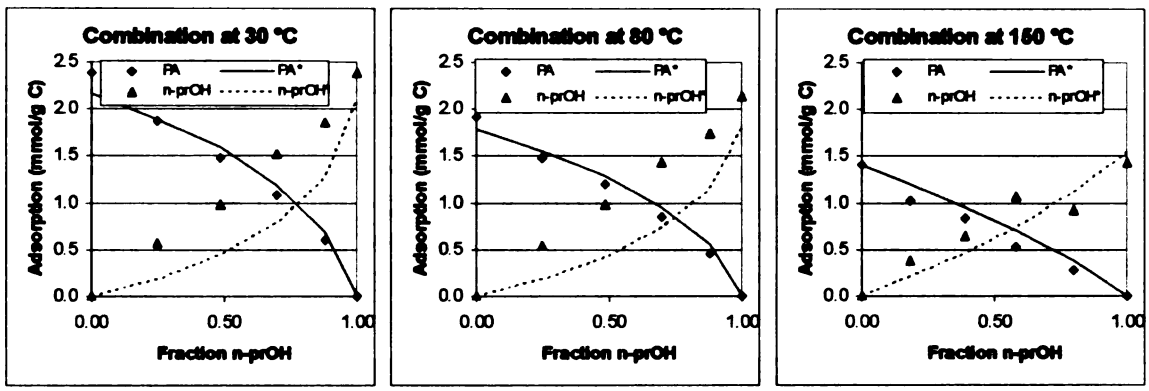

Figure 7-21: Experimental and predicted DWL isotherms for mixture of PA and n-prOH on 3310 carbon at 0.5 M total species concentration and 30 °C, 80 °C, and 150 °C. Abscissa is fraction of n-prOH in the total species (PA + n-prOH) present. Lines are the predicted isotherms.

Figure 7-22 shows the predicted isotherms for PA+PG at a total initial concentration of 0.5 M and temperatures of 30 °C, 80 °C, and 150 °C. PA greatly inhibits the adsorption of PG, and therefore PA is adsorbs much more strongly than PG. The predicted values for PA show good agreement with experimental values except at high temperatures. This deviation is not due to competition from PG but due to a bias in the DWL model, which tends to overpredict adsorption at high temperatures while underpredicting the adsorption at low temperatures. **Figure 7-23** clearly shows this bias. Attempts were made to eliminate this observed bias by adjusting the parameters but these attempts resulted in a

significantly worse fit. Lacking a logical basis to eliminate data points that resulted in this bias, the best fit was used and is reported.

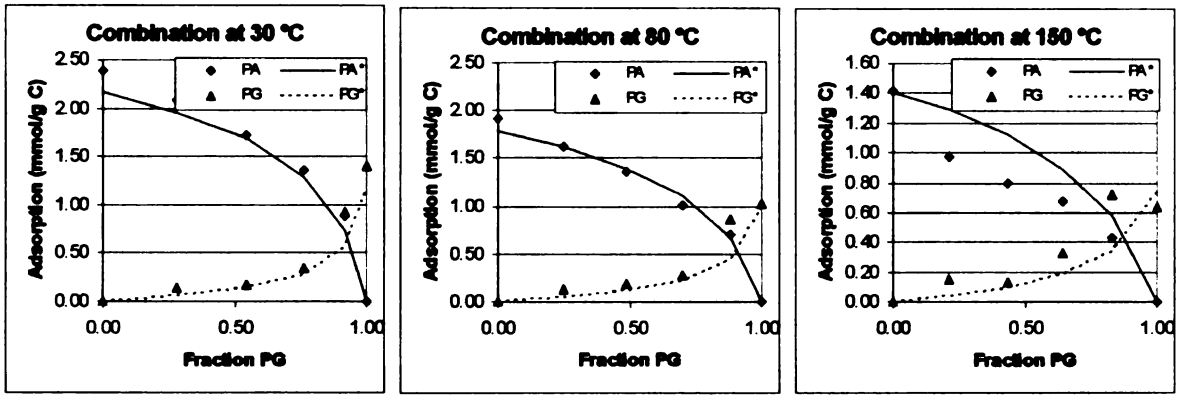

Figure 7-22: Experimental and predicted DWL isotherms for mixture of PA and PG on 3310 carbon at 0.5 M total species concentration and 30 °C, 80 °C, and 150 °C. Abscissa is fraction of PG in the total species (PA + PG) present. Lines are the predicted isotherms.

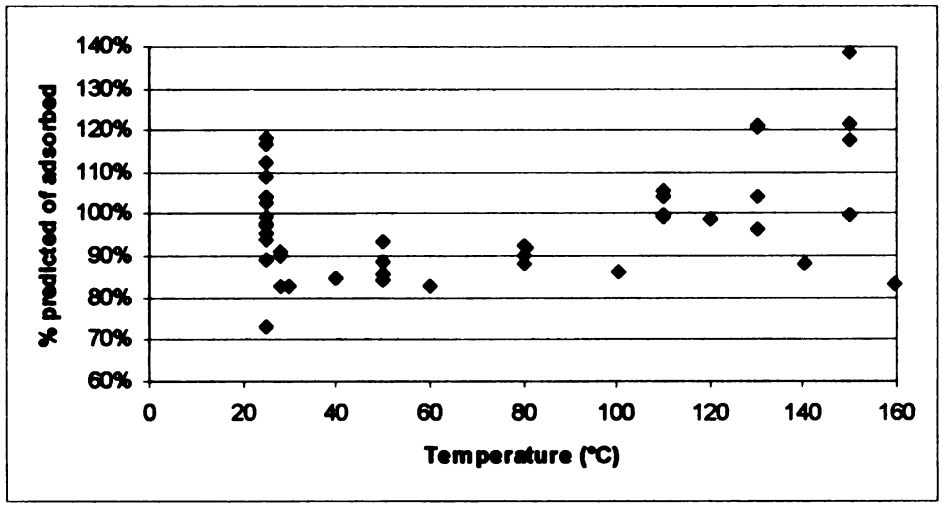

Figure 7-23: DWL predicted adsorptions of PA as percentage of actual adsorbed on 3310 carbon at initial concentration from 10 mM to 2000 mM.

The DWL model's performance in dual compound systems is best summarized by looking at the parity plots in **Figure 7-24**. LA and PA show linearity to X = Y while n-prOH is generally underpredicted. PG shows a significant amount of scatter. The cluster of points between 0.6 and 1.0 mmol/g C are from one experiment with a 4:1 PG to PA ratio.

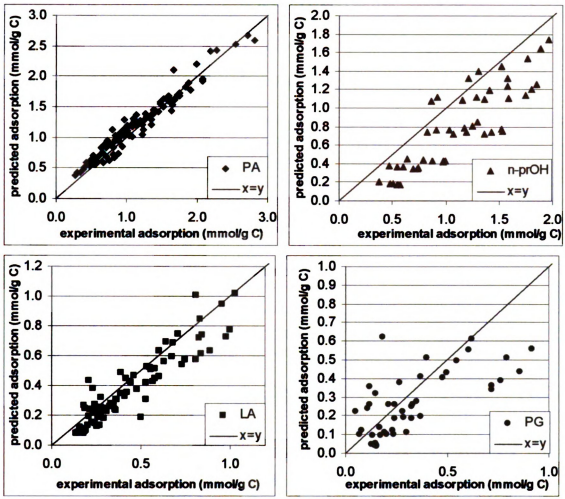

Figure 7-24: Experimental vs predicted adsorption of PA, LA, n-prOH and, PG on 3310 carbon in binary mixtures only.

7.6 Additional notes on adsorption modeling

n-Propanol data was inconsistent with model. The question arises whether n-prOH behaves differently or the experimental data were flawed some how. Control experiments were run to validate the variable temperature experimental design. Experiments were performed as described earlier, except that no carbon was added. Even though no carbon was added, a carbon loading of 1 gram was

assumed to maintain consistency in the calculations. **Figure 7-25** shows single component measured adsorption of 100mM n-prOH, LA and, PA without any carbon over a temperature range 25 - 160 °C.

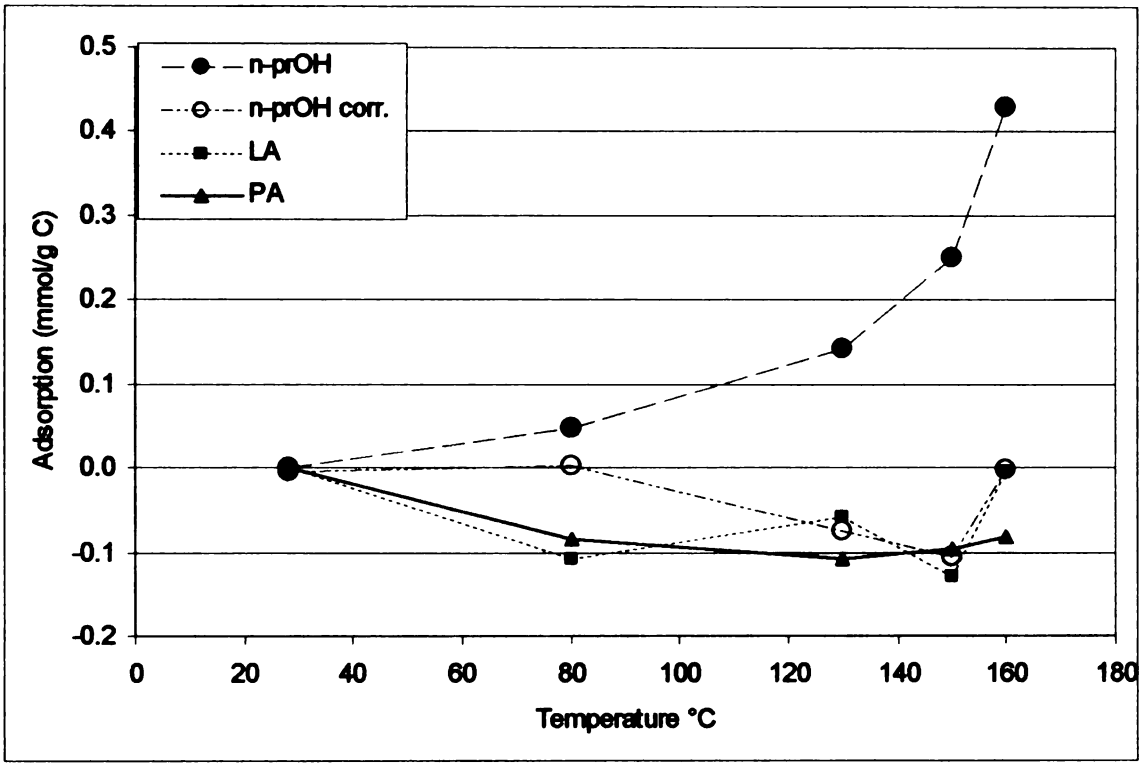

Figure 7-25: Apparent species adsorption in control experiments without carbon showing the need to correct for vapor fraction of n-prOH. (note data for 150 °C after 14 hours is plotted at 160°C for clarity.)

PA and LA show no significant deviation from zero as expected. For n-prOH there is a significant deviation at high temperatures due to high vapor pressure of n-prOH. To correct for the fraction of n-propanol in the vapor phase, partial pressure (yP), vapor volume and temperature were used to calculate the quantity (mmols) of n-propanol in the vapor phase. Partial pressure was calculated using modified Raoult's law($yP = x\gamma P^{sat}$) and the following assumptions:

1. Gas phase acts as ideal gas.

2. P^{sat} for n-prOH can be described by Antoine's Equation

3. Solution density is ~1 g/ml

4. γ (gamma) is a linear function of x and T with the form γ = DT + Ex + F

Antoine coefficients (A=7.77374, B=1518.16, C =213.076) where taken from Yaws' Handbook of Antoine Coefficients[74]. Aspen properties was used to calculate gamma's over range 0≤x≤.02, 25≤T≤160. Least square fitting was used to find D, E and F (D=0.009439, E=-196.09, F=16.955). This correction was applied to all n-prOH data at temperatures greater then 80 °C.

8 CONCLUSIONS AND RECOMMENDATIONS

8.1 Conclusions

A study of substrate-catalyst interactions has been completed; both metal and carbon support adsorb reacting species and influence apparent reactivity.

Methods and a recirculating microreactor apparatus for measuring adsorption on metal surfaces from the aqueous phase have been developed. The key features are a large metal to solution volume ratio, automated sampling, an operating range of 25-200 °C, and headspace gas control.

Adsorption of organic acids and polyols on Ru sponge metal from water was characterized.

- The extent of lactic acid is ~4 μmol/g Ru and is independent of hydrogen saturation of the metal surface.
- C3 polyols with terminal hydroxyl groups adsorb irreversibly through a dehydrogenation step to an "aldehyde like" species followed by degradation. This adsorption is inhibited by presaturating the metal surface with hydrogen.
- Adsorption of isopropanol shows little adsorption on either a H_2-free or H_2-saturated Ru surface. On the H_2-free surface formation of acetone, a dehydrogenation product, is seen.
- Primary alcohols, when adsorbed on a H_2-free Ru surface, show the formation of acids, an oxidation product.

Single component and multicomponent competitive adsorption on activated carbon at a range of concentrations and temperatures was characterized.

- For glycerol and propylene glycol, adsorption of individual species is well-represented by the Langmuir isotherm, and simultaneous adsorption of the two species is described by an extended Langmuir model that uses the single-component adsorption constants and accounts for competitive adsorption between the two species.
- Propanoic acid (PA) and lactic acid (LA) adsorption is competitive and PA adsorbs three times more strongly than LA.
- A two part adsorption model consisting of adsorption into the micro pore and adsorption on the surface of the macropores was developed. The model accurately predicts the individual species adsorption and when the individual adsorption parameters are used, competitive adsorption was accurately predicted with the noted exception of n-propanol.
- Incorporation of the competitive adsorption model into our kinetic model for the hydrogenation of LA and PA was done by Chen[68]. The combined model performed reasonable well when using reaction rate constants found on unsupported Ru catalyst and the pore concentrations predicted based on competitive adsorption on carbon.

H-D exchange on H_2O-D_2O-H_2-D_2 over metal catalyst was characterized. The dissociation of water is the limiting step on 5% Ru/C but not on 5% Pt/C. The experimental data can accurately fit the kinetic model.

8.2 Recommendations

There are several areas that warrant further investigation to elucidate the mechanisms of adsorption that were observed in this work.

- Simpler systems with substrates containing no carbon atoms or only one carbon atom should be looked at in more detail.
    a. A thorough study of the interactions, in liquid phase, between water and the metal surface focusing on the actual oxidation state for the metal.
    b. Characterization of interaction between Ru surfaces and C_1 species (ie. methane, methanol, formaldehyde, formic acid, and carbonate). This should include hydrogen saturation affects and temperature dependence.
- The reversibility of lactic acid adsorption on Ru sponge metal should be examined.
- Adsorption behaviors on different metal surfaces should be investigated. One option is adsorption on Raney nickel, which is a known active hydrogenation catalyst.

APPENDICES

Appendix A: Master experiment list

			Concentration		Catalyst			Conditions			
Exp#	Date	Reactants	mol	Type	Type	g.	cat. prep.	T (°C)	Gas	P (psi)	Description and Results
4	03/18/03	Sorbitol	100	Loop to system	Ru (sponge)	8.7	standard	25	He		fail problems with HPLC
5	03/31/03	Sorbitol	100	Loop to system	Ru (sponge)	8.7	standard	25	He	<5	~1.5umol/g adsorbed
6	04/08/03	Glucose	100	Loop to system	Ru (sponge)	8.7	standard	25	He	<5	~1.5umol/g adsorbed gluconic acid and sorbitol formed at same rate
7	04/10/03	Glucose	100	Loop to system	Ru (sponge)	8.7	standard	25	He	<5	The HPLC had problems big waves. There also appeared to be contamination. Gluconic acid formed right away and only some sorbitol. After addition of hydrogen, gluconic acid and glucose disappeared while sorbitol started to form
8	04/14/03	Glucose	100-200	Loop to system	Ru (sponge)	8.7	standard?	25	He	<5	hardly any adsorbed
9	04/21/03	Glucose	100-200	Loop to system	Ru (sponge)	8.7	H_2 saturated	25	He,H_2	100	~1-2mg adsorbed and glucose converts to sorbitol
10	05/05/03	Glucose	100	Loop to system	-	-		25	He	<5	as expected no adsorption with no catalyst

Appendix A: (cont'd).

11	05/13/03	Sorbitol	100	Loop to system	-	-		25	He	<5	as expected noadsorption with no catalyst
12	05/21/03	Sorbitol	10,20	Loop to system	Ru (sponge)	8.7	standard	25	He	<5	added 10umol and let adsorb for 18 hours ~0.8umol/g adsorbed then added 10umol more adsorbed to ~1.5umol/g
13	05/29/03										fail problems with HPLC system testing
14	05/29/03	Sorbitol	10,20	Loop to system	Ru (sponge)	9	standard then washed 5mM H_2SO4	25	He	<5	This is multi part experiment first 10uml SO is adsorbed in 4mM H_2SO4 which results in the formation on one product byciclict sorbitol? After time mor sorbitol was added 10umol 1,4-dehydrosorbitol
15	06/11/03	Sorbitol	10,20	Loop to system	Ru (sponge)	9	standard then washed 5mM H_2SO4	25	He	<5	acid present forms main product at 10.8 HPLC had problems some contamination
16		Sorbitol	10mg	Loop to system	Ru (sponge)	9	standard	25	He	<5	What does it show some adsorption
17		Sorbitol	10mg	Loop to system	Ru (sponge)	9	standard	25	He	<5	
18		Sorbitol	10mg	Loop to system	Ru (sponge)	9	standard	25	He	<5	

Appendix A: (cont'd).

20	03/01/04	Sorbitol	~2mg total	ramp 0.2mg	Ru (sponge)	10	standard	25	He	20	~1mg total adsorbed
21	03/03/04	Sorbitol	~2mg total	ramp 0.2mg	Glass beads	~3	wash water	25	He	20	no reaction and no adsorption
22	03/05/04	Sorbitol	~2mg total	ramp 0.2mg	Glass beads	~3	wash water	25	He	20	this is using controlled pore glass 2g this should have ~7.4m^2/g showed no adsorption
23	03/11/04	Glucose	~2mg total	ramp 0.2mg	Ru (sponge)	10	standard	25	He	20	guconic acid and sorbitol for equal amounts adsored ~1umol/g Ru
24	03/12/04	Glucerol ramped	~4mg total	ramp 0.2mg	Ru (sponge)	10	standard	25	He	20	~0.3umol/g Ro
25	03/15/04	Gluconic acid	~4mg total	ramp 0.2mg	Ru (sponge)	10	standard	25	He	20	0.6mg adsorbed ~0.3umol/g Ru
-											
-											
30	04/28/04	Glycerol 0.4mg			Ru (sponge)	10	H_2 sat.	50	H_2	50	Adsorbtion on a H_2 saturated surface under Ar T=50 °C This system shows a lot slower adsorbtion
31	05/03/04	Glycerol	0.4mg-2.8mg	ramp 0.2mg	Ru (sponge)	10	standard	60	He	20	CO is formed and EG and PG seem to keep forming. There seems to be a adsorption of ~0.2mg followed by a constant reaction rate

Appendix A: (cont'd).

32	05/10/04	Glycerol	0.4mg-2.8mg	ramp 0.2mg	Ru (sponge)	10	standard	80	He	20	Adsorption with concentration ramping. EG and PG were also ramped to T=80°C. CO is formed and EG seems to still react but PG is dropping at injection rate no clear adsorption level
33	06/09/04	Sorbitol 50mg			Ru (sponge)	10	H_2 sat.	80	He		Adsorption on a H_2 saturated surface under He T=80 °C
34											
35											
36		GO	1mg	Loop to system	Ru (sponge)	10	standard +water wash at 30 °C	80	Ar	20	Calculations are old style and not clear might be useless
37		GO	1mg	Loop to system	Ru (sponge)	10	standard	25?	Ar	20	shows ~0.7mg GO adsorbed
38		GO	0.4mg	Loop to system	Ru (sponge)	10	standard	25	Ar	20	All adsorbed ~0.4mg
39		GO	0.4mg	Loop to system	Ru (sponge)	10	standard	25	Ar	20	~3.2umol adsorbed
40		GO	2mg	Loop to system	Ru (sponge)	10	standard	25	Ar	20	?

Appendix A: (cont'd).

41		PG	5.mg	Loop to system	Ru (sponge)	10	standard	25,60	Ar	20	~7-8umol PG adsorbed and after increasing temperature to 60 this went to 13umol
42		PG then GO	0.5mg PG 0.4mg GO	Loop to system	Ru (sponge)	10	standard	25	Ar	20	first adsorbed PG ~2umol then added GO and it adsorbed ~2.3umol
43a		H_2 D_2O		10 ml reactor+MS	none			25(rt)			10ml reactor with 2ml D_2O and H_2 gas at 100 psi there was no formation of D_2 or HD
43b		H_2 D_2O		10 ml reactor+MS	Ru/C 5%	0.1		25(rt)			10ml reactor with 2ml D_2O and H_2 gas at 100 psi +0.2g wet catalyst (0.1g dry) there was formation of HD followed by the formation of D_2
43c		H_2 D_2O		10 ml reactor+MS	Pt/C 5%	0.1		25(rt)			10ml reactor with 2ml D_2O and H_2 gas at 100 psi +0.1g dry catalyst there was rapid formation of HD and D_2
44		PG then GO	5mg PG 0.4mg GO	Loop to system	Ru (sponge)	10	standard	25	Ar	20	first adsorbed PG ~6.0-7umol then added GO and it adsorbed ~1umol
45		GO then PG	0.6mg GO 0.5mg PG	Loop to system	Ru (sponge)	10	standard	25	Ar	20	GO was added first and adsorbed ~3umol addition of PG resulted in no change no PG adsorbed (* the adsorbed amount of GO is less then expected)

Appendix A: (cont'd).

46		H_2+D_2 D_2O		70 ml reactor+MS	none			25(rt)			70ml reactor with 10ml D2O and 50 psi each of H_2 and D_2 there seems to be a slow conversion to HD and D_2 (from the SS?) there seems to be no incorporation of D from solution
47		H_2 DOethanol		10 ml reactor+MS	Ru/C 5%			25(rt)			10ml reactor with 3ml DOethanol and H_2 gas at 100 psi +0.2g wet catalyst(0.1g dry) there was formation of HD but almost no D_2 was formed
48		H_2 + D_2 D_2O		70 ml reactor+MS	Ru sponge			25(rt)			70ml reactor with 10ml D_2O and 50 psi each of H_2 and D_2 and 1g Ru sponge (system was reduced at 200 °C for 4 hours). Does not seem different from exp 46 (I checked there was Ru in reactor)
49		PG+GO	.25mg PG 0.2mg GO	Loop to system	Ru sponge	10	standard	25	Ar	20	GO adsorbed faster ~1.8 umol (almost all) while PG adsorbtion was only 0.6umol
50	10/27/04	H_2,D_2	50psi each	70 ml reactor+MS	5%Ru/C	0.1	non	25(rt)			H_2 + D_2 over D_2O with 0.1g Ru/C 5% (50psi each in 70ml reactor)
51	11/23/04	PG	5.0mg	Loop to system	Ru (sponge)	10	H2 sat.	20	H2	75	~1umol PG adsorbed. There was a periodic noise in the data ~.3mg interesting.

Appendix A: (cont'd).

52	01/12/05	EG	5.0mg	Loop to system	Ru (sponge)	10	standard	25	Ar	20	~9umol EG adsorbed
53	01/20/05	EG	5.0mg	Loop to system	Ru (sponge)	10	standard	25	Ar	20	~8umol EG adsorbed. Subsequent additions of EG did give a higher adsorption but this may be due to uncertainties in the system
54	01/24/05	Lactic Acid	0.5mg	Loop to system	Ru (sponge)	10	standard	25	Ar	20	Lactic acid seemed to convert to pyruvic acid in the loop but when column was in line there was no evidence of pyruvic acid and ~1.2umol of LA adsorbed
54B	01/25/05	Lactic Acid	0.5mg	Loop only	...	...	....	25	Air	0	Lactic acid converted to pyruvic acid that also disappeared from solution. This experiment would have been better if I did not hav it open to air. There seems to be some oxidation that can take place over the stainless steel tubing.
55	01/31/05	Lactic Acid	0.5mg	Loop to system	Ru (sponge)	10	H2 sat.	25	H2	10	Some formation of pyruvic acid in loop. Adsorbtion of ~1.2umol of LA but this seemed slower then with a H_2 free surface.
56	02/02/05	Lactic Acid	50umol	Loop to system	Ru (sponge)	10	standard	25	Ar	15	~13umol LA adsorbed. The pH at end was ~5.5 this is higher then expected
57	02/07/05	Lactic Acid	93umol	Loop to system	Ru (sponge)	10	standard	25	Ar	15	~25mg LA adsorbed. Ending pH was 3.35

Appendix A: (cont'd).

58	02/08/05	Lactic Acid	190umol	Loop to system	Ru (sponge)	10	standard	25	Ar	15	This experiment had som problems and gave ~44umol LA I don't trust this experiment
59	02/10/05	n-propanol + PG	20umol 27umol	Loop to system	Ru (sponge)	10	standard	25	Ar	20	5umol of n-propanol adsorbed and 7 umol of PG.
60	02/14/05	Lactic Acid	100umol	Loop to system	Ru (sponge)	10	H_2 sat.	25	H_2	10	~27umol LA adsorbed. The pH was ~3-4
61	2-15-2005	Lactic Acid	50umol	loop only	Ru (sponge)	10	standard	25	Ar	20	no significant change ove time
62	02/16/05	Lactic Acid	50umol	Loop to system	Ru (sponge)	10	standard	25	Ar	20	~23umol LA adsorbed but at a slower rate. This was different then the previous 50umol run exp 56
63	02/25/05	Lactic Acid	5umol	Loop to system + pH probe	Ru (sponge)	10	standard	25	Ar	20	No significant adsorption seen but the pH went up to 10 in the first 3 hours. There is also the problem of Potasium Nitrate leaching in to the system. A peak also grew at 25.8 min that is UV active. Simona says that she has seen peaks from there.
64	03/02/05	Lactic Acid			Ru (sponge)						This was a flow trough experiment with pulses of lactic acid on the 150mm column broad peaks not simple to interpide

Appendix A: (cont'd).

65	03/03/05	?????			Ru (sponge)?						simmilar to exp 64 no good note also ran some glass bead column that showed adsorbtion of acid
66	04/04/05	Lactic Acid GO?			Ru (sponge)						atempts in 70ml reactors did not work well no clear results or experimental data
67	05/15/05	GO	5+5umol	Loop to system	Ru (sponge)	10	standard then water wash several days	25	Ar	10	show that 5umols adsorbed each time (added 5 more after day)
68	05/16/05	GO	5+10umol	Loop to system	Ru (sponge)	10	dry reduction	25	Ar	10	show that 5umols adsorbed each time (added 6 more after day slower then wet reduction could be not fuidized?)
69	05/23/05	GO	~2umol	vial	Ru (sponge)	~0.5-0.7	dry reduction	25	N2		atempts to do adsorbtion in a vial batch style transferred Ru in glove bag (did not give clear results
70	09/01/05	LA+PA	126LA 128PA	Loop to system	Ru (sponge)	10	standard	25	Ar	15	~26umol PA adsorbed and 30umol LA at about the same rate
90	03/22/06	GO	50	Loop to system	Ru (sponge)	10	standard	25	Ar	20	not procesed data look ok (might need reprocess)

Appendix A: (cont'd).

91	03/27/06	GO	50	Loop to system	Ru (sponge)	10	standard	25	Ar	20	~8umol GO adsorbed (but data scatered and no clear maximum
92	03/30/06	GO	50	Loop to system	Ru (sponge)	10	water wash only	25	Ar	20	only washed with rt water after last run 2.5umol GO adsorbed
93	04/12/06	GO	50	Loop to system	Ru (sponge)	20	Standard	25,60	Ar	20	First run with 20g Ru(s) total GO adsorbed at 25 °C ~15umol when T increased to 60 °C adsorption went to ~25umol
94	04/19/06	GO	50	Loop to system	Ru (sponge)	20	Standard	60	Ar	20	adsorbed 0.8umol/g also shows recovery at 200 °C of carbon
95	04/24/06	GO	50	Loop to system	Ru (sponge)	20	Standard	40	Ar	20	GO adsorbed 0.9umol/g when shitching to 60 no real increase adding H_2 recovered all Crbon adosrbed at 60 °C
96	04/27/06	GO	50	Loop to system	Ru (sponge)	20	Standard	80	Ar	20	GO adsorbtion ~1umol/g gas data , also shows recovery of all carbon upon heating with H_2
97	05/03/06	PG	50	Loop to system	Ru (sponge)	20	Standard	25	Ar	20	adsorbtion low 5-6umol
98	05/09/06	PG	50	Loop to system	Ru (sponge)	20	Standard	25	Ar	20	recirculating pump stoped over night after that next day was heated to 80
99	05/15/06	GO	50	Loop to system	Ru (sponge)	20	Standard	80	Ar	20	HPLC had irregular flow so retention time were changing could possibly make a correction scheme but not worth it

Appendix A: (cont'd).

100	06/02/06	GO	50	Loop to system	Ru (sponge)	20	H_2 saturated	25,	Ar	20	prepared by reducing followed by cooling on H_2 followed by water wash with argon Adsorbed 6umol(0.3umol/g GO (note this in on 20g Ru)
101	06/05/06	GO	50	Loop to system	Ru (sponge)	20	standard	25,	Ar	20	adsorption only ~7umol (~0.3umol/g problem
102	06/12/06	GO	50	Loop to system	Ru (sponge)	20	standard	25,	Ar	20	showed 6-7 umols(0.2-0.3umol/g) adsorbed from start not sure what happened suspect that sponge was kaked in column
103	06/15/06	GO	50	Loop to system	Ru (sponge)	20	standard	25,	Ar	20	checking system with normal GO adsorbtion failed
104	06/16/06		50	Loop to system	Ru (sponge)	20					reduction only
105	06/22/06	GO	50		Ru (sponge)	20	standard?	25,	Ar	20	no calculation has full reduction sampeling should be ok
106	06/30/06	GO	50	Loop to system	Ru (sponge)	20	standard	25	Ar	20	Failed after 2 hours not usefull
107	07/07/06	GO	50	Loop to system	Ru (sponge)	20	standard	80	Ar	20	only have data for the first 4hours system failed trend looks normal
108	07/11/06	GO	50	Loop to system	Ru (sponge)	20	standard?	25?	Ar	20	computer crashed over night does have data calculations are questionable might be at 80 °C

Appendix A: (cont'd).

109	07/17/06	IPA	50	Loop to system	Ru (sponge)	20	standard	25,	Ar	20	IPA formed acetone anly ~0.2umol/g adsorbed
110	07/21/06	IPA	50	Loop to system	Ru (sponge)	20	standard	25,	Ar	20	IPA converted to acetone adsorbtion ~0.25umol/g system failed after 11 samples
111	07/28/06	IPA	50	Loop to system	Ru (sponge)	20	H_2 saturated	25,	H_2	20	IPA ~0.25umol/g adsorbed
112	08/02/06	GO and IPA	50 each	Loop to system	Ru (sponge)	20	standard	25,	Ar	20	~1umol/g of GO adsorbed but no IPA. Some acetone was formed upon adding H_2 no mo GO adsorbed
113	08/10/06	1,3PD	50	Loop to system	Ru (sponge)	20	standard	25,	Ar	20	~1.1umol/g of 1,3-BDO adsorbed note there were several side products ~5-10% of adsorbe material (there was a leak in the middle of the run
114	08/15/06	Ethanol	50	Loop to system	Ru (sponge)	20	standard	25,	Ar	20	~0.7umol/g were adsorbed with the formation of some acetic acid there was also an unidentified peak (not acetal) the adsorbtion stoped on the adition of H_2 with a step decrease in acid
115	08/23/04	Acetone	50	Loop to system	Ru (sponge)	20	standard	25,	Ar	20	it ran for 1 day on loop only when on column the acetone converted to IPA and there was ~0.2-0.3umol/g adsorbtion

Appendix A: (cont'd).

116	09/06/06	GO then acetone	50 each	Loop to system	Ru (sponge)	20	standard	25,	Ar	20	GO adsorbed to ~20umol The acetone did not adsorb but did get converted to IPA to a larger extent then acetone alone.
117	09/14/06	THF	50	Loop to system	Ru (sponge)	20	standard	25,	Ar	20	~0.25umol/g THF adsorbed. The HPLC was iradic and skiped samples not sure why
118											
119	10/27/06	GO	50	Loop to system	Ru (sponge)	20	standard	60	Ar	20	~30umols adsorbed long run with gas
120	11/03/06	n-prOH	50	Loop to system	Ru (sponge)	20	standard	25	Ar	20	system failed leaks
121	12/01/06	n-prOH	50	Loop to system	Ru (sponge)	20	standard	25	Ar	20	~23umol adsorbed
122	12/04/06	n-prOH	50	Loop to system	Ru (sponge)	20	standard	25	Ar	20	~8-10umols adsorbed

Appendix B: Supplemental data

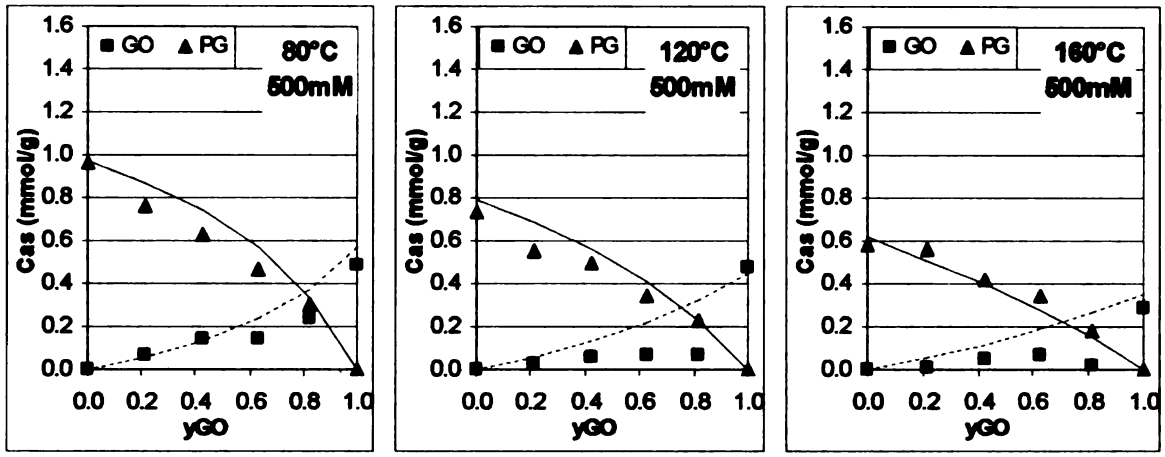

Figure B-1: Experimental and predicted Langmuir isotherms for mixture of GO and PG on 3310 carbon at 0.5 M total species concentration and 80°C, 120°C, and 160°C. Abscissa is fraction of GO in the total species (GO + PG) present. Lines are the predicted isotherms.

	H_2	HD	DH	D_2	M-H	M-D	M	M-OH	M-OD	H_2O	DHO	HDO	D_2O
H	2	1	1	0	1	0	0	1	0	0	0	0	0
D	0	1	1	2	0	1	0	0	1	0	0	0	0
O	0	0	0	0	0	0	0	1	1	1	1	1	1
M	0	0	0	0	1	1	1	1	1	0	0	0	0

Rn= #cp –Rank(FM)= 13-4 =9

Figure B-2: Formula matrix calculation of number of reactions needed.

		k2y6y6	k2y6y8	k2y8y8	k1y7y7y1	k1y7y7y2	k1y7y7y3	k1y7y7y4	k4y7y7y10	k4y7y7y11	k4y7y7y12	k4y7y7y13	k3y5y8	k3y5y9	k3y6y8	k3y6y9	k5y10y13	k5y11y12
H2	y(1)	1	0	0	-1	0	0	0	0	0	0	0	0	0	0	0	0	0
HD	y(2)	0	1	0	0	-1	0	0	0	0	0	0	0	0	0	0	0	0
DH	y(3)	0	1	0	0	0	-1	0	0	0	0	0	0	0	0	0	0	0
D2	y(4)	0	0	1	0	0	0	-1	0	0	0	0	0	0	0	0	0	0
M-H	y(5)	-2	-2	0	2	1	1	0	1	1	0	0	-1	-1	0	0	0	0
M-D	y(6)	0	-2	-2	0	1	1	2	0	0	1	1	0	0	-1	-1	0	0
M	y(7)	2	4	2	-2	-2	-2	-2	-2	-2	-2	-2	2	2	2	2	0	0
M-OH	y(8)	0	0	0	0	0	0	0	1	0	1	0	-1	0	-1	0	0	0
M-OD	y(9)	0	0	0	0	0	0	0	0	1	0	1	0	-1	0	-1	0	0
H2O	y(10)	0	0	0	0	0	0	0	-1	0	0	0	1	0	0	0	-1	1
DHO	y(11)	0	0	0	0	0	0	0	0	-1	0	0	0	1	0	0	1	-1
HDO	y(12)	0	0	0	0	0	0	0	0	0	-1	0	0	0	1	0	1	-1
D2O	y(13)	0	0	0	0	0	0	0	0	0	0	-1	0	0	0	1	-1	1

Figure B-3: Matrix of coefficients for ODE's

Table B-1: Unique rate terms for elementary reactions

r1f = k1y7y7y1	**r1r = k2y5y5**
r2f = k1y7y7y2	**r2r = k2y5y6**
r3f = k1y7y7y3	**r3r = r2r**
r4f = k1y7y7y4	**r4r = k2y6y6**
r5f = k3y5y8	**r5r = k4y7y7y10**
r6f = k3y5y9	**r6r = k4y7y7y11**
r7f = k3y6y8	**r7r = k4y7y7y12**
r8f = k3y6y9	**r8r = k4y7y7y13**
r9f = k5y10y13	**r9r = k5y11y12**

Matlab Code

H2D2model.m

```
1 clear all
2 %hold on
3 global Mt Dt Nt Nl Ng Ns Ht XX reactor_V
4 optz=0
5 %this section defines initial conditions the fixed parameters
6 D2O_i=0; H2O_i=10;%ml
7 H2=0; D2=180%psi
8 grams_Ru=13;
9 reactor_V=23;
10 Gas_V=reactor_V-D2O_i-H2O_i-grams_Ru/3;
11 % calculated invariants
12 Ng=(H2+D2)/14.5*Gas_V/22400; Ns=0.4/22400*2*grams_Ru;
13 Nl=(H2O_i+D2O_i)/18*2; S_i=Ns*1; Nt=Ns+Nl+Ng;
14 Dl=D2O_i/18*2; Ds=Dl/Nl*Ns; Dg=D2/(D2+H2)*Ng; Dt=Dg+Ds+Dl;
15 %initial conditions
16 Yo(1:3)=[(H2)/14.5*Gas_V/22400 ,0,0];
17 Yo(4:13)=[(Ng-Yo(1)),0,0,S_i*.9999,0,0,(Nl-Dl),0,0,Dl];
18 %changeable parameters
19 % k1=4093; Kr=2.0048; Kg=5.3232; Kl=94.379; k5=10000;
20 % k1=50586; Kr=129.54; Kg=6.9848; Kl=8.6846; k5=1000000;
21 % k1=90938; Kr=308.28; Kg=13.365; Kl=1.5545; k5=1000000;
22 k1=50586; Kr=129.54; Kg=6.9848; Kl=8.6846; k5=10000;
23 % k1=31093; Kr=2.0048; Kg=5.3232; Kl=94.379; k5=10000
24 k1=5000586; Kr=1000; Kg=1; Kl=.1; k5=1000000;
25 k=[k1,Kr,Kg,Kl,k5];
26 %solve ODE's from 0 to 1000
27 options = odeset( 'RelTol',.00000001,'MaxStep' ,10);
28 [t,Y] = ode15s(@(t,Y) larsf(t,Y,k),[.000010 1000],Yo,options);
29 %calculate fractional info
```

```
30 calfractions;
31 % plot results (data was really move back to excel and ploted from there!)
32 subplot(3,1,1);plot (t,g);
33 subplot(3,1,2);plot (t,(Y(:,11)/2+Y(:,12)/2+Y(:,13))/((D2O_i+H2O_i)/500));
34 subplot(3,1,3);plot (t,HD);
35 % %*****************************************************************
36 % % % optimization atempts
37 % % %*****************************************************************
38 if ( optz > 0 )
39 getdata %get experiment 1 data
40 Va= zeros(5,1);temp=1; temp2=1;sheet=0;
41 k=[k1,Kr,Kg,Kl,k5];
42 R=objectivef(k,tdata1,ydata1,Yo);Ro=R+10;
43 while R>.01;
44 dp=1;
45 a = randint(1,1,[1,4]); %randomly pick one to change
46 KTemp=k(a);
47 k(a)=k(a)+(0.5-rand)*k(a)*dp*2;
48 %solve ODE's from 0 to 1000
49 R=objectivef(k,tdata1,ydata1,Yo);
50 if (R < Ro) ; %if improvement then keep it and save the conditions
51 KR(temp,:)=[R,k];
52 temp=temp+1;
53 Ro=R
54 else %restore original value and continue
55 KF(temp2,:)=[R,k];
56 k(a)=KTemp;
57 temp2=temp2+1;
58 end
59 if temp2>1000
60 sheet=sheet+1
```

```
61 xlswrite( 'H2Omodeltempdata.xls', KF ,sheet)
62 temp2=1
63 end
64 Va(a)=Va(a)+1; [Ro,a,temp2]
65 end
66 end
67
```

larsf.m

```
1 function dy = larsf(t,Y,k)
2 global Mt Dt Nt Nl Ng Ns Ht XX reactor_V
3 %calculate k values
4 y=Y;
5 y(1:4)=exp(-t/2000)*Y(1:4);
6 k1=k(1);k2=k(1)/k(3);k3=k(1)/k(2);k4=k3/k(4);k5=k(5);
7 %k1=0;k2=0;k3=0;k4=0;k5=k(5);
8 % clear
9 dydy = zeros(13,1);
10 % calculate
11 V=reactor_V/1000;% vol in liters
12 %calculate each reaction rate pates
13 k1y7y7=k1*y(7)*y(7); k4y7y7=k4*y(7)*y(7) ;
14 xx=[k2*y(5)*y(5)/V; k2*y(5)*y(6)/V; k2*y(6)*y(6)/V; ...
15 k1y7y7*y(1)/V/V; k1y7y7*y(2)/V/V; k1y7y7*y(3)/V/V; ...
16 k1y7y7*y(4)/V/V; k4y7y7*y(10)/V/V; k4y7y7*y(11)/V/V; ...
17 k4y7y7*y(12)/V/V; k4y7y7*y(13)/V/V; k3*y(5)*y(8)/V; ...
18 k3*y(5)*y(9)/V; k3*y(6)*y(8)/V; k3*y(6)*y(9)/V; ...
19 k5*y(10)*y(13)/V; k5/4*(y(11)+y(12))^2/V];%try using average of the HDO and
   HOD
20 % difine the coef for all the ODE
21 A= [1 0 0 -1 0 0 0 0 0 0 0 0 0 0 0 0 ;...
```

```
22 0 1 0 0 -1 0 0 0 0 0 0 0 0 0 0 0 ;...
23 0 1 0 0 0 -1 0 0 0 0 0 0 0 0 0 0 ;...
24 0 0 1 0 0 0 -1 0 0 0 0 0 0 0 0 0 ;...
25 -2 -2 0 2 1 1 0 1 1 0 0 -1 -1 0 0 0 0 ;...
26 0 -2 -2 0 1 1 2 0 0 1 1 0 0 -1 -1 0 0 ;...
27 2 4 2 -2 -2 -2 -2 -2 -2 -2 -2 -2 2 2 2 2 0 0 ;...
28 0 0 0 0 0 0 0 0 1 0 1 0 -1 0 -1 0 0 0 ;...
29 0 0 0 0 0 0 0 0 0 1 0 1 0 -1 0 -1 0 0 ;...
30 0 0 0 0 0 0 0 0 -1 0 0 0 1 0 0 0 -1 1;...
31 0 0 0 0 0 0 0 0 -1 0 0 0 1 0 0 1 -1 ;...
32 0 0 0 0 0 0 0 0 0 -1 0 0 0 1 0 1 -1 ;...
33 0 0 0 0 0 0 0 0 0 0 -1 0 0 0 1 -1 1 ];
34 %calculate all the ODE's
35 dy=A*xx;
36
37
```

calfractions.m

```
1 % calculate fractions for each spieces
2 g(:,1:3)= [Y(:,1)/Ng, (Y(:,2)+Y(:,3))/Ng, Y(:,4)/Ng];
3 l(:,1:3)= [Y(:,10)/Nl, (Y(:,11)+Y(:,12))/Nl, Y(:,13)/Nl];
4 s(:,1:5)= [Y(:,5:6)/Ns, Y(:,7)/Ns, (Y(:,8:9))/Ns];
5 % calculate free site fraction and M-X M-OX fractions
6 ss(:,1:3)= [Y(:,7),(Y(:,5)+Y(:,6))/Ns, (Y(:,8)+Y(:,9))/Ns ];
7 % calculate H/D ration in G,S,L
8 HD(:,1:3)= [(Y(:,1)+Y(:,2)/2+Y(:,3)/2)/Ng, (Y(:,5)+Y(:,8))./(Ns-Y(:,7)),
    (Y(:,10)+Y(:,11)/2+Y(:,12)/2)/Nl];
9
```

H2D2modelfunctions.m

```
%this is a script ---- getdate.m
%get experimental data
tdata1=xlsread('f:\che 801\data.xls', 'data2', 'time2');
ydata1=xlsread('f:\che 801\data.xls', 'data2','HDF2');
%-----------------------------------------
function dy = larsf(t,y,k)
global Mt Dt Nt Nl Ng Ns Ht XX reactor_V
%calculate k values
k1=k(1);k2=k(1)/k(3);k3=k(1)/k(2);k4=k3/k(4);k5=k(5);
% clear
dydy = zeros(13,1);
% calculate
V=reactor_V/1000;% vol in liters
%calculate each reaction rate pates
k1y7y7=k1*y(7)*y(7); k4y7y7=k4*y(7)*y(7) ;
xx=[k2*y(5)*y(5)/V; k2*y(5)*y(6)/V; k2*y(6)*y(6)/V; ...
k1y7y7*y(1)/V/V; k1y7y7*y(2)/V/V; k1y7y7*y(3)/V/V; ...
k1y7y7*y(4)/V/V; k4y7y7*y(10); k4y7y7*y(11)/V/V; ...
k4y7y7*y(12)/V/V; k4y7y7*y(13)/V/V; k3*y(5)*y(8)/V; ...
k3*y(5)*y(9)/V; k3*y(6)*y(8)/V; k3*y(6)*y(9)/V; ...
k5*y(10)*y(13)/V; k5*y(11)*y(12)/V];
% difine the coef for all the ODE
A= [1 0 0 -1 0 0 0 0 0 0 0 0 0 0 0 0 0;...
0 1 0 0 -1 0 0 0 0 0 0 0 0 0 0 0 0;...
0 1 0 0 0 -1 0 0 0 0 0 0 0 0 0 0 0;...
0 0 1 0 0 0 -1 0 0 0 0 0 0 0 0 0 0;...
-2 -2 0 2 1 1 0 1 1 0 0 -1 -1 0 0 0 0;...
0 -2 -2 0 1 1 2 0 0 1 1 0 0 -1 -1 0 0;...
2 4 2 -2 -2 -2 -2 -2 -2 -2 -2 2 2 2 2 0 0;...
0 0 0 0 0 0 0 0 1 0 1 0 -1 0 -1 0 0 0;...
```

```
31 0 0 0 0 0 0 0 0 1 0 1 0 -1 0 -1 0 0;...
32 0 0 0 0 0 0 0 -1 0 0 0 1 0 0 0 -1 1;...
33 0 0 0 0 0 0 0 0 -1 0 0 0 1 0 0 1 -1;...
34 0 0 0 0 0 0 0 0 0 -1 0 0 0 1 0 1 -1;...
35 0 0 0 0 0 0 0 0 0 0 -1 0 0 0 1 -1 1];
36 %calculate all the ODE's
37 dy=A*xx;
38 %-----------------------------------------------------------
39 function RR = objectivef(k,tdata,ydata,Yo);
40 global Mt Dt Nt Nl Ng Ns Ht XX reactor_V
41 %solve ODE's from 0 to 1000
42 options = odeset( 'RelTol',.00000001,'MaxStep' ,10);
43 [t,Y] = ode15s(@(t,Y) larsf(t,Y,k),[0 995],Yo,options);
44 %calculate fractional info
45 calfractions;
46 % extrapolate Experimental data to calculated data
47 Yexp = interp1(tdata,ydata,t, 'pchip');
48 %calculate least squares
49 R=(g-Yexp).^2;
50 %add all least square values
51 RR=sum(sum(R, 'double'), 'double');
```

References

1. B. Hogle, D. S., K. Nagarajan, J.E. Jackson, D.J. Miller Formation and recovery of itaconic acid from aqueous solutions of citraconic acid and succinic acid. *Industrial and Engineering Chemistry Research* **2002,** 41, (9), 2069-2073.

2. Z. Zhang, J. E. J., D.J. Miller, Aqueous-phase hydrogenation of lactic acid to propylene glycol. *Applied Catalysis A: General* **2001,** 219, 89-98.

3. Jere, F. T.; Miller, D. J.; Jackson, J. E., Stereoretentive C-H bond activation in the aqueous phase catalytic hydrogenation of amino acids to amino alcohols. *Organic Letters* **2003,** 5 (4), 527-530.

4. Chopade, S. P.; Miller, D. J.; Jackson, J. E.; Werpy, T. A.; Frye, J. G., Jr.; Zacher, A. H. Catalysts and process for hydrogenolysis of sugar alcohols to polyols. 2001-US536,2001066499, 2001, 2001.

5. Shafer, M. W. Catalytic processing of monosaccharides and sugar alcohols to value-added products. Michigan State University, East Lansing, 2004.

6. Kovacs, D. G.; Jackson, J. E.; Miller, D. J., Mechanistic investigation of glycerol hydrogenolysis. *Abstracts of Papers of the American Chemical Society* **2001,** 221, U177-U178.

7. Crabtree, S. P.; Tyers, D. V. Process for the catalytic hydrogenolysis of sugar feedstocks into glycols and glycerol. 2004-GB4391,2005051874, 2004, 2005.

8. Suppes, G. J.; Sutterlin, W. R.; Dasari, M. A. Method of producing lower alcohols from glycerol. 2005-US9901,2005095536, 20050324., 2005.

9. Lahr, D. G.; Shanks, B. H., Effect of sulfur and temperature on ruthenium-catalyzed glycerol hydrogenolysis to glycols. *Journal of Catalysis* **2005,** 232, (2), 386-394.

10. Lahr, D. G.; Shanks, B. H., Kinetic analysis of the hydrogenolysis of lower polyhydric alcohols: Glycerol to glycols. *Industrial & Engineering Chemistry Research* **2003,** 42, (22), 5467-5472.

11. Kusunoki, Y.; Miyazawa, T.; Kunimori, K.; Tomishige, K., Highly active metal-acid bifunctional catalyst system for hydrogenolysis of glycerol under mild reaction conditions. *Catalysis Communications* **2005,** 6, (10), 645-649.

12. Dasari, M. A.; Kiatsimkul, P. P.; Sutterlin, W. R.; Suppes, G. J., Low-pressure hydrogenolysis of glycerol to propylene glycol. *Applied Catalysis a-General* **2005,** 281, (1-2), 225-231.

13. Chaminand, J.; Djakovitch, L.; Gallezot, P.; Marion, P.; Pinel, C.; Rosier, C., Glycerol hydrogenolysis on heterogeneous catalysts. *Green Chemistry* **2004,** 6, (8), 359-361.

14. Perosa, A.; Tundo, P., Selective Hydrogenolysis of Glycerol with Raney Nickel. *Industrial & Engineering Chemistry Research* **2005,** 44, (23), 8535-8537.

15. Montassier, C.; Menezo, J. C.; Hoang, L. C.; Renaud, C.; Barbier, J., Aqueous polyol conversions on ruthenium and on sulfur-modified ruthenium. *Journal of Molecular Catalysis* **1991,** 70, (1), 99-110.

16. Hahn, R.; Tscheliessnig, A.; Zochling, A.; Jungbauer, A., Shallow bed adsorption: Theoretical background and applications. *Chemical Engineering & Technology* **2005,** 28, (11), 1241-1251.

17. Alduri, B., A Review in Equilibrium in Single and Multicomponent Liquid Adsorption Systems. *Reviews in Chemical Engineering* **1995,** 11, (2), 101-143.

18. Cornelissen, G.; Gustafsson, O.; Bucheli, T. D.; Jonker, M. T. O.; Koelmans, A. A.; Van Noort, P. C. M., Extensive sorption of organic compounds to black carbon, coal, and kerogen in sediments and soils: Mechanisms and consequences for distribution, bioaccumulation, and biodegradation. *Environmental Science & Technology* **2005,** 39, (18), 6881-6895.

19. Smith, E. H., Evaluation of Multicomponent Adsorption Equilibria for Organic Mixtures onto Activated Carbon. *Water Research* **1991,** 25, (2), 125-134.

20. Xing, B. S.; Pignatello, J. J.; Gigliotti, B., Competitive sorption between atrazine and other organic compounds in soils and model sorbents. *Environmental Science & Technology* **1996,** 30, (8), 2432-2440.

21. Li, F. S.; Yuasa, A.; Ebie, K.; Azuma, Y.; Hagishita, T.; Matsui, Y., Factors affecting the adsorption capacity of dissolved organic matter onto activated carbon: modified isotherm analysis. *Water Research* **2002,** 36, (18), 4592-4604.

22. Antonjuk, A. A.; Redkovsky, N. N.; Carl, P. S.; Seidel, A.; Marutovsky, R. M., Determination of Intraparticle Kinetic-Parameters for Adsorption of Binary-Solutions on Activated Carbon. *Chemical Engineering Science* **1991,** 46, (4), 1035-1039.

23. Leitao, A.; Serrao, R., Adsorption of phenolic compounds from water on activated carbon: Prediction of multicomponent equilibrium isotherms using single-component data. *Adsorption-Journal of the International Adsorption Society* **2005,** 11, (2), 167-179.

24. Abburi, K., Adsorption of phenol and p-chlorophenol from their single and bisolute aqueous solutions on Amberlite XAD-16 resin. *Journal of Hazardous Materials* **2003,** 105, (1-3), 143-156.

25. Yaacoubi, A.; Mazet, M.; Dusart, O., Competitive Effect in Bi-Solute Adsorption onto Activated Carbon - Dss, Alcohols and Phenols as Solutes. *Water Research* **1991,** 25, (8), 929-937.

26. Lu, Q. L.; Sorial, G. A., Adsorption of phenolics on activated carbon - impact of pore size and molecular oxygen. *Chemosphere* **2004,** 55, (5), 671-679.

27. Dekock, F. P.; Vandeventer, J. S. J., Stochastic-Model for Equilibrium Adsorption onto Activated Carbon. *Chemical Engineering Journal and the Biochemical Engineering Journal* **1995,** 59, (3), 205-220.

28. Lee, J. W.; Kwon, T. O.; Moon, I. S., Adsorption of mono saccharides, disaccharides, and maltooligosaccharides on activated carbon for separation of maltopentaose. *Carbon* **2004,** 42, (2), 371-380.

29. Liu, X.; Pinto, N. G., Ideal adsorbed phase model for adsorption of phenolic compounds on activated carbon. *Carbon* **1997,** 35, (9), 1387-1397.

30. Kumar, A.; Kumar, S.; Kumar, S., Adsorption of resorcinol and catechol on granular activated carbon: Equilibrium and kinetics. *Carbon* **2003,** 41, (15), 3015-3025.

31. Lu, Q. L.; Sorial, G. A., The role of adsorbent pore size distribution in multicomponent adsorption on activated carbon. *Carbon* **2004,** 42, (15), 3133-3142.

32. Braeken, L.; Boussu, K.; Van der Bruggen, B.; Vandecasteele, C., Modeling of the adsorption of organic compounds on polymeric nanofiltration membranes in solutions containing two compounds. *Chemphyschem* **2005,** 6, (8), 1606-1612.

33. Frimmel, F. H.; Assenmacher, M.; Kumke, M. U.; Specht, C.; Abbt-Braun, G.; Grabe, G., Removal of hydrophilic compounds from water with organic polymers - Part II: Adsorption behavior of industrial wastewater. *Chemical Engineering and Processing* **2002,** 41, (9), 731-736.

34. Matsui, Y.; Yuasa, A.; Ariga, K., Removal of a synthetic organic chemical by PAC-UF systems - I: Theory and modeling. *Water Research* **2001,** 35, (2), 455-463.

35. Bonalumi, N.; Vargas, A.; Ferri, D.; Burgi, T.; Mallat, T.; Baiker, A., Competition at chiral metal surfaces: Fundamental aspects of the inversion of enantioselectivity in hydrogenations on platinum. *Journal of the American Chemical Society* **2005,** 127, (23), 8467-8477.

36. Vargas, A.; Ferri, D.; Baiker, A., DFT and ATR-IR insight into the conformational flexibility of cinchonidine adsorbed on platinum: Proton exchange with metal. *Journal of Catalysis* **2005,** 236, (1), 1-8.

37. Keresszegi, C.; Ferri, D.; Mallat, T.; Baiker, A., Unraveling the surface reactions during liquid-phase oxidation of benzyl alcohol on Pd/Al2O3: an in situ ATR-IR study. *Journal of Physical Chemistry B* **2005,** 109, (2), 958-967.

38. Hamminga, G. M.; Mul, G.; Moulijn, J. A., Real-time in situ ATR-FTIR analysis of the liquid phase hydrogenation of gamma-butyrolactone over Cu-ZnO catalysts: A mechanistic study by varying lactone ring size. *Chemical Engineering Science* **2004,** 59, (22-23), 5479-5485.

39. Lefevre, G., In situ Fourier-transform infrared spectroscopy studies of inorganic ions adsorption on metal oxides and hydroxides. *Advances in Colloid and Interface Science* **2004,** 107, (2-3), 109-123.

40. Mul, G.; Hamminga, G. M.; Moulijn, J. A., Operando ATR-FTIR analysis of liquid-phase catalytic reactions: can heterogeneous catalysts be observed? *Vibrational Spectroscopy* **2004,** 34, (1), 109-121.

41. Hind, A. R.; Bhargava, S. K.; McKinnon, A., At the solid/liquid interface: FTIR/ATR - the tool of choice. *Advances in Colloid and Interface Science* **2001,** 93, (1-3), 91-114.

42. Ninness, B. J.; Bousfield, D. W.; Tripp, C. P., In situ infrared technique for studying adsorption onto particulate silica surfaces from aqueous solutions. *Applied Spectroscopy* **2001,** 55, (6), 655-662.

43. Lazorenko-Manevich, R. M., Adatom hypothesis as a predominant mechanism of surface enhanced Raman scattering: A review of experimental argumentation. *Russian Journal of Electrochemistry* **2005,** 41, (8), 799-831.

44. Tian, Z. Q.; Ren, B., Adsorption and reaction at electrochemical interfaces as probed by surface-enhanced Raman spectroscopy. *Annual Review of Physical Chemistry* **2004,** 55, 197-229.

45. Brolo, A. G.; Irish, D. E.; Smith, B. D., Applications of surface enhanced Raman scattering to the study of metal-adsorbate interactions. *Journal of Molecular Structure* **1997,** 405, (1), 29-44.

46. Urban, M. W., Surface and Interface Vibrational Spectroscopy - Relevance to Adhesion. *Journal of Adhesion Science and Technology* **1993,** 7, (1), 1-47.

47. Otto, A., Surface-Enhanced Raman-Scattering of Adsorbates. *Journal of Raman Spectroscopy* **1991,** 22, (12), 743-752.

48. Guo, Q. L.; Wang, E. G., Geometric and electronic structure of Cu on corundum (0001) surfaces. *Science and Technology of Advanced Materials* **2005,** 6, (7), 795-798.

49. Reniers, F.; Tewell, C., New improvements in energy and spatial (x, y, z) resolution in AES and XPS applications. *Journal of Electron Spectroscopy and Related Phenomena* **2005,** 142, (1), 1-25.

50. Duwez, A. S., Exploiting electron spectroscopies to probe the structure and organization of self-assembled monolayers: a review. *Journal of Electron Spectroscopy and Related Phenomena* **2004,** 134, (2-3), 97-138.

51. Marcus, P.; Galtayries, A., ESCA and metal surfaces - Alloys, corrosion and surface treatments. *Vide-Science Technique Et Applications* **2003,** 58, (308), 230-+.

52. Sun, C. H.; Berg, J. C., A review of the different techniques for solid surface acid-base characterization. *Advances in Colloid and Interface Science* **2003,** 105, 151-175.

53. Pollini, I.; Mosser, A.; Parlebas, J. C., Electronic, spectroscopic and elastic properties of early transition metal compounds. *Physics Reports-Review Section of Physics Letters* **2001,** 355, (1), 1-72.

54. Zemek, J., Electron spectroscopy of solid surfaces. *Acta Physica Slovaca* **2000,** 50, (5), 577-589.

55. Ronning, C.; Feldermann, H.; Merk, R.; Hofsass, H.; Reinke, P.; Thiele, J. U., Carbon nitride deposited using energetic species: A review on XPS studies. *Physical Review B* **1998,** 58, (4), 2207-2215.

56. Weitzsacker, C. L.; Xie, M.; Drzal, L. T., Using XPS to investigate fiber matrix chemical interactions in carbon-fiber-reinforced composites. *Surface and Interface Analysis* **1997,** 25, (2), 53-63.

57. Wang, J. X.; Marinkovic, N. S.; Zajonz, H.; Ocko, B. M.; Adzic, R. R., In situ X-ray reflectivity and voltammetry study of Ru(0001) surface oxidation in electrolyte solutions. *Journal of Physical Chemistry B* **2001,** 105, (14), 2809-2814.

58. Ciobica, I. M.; Kleyn, A. W.; Van Santen, R. A., Adsorption and coadsorption of CO and H on ruthenium surfaces. *Journal of Physical Chemistry B* **2003,** 107, (1), 164-172.

59. Riedmuller, B.; Ciobica, I. M.; Papageorgopoulos, D. C.; Frechard, F.; Berenbak, B.; Kleyn, A. W.; van Santen, R. A., CO adsorption on hydrogen saturated Ru(0001). *Journal of Chemical Physics* **2001,** 115, (11), 5244-5251.

60. Peebles, D. E.; Schreifels, J. A.; White, J. M., The Interaction of Coadsorbed Hydrogen and Carbon-Monoxide on Ru(001). *Surface Science* **1982,** 116, (1), 117-134.

61. Pallassana, V.; Neurock, M., Reaction paths in the hydrogenolysis of acetic acid to ethanol over Pd(111), Re(0001), and PdRe alloys. *Journal of Catalysis* **2002,** 209, (2), 289-305.

62. Haile, J. M., *Molecular dynamics simulation : elementary methods*. Wiley: New York, 1992; p xvii, 489 p.

63. Jacob, T.; Goddard, W. A., Agostic interactions and dissociation in the first layer of water on Pt(111). *Journal of the American Chemical Society* **2004,** 126, (30), 9360-9368.

64. Ogasawara, H.; Brena, B.; Nordlund, D.; Nyberg, M.; Pelmenschikov, A.; Pettersson, L. G. M.; Nilsson, A., Structure and bonding of water on Pt(111). *Physical Review Letters* **2002,** 89, (27).

65. Ito, M.; Nakamura, M., Hydration processes of electrolyte anions and cations on Pt(111), Ir(111), Ru(001) and Au(111) surfaces: Coadsorption of water molecules with electrolyte ions. *Faraday Discussions* **2002,** 121, 71-84.

66. Thor Dozeman, G. J., TLE Catalytic conversion of D-glucitol and isosorbide using zeolite.

67. Dozeman, G. J., Catalytic conversion of D-glucitol and isosorbide using zeolite catalysts. In 1989.

68. Chen, Y. Aqueous-Phase Catalytic Hydrogenation of Organic Acids and Theit Mixtures. Michigan State University, East Lansing, 2007.

69. Parsons, M. T.; Westh, P.; Davies, J. V.; Trandum, C.; To, E. C. H.; Chiang, W. M.; Yee, E. G. M.; Koga, Y., A thermodynamic study of 1-propanol-glycerol-H2O at 25 degrees C: Effect of glycerol on molecular organization of H2O. *Journal of Solution Chemistry* **2001,** 30, (11), 1007-1028.

70. Parsons, M. T.; Koga, Y., Interactions in 1-propanol-(1,2-and 1,3-)propanediol-H2O: The effect of hydrophobic vs hydrophilic moiety on the molecular

organization of H2O. *Journal of Physical Chemistry B* **2002,** 106, (28), 7090-7095.

71. Hansch, C.; Hoekman, D.; Leo, A.; Zhang, L. T.; Li, P., The Expanding Role of Quantitative Structure-Activity-Relationships (Qsar) in Toxicology. *Toxicology Letters* **1995,** 79, (1-3), 45-53.

72. Sorial, G. A.; Suidan, M. T.; Vidic, R. D.; Maloney, S. W., Competitive Adsorption of Phenols on Gac .1. Adsorption Equilibrium. *Journal of Environmental Engineering-Asce* **1993,** 119, (6), 1026-1043.

73. McKay, G.; Alduri, B., Multicomponent Dye Adsorption onto Carbon Using a Solid Diffusion Mass-Transfer Model. *Industrial & Engineering Chemistry Research* **1991,** 30, (2), 385-395.

74. Yaws, C. L. N., Prasad, K.; Gabbula, Chaitanya . Yaws' Handbook of Antoine Coefficients for Vapor Pressure (Electronic Edition). Knovel.